Anal. Methods Environ. Chem. J. 4 (2) (2021) 5-24

AMECJ

Research Article, Issue 2
Analytical Methods in Environmental Chemistry Journal
Journal home page: www.amecj.com/ir

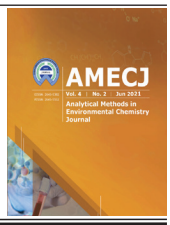

Reusable and sustainable graphene oxide/metal–organic framework-74/Fe_3O_4/polytyramine nanocomposite for simultaneous trace level quantification of five fluoroquinolones in egg samples by high performance liquid chromatography

Fatemeh Pourbahman[a], Mohsen Zeeb[a,*], Amirhossein Monzavi[b], Zahra Khodadadi[a] and Seyed Saied Homami[a]
[a]*Department of Applied Chemistry, Faculty of Science, South Tehran Branch, Islamic Azad University, Tehran, Iran*
[b]*Department of Polymer and Textile Engineering, South Tehran Branch, Islamic Azad University, Tehran, Iran*

ARTICLE INFO:

Received 2 Mar 2021
Revised form 5 May 2021
Accepted 27 May 2021
Available online 28 Jun 2021

Keywords:
Magnetic dispersive micro-solid phase extraction,
Metal–organic framework,
Graphene oxide,
Polytyramine,
Fluoroquinolones

ABSTRACT

A nanohybrid material termed graphene oxide/metal-organic framework-74/Fe_3O_4/polytyramine (GO/MOF-74/Fe_3O_4/PTy) was fabricated and applied in magnetic dispersive micro-solid phase extraction (MD-μ-SPE) coupled with high performance liquid chromatography (HPLC) for simultaneous determination of fluoroquinolones compounds including, ofloxacin, ciprofloxacin, lomefloxacin, enrofloxacin and sperfloxacin in egg samples. The GO/MOF-74/Fe_3O_4/PTy nanocomposite was fabricated through an in situ synthesis of MOF-74 in the presence of magnetic GO and followed with an oxidative polymerization of tyramine using horsedish peroxide (HRP) enzyme. The modifier agents improved the merits of the nanoporous sorbent. Extraction protocols based on GO/MOF nanocomposites have various benefit such as, the high stability, the tunable porosity, the fast mast transfer and reasonable enrichment factor. The fabricated material was characterized via energy dispersive x-ray analysis (EDX), the scanning electron microscopy (SEM), Fourier-transform infrared spectroscopy (FT-IR), and the x-ray diffraction (XRD). The calibration curves revealed linearity ($0.9992 \leq r^2 \leq 0.9997$) in the ranges of 1.0-475.0, 0.5-350.0, 0.5-350.0, 0.5-375.0 and 1.5-300.0 ng mL^{-1} with limit of detections (LODs, S/N=3) of 0.3, 0.1, 0.2, 0.1 and 0.4 ng mL^{-1} for ofloxacin, ciprofloxacin, lomefloxacin, enrofloxacin and sperfloxacin, respectively. The intra-assay (≤7.7%, n = 9) and inter-assay (≤7.0%, n = 9) precisions along with accuracy less than 9.0% showed the reliability of the method.

1. Introduction

Fluoroquinolones (FQs) such as ofloxacin, ciprofloxacin, lomefloxacin, enrofloxacin and sparfloxacin (Fig. 1) have great importance due to their high antibacterial activity and considerable bioavailability which makes these compounds as efficient drugs not only for treatment of human's diseases but also for prevention and treatment of veterinary illnesses [1]. In recent years, the FQs have been widely used in different infectious diseases due to resistance against these drugs,

*Corresponding Author: Mohsen Zeeb
Email: zeeb.mohsen@gmail.com
https://doi.org/10.24200/amecj.v4.i02.135

the various hazardous side effects and allergic problems [2]. Based on FQs application in animal husbandry, the impact of FQs has been found in a variety of food samples like milk, the bee products, chicken and eggs. Since eggs and egg yolk products have high protein content and some essential minerals, they are tremendously utilized in the diet of breastfed children, infants, premature babies and adults. Hence, it is necessary to expand reliable and cost-effective analytical methods to quantify trace amount of FQs residue in egg samples to ensure public health safety in humans [3-5].

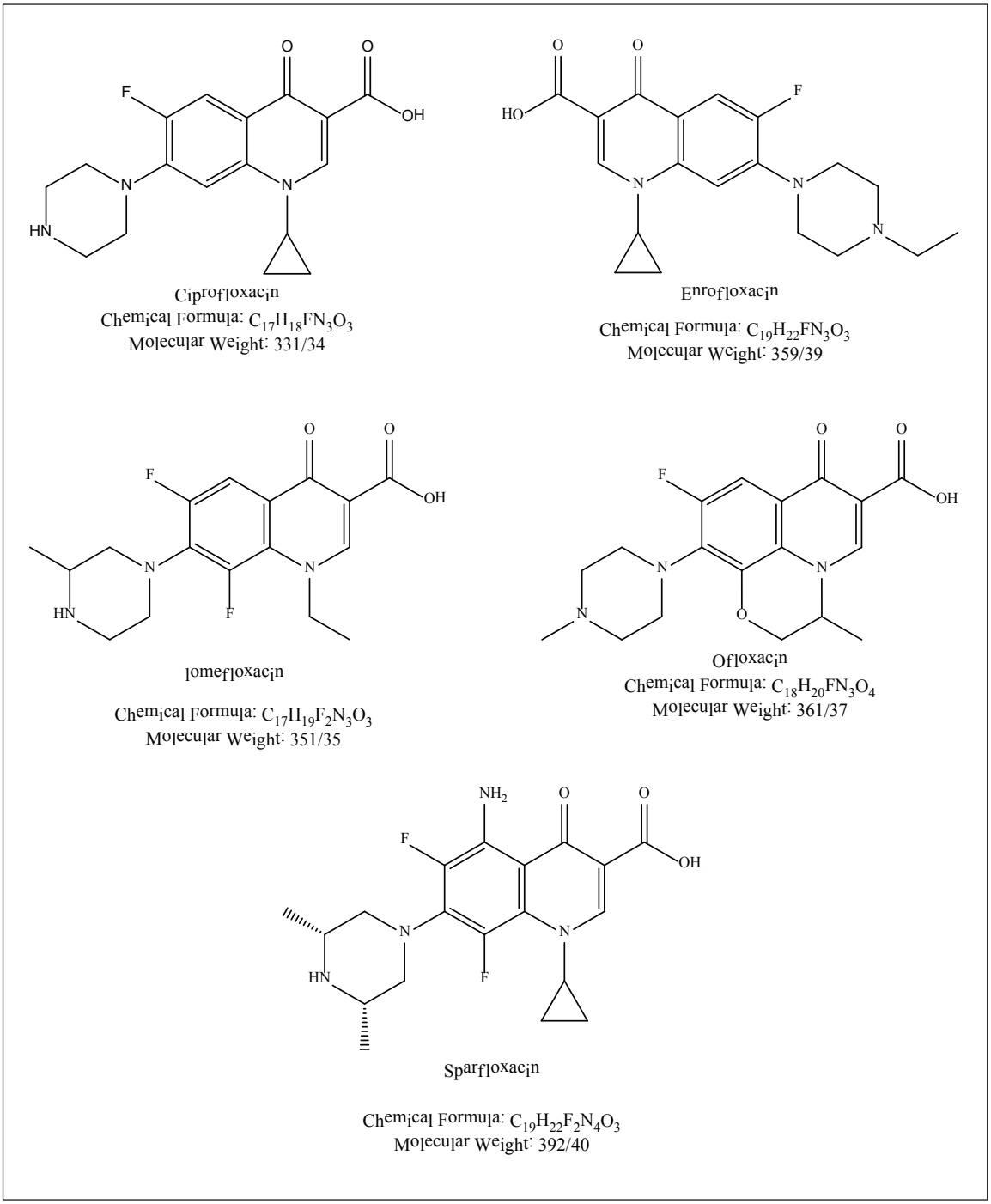

Fig. 1. Structures of target of fluoroquinolones (FQs) such as ofloxacin, ciprofloxacin, lomefloxacin, enrofloxacin and sparfloxacin

Literature survey shows that different analytical protocols have been reported for the determination of FQs which suffer from major drawbacks including high matrix effect, low sensitivity, unacceptable reproducibility, high usage of hazardous reagents and etc. [1, 4-6]. In order to overcome these weaknesses, the development a sustainable sample preparation strategy prior to measurement is essential. Magnetic dispersive micro-solid phase extraction (MD-μ-SPE) as a promising kind of solid-phase extraction (SPE) offers many merits over other traditional sample preparation methods and reveals notable applications in enrichment and isolation of target analyses from complex matrices like environmental, natural, drug and food samples [7-10]. The major advantages of this new kind of extraction method involve significant reduction of toxic reagent usage, removal of time consuming steps like filtration and centrifugation, considerable automation ability and reasonable extraction yields along with a meaningful decrease of interference effects [1]. Researchers have conducted extensive studies over new magnetic sorbents MD-μ-SPE and used in different analytical purposes. However, the developed sorbets show some disadvantages involving the lack of reusability, low surface area, insufficient porosity, low satiability and so on [11]. To deal with these issues, graphene oxide (GO) nanosheet as a novel allotrope of carbon seems superior choice to fabricate a new nanohybrid material for extraction goals. Its high surface area, strong hydrophobic properties, notable mechanical characteristics, outstanding acid and alkaline resistance as well as high chemical and thermal stability, enable it to create increasing π-π interactions [12, 13]. Lately, various materials with individual properties such as silicon-based compounds [14], inorganic nano-materials [15], metal oxides [16, 17], conducting metal polymers [18] and MOFs [19-21] have been introduced as surface modifiers to enhance the merits of the GO. MOFs are classified a new type of highly porous materials which can be synthesized through an interaction between coordinates of metal ions (nodes) and bridging ligands, under appropriate conditions. MOFs as 3-dimensional structures exhibit various topologies along with individual properties like tunable porosity, high surface area from 1000 to 10400 m^2g^{-1}, simple synthesis routes, and adequate resistance. Owing to these possessions, these materials have been applied in different areas like the adsorption phenomena [22], the separation [23-25], the gas storage [26, 27] and the drug delivery [28]. Literature survey shows that some MOFs including Hkust-1 [29], MIL-101 [30], MOF-5 [31], UiO-66 [32], MIL-100 [33] have been applied in SPE as successful sorbents. Among of MOFs crystals, the MOF-74 is resulted from the reaction of divalent metal cations like Mg, Mn, Fe, Co, Ni and Zn with divergent organic ligand called 2,5-dihydroxybenzene-1,4-dicarboxylate (DBDC) [34-36]. In order to enhance the qualities of a carbon based material for extraction purposes, conductive polymers such as polythionine, polyaniline, polythiophene, polytyramine (PTy) seem appreciable alternatives which significantly increase π-π interaction, hydrophobic property, extraction capacity, diffusion rate and reusability [37-43]. Among these polymers, PTy can be synthesized through a simple and inexpensive oxidative polymerization route in the presence of horseradish peroxidaze (HRP) enzyme as a catalyst and furthermore existence of alkyl groups in this polymer results the establishment of macropores on the surface of sorbent. The synthesized nanosorbent have been used in a similar way to investigate the prokinetic drugs on human plasma but in this study, as a novel research, we used synthesized sorbent to quantitatively probe the simultaneous, five type of fluroquinolone in egg sample [44].

In the presented study, the surface of GO nanosheet was modified with MOF-74 to result GO/MOF-74 and furthermore in order to provide a super-magnetic material, precipitation of Fe_3O_4 on the fabricated sorbent was followed. In the last step, the polymerization of tyramine was carried out using HRP enzyme to prepare recyclable GO/MOF-74/Fe_3O_4/PTy nanocomposite as a sustainable sorbent for the MD-μ-SPE process. Ultimately, the extraction protocol was followed with HPLC-

UV for simultaneous extraction and quantitation of five fluoroquinolones including ofloxacin, ciprofloxacin, lomefloxacin, enrofloxacin and sperfloxacin in egg samples and satisfactory precisions along with desirable accuracies were obtained.

2. Experimental

2.1. Chemicals

In this study, the analytical grade of chemicals and reagents were applied. These chemicals involviung 2, 5- Dihydroxy triphetalic acid, N, N- dimethylformamide, tyramine, horseradish peroxidaze and graphite powder (mesh of 100) were obtained from Merck Company (Darmstadt, Germany). Iron (III) chloride hexahydrate ($FeCl_3.6H_2O$), iron (II) chloride tetrahydrate ($FeCl_2.4H_2O$), the sodium nitrate ($NaNO_3$), the potassium permanganate ($KMnO_4$), the sulfuric acid (H_2SO_4, 98%), the nickel (II) nitrate hexahydrate [$Ni(NO_3)_2.6H_2O$], the sodium hydroxide (NaOH), the hydrochloric acid (HCl 37%), the hydrogen peroxide (H_2O_2, 30%), the ethanol (C_2H_5OH) and triethylamine were obtained from Sigma-Aldrich Company (St. Luise, MO, USA). The standards of fluoroquinolones were provided from Kusum Healthcare (Punjab, India). Ultrapure water (Millipore, Bedford, MA, USA) was used in all experminets. HPLC grades of methanol, acetonitrile, acetone and potassium dihydrogen phosphate were bought from Merck company (Darmstadt, Germany).

2.2. Instrumentation

Energy dispersive x-ray (EDX) spectra and scanning electron microscopy (SEM) images were investigated in detail via a TESCAN-Vega 3 (TESCAN, Czech Republic), machines. All the X-ray diffraction (XRD) spectra were recorded and studied within angular range of 0-80°, using Kα radiation (λ= 1.54 ˚A) created by Cu element on a D8 Advance AXS diffractometer instrument (Bruker, Germany). All the FTIR spectra were recorded on a Perkin Elmer FTIR spectrometer (RXI, Germany).

2.3. Chromatographic analysis

Chromatographic data were obtained using a waters alliance e2695 instrument (Massachusetts, USA) equipped with two pumps for delivering the mobile phase during gradient elution. UV-VIS detector (wavelengths of 275 and 288 nm) and C_{18} reversed phase column (5 µm, 250×4.6 mm id, phenomenex Co, Torrance, CA) at 30°C temperature were utilized to complete separation process. A gradient elution containing two types of mobile phases (A: phosphate buffer at pH 3 and B: acetonitrile) was programmed as follows: it was started at 70% A for 12 min, increased to 85% A over 1 min and retained at this value for 6 min and decreased to 70% A for 4 min. The flow rate of pump was regulated at 1 mL min^{-1} in all experiments while the injection volume was set at 20 µL. The applied mobile phase was filtered through a 0.2 µm membrane filter (Millipore, Bedford, MA, USA) for further purification.

2.4. Synthesis

2.4.1.Synthesis of GO/MOF-74

0.25 g graphene oxide (GO was fabricated using hummer's method [45] and 0.23 g of 2, 5-dihydroxyphthalic acid and 1.13 g of Ni $(No_3)_2.6H_2O$ were mixed completely and a mixture containing N,N-Dimethylformamide (DMF), ethanol and once ionized water (1:1:1, V/V/V, 100 ml) was added slowly to the above materials. For making a suspension, the obtained solution was sonicated in an ultrasound bath for 10 minutes [46]. The resultant was kept inside an oven for 24 hours at a temperature of 100 °C and then it was cooled to 25 °C. The upper phase was decanted off and the sedimented phase was washed with methanol for 6 times to remove any impurities.

2.4.2.Synthesis of GO/MOF-74/Fe_3O_4

For synthesis of GO/MOF-74/Fe_3O_4, 0.8 g $FeCl_3.6H_2O$ and 0.3 g of $FeCl_2.4H_2O$ were mixed and dissolved in 25 mL deionized water. The fabricated GO/MOF-74 was added slowly to the solution under a stream of nitrogen and the pH of the solution was fixed at 10 using ammonia. The

resulting solution was placed into an oven at 100 °C for 24 hours and afterwards it was cooled to 25 °C (room temperature). To remove probable impurities, the upper phase was poured off and residue was washed for 3 times with methanol. The final compound was transferred into an oven with a temperature of 250°C and kept there for 2 hours to achieve a brown powder.

2.4.3.Synthesis of GO/MOF-74/Fe_3O_4/ polytyramine

In order to fabricate GO/MOF-74/Fe_3O_4/PTy, an in situ oxidative polymerization was performed on the surface of GO/MOF-74/Fe_3O_4 through an enzymatic cross-linking of poly-tyramine in the presence of HRP enzyme as a catalyst. HRP is considered as a heme-containing oxidoreductase which composes of two broad classes of iron centers including a single heme group [iron (iii) protoporphyrin IX] and two calcium atoms, which catalyzes the oxidation of different organic substrates by hydrogen peroxide. The chemical equation below describes the relevant chemical reaction:

where tyramine as an enzyme substrate, conjugates with hydrogen peroxide and thus catalyzed by HRP. Synthesis route was as follows: 200 mg GO/MOF-74/Fe_3O_4, 160 mg tyramine, 1 mg HRP, 8 mL acetone and 4 mL phosphate buffer (0.1 M, pH 7) were completely mixed together. Then, 240 µL hydrogen peroxide was used to proceed the reaction at a temperature of 30°C. The obtained solution was filtered and placed into an oven and kept there until dryness.

2.5. Preparation of standard solutions and quality control samples of FQs

In order to prepare stock solutions, required amount of each FQs including ofloxacin, ciprofloxacin, lomefloxacin, enrofloxacin and sperfloxacin was independently dissolved in methanol to result a concentration of 10.0 mg L^{-1}. To prevent the decomposition of FQs, the stock solutions of these drugs were prepared every week and stored in the dark place at 4 °C. To obtain working standard solutions of FQs, stock solutions were diluted step wise. Egg samples were spiked with various levels of the working standard solutions for plotting calibration curve and further measuring. To demonstrate the accuracy and reproducibility of the presented method, different quality control samples of target FQs at concentration levels of 10.0, 150.0 and 350.0 ng mL^{-1} were prepared.

2.6. Preparation of egg samples

Two kinds of egg samples (subject) were collcted and prepared before using by the proposed method. The egg samples 1 from healthy hens without feeding any drugs for evaluation of inter-day/ intra-day precisions and accuraies were used. The egg samples 2 from hens which had been fed a certain amount of five FQs once a day for 7 day for conduting recovery experiments and evaluating the reliabilty of the method were selected. In order to prepare egg samples, 5 g of eggs was added to centrifuge tubes and after that 10 mL methanol was added to them and centrifuged at 5000 rpm for 10 min. The upper phase was decanted to the new tubes and evaporated to dryness under a stream of nitogen. Finally, 5 mL deionzed water was added to each tube and subjected to the presented extration protocol.

2.7. The procedure of MD-µ-SPE-HPLC-UV

The steps of MD-µ-SPE-HPLC-UV procedure for isolation, enrichment and quatitation of FQs are shown in schema 1. Firstly, 5.0 mL of the prepared egg sample was placed into a centrifuge tube and then 10.0 mg of GO/MOF-74/Fe_3O_4/PTy was added to the tube containing the real sample. After that, ultrasonic irradiation was utilized for 10 min, to disperse the supermagnetic nanoporous sorbent into the solution and isolate the analytes of interest. The tube containing the sample was exposed to a powerful magnet Nd-Fe-B with a magnitude of 0.8 tesla to collect the particles of nanosorbent at the bottom of the vessel. In the next step, the aqueous media was discarded and the remaining extractor was washed with 2.5 mL acetonitrile through the applying ultrasonic irradiation for 2 min. Then, the sample containing desorbed FQs was exposed to

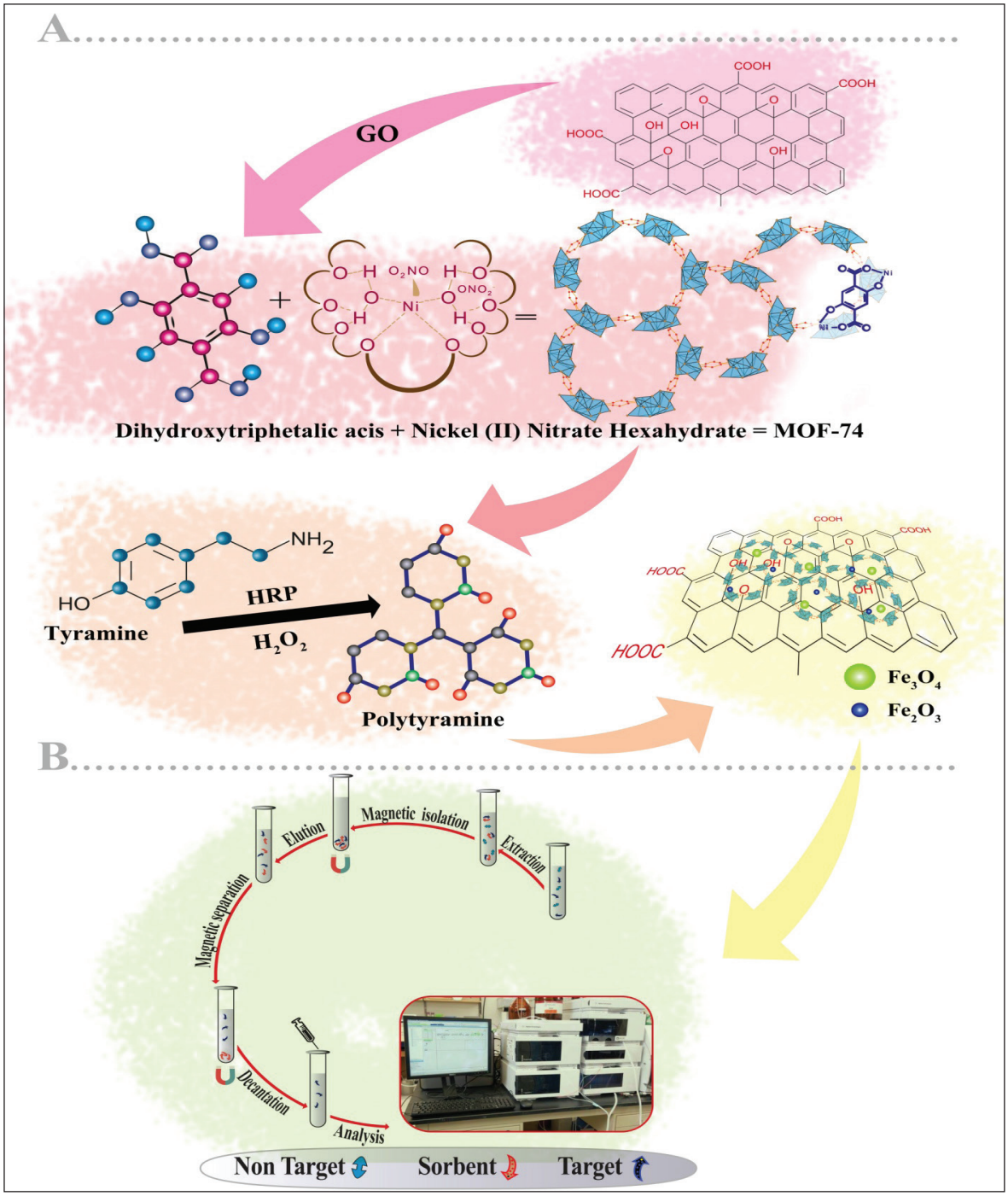

Schema 1. A: Schematic diagram of the synthesis routes of GO/MOF-74/Fe3O4/PTy. B: different steps of MD-μ-SPE-HPLC-UV method in extraction, enrichment and isolation of FQs

the magnet again to collect solution. The collected solution was evaporated under a stream of nitrogen to dryness and the resultant residue was dissolved in 100.0 μL of the optimized mobile phase of HPLC. Finally, 20.0 μL of the obtained sample was injected into HPLC for analyzing FQs.

3. Results and Discussion

3.1. Characterizations

The illustrates of the FTIR spectrum of GO/MOF-74/Fe_3O_4/PTy, recorded in the range of 400–4000 cm^{-1}(Fig.2) The FTIR spectrum of the synthesized nanocomposite sorbent indicates all the components of this structure evidently. As clearly exhibited in the spectrum, the broad peak at 3200-3648

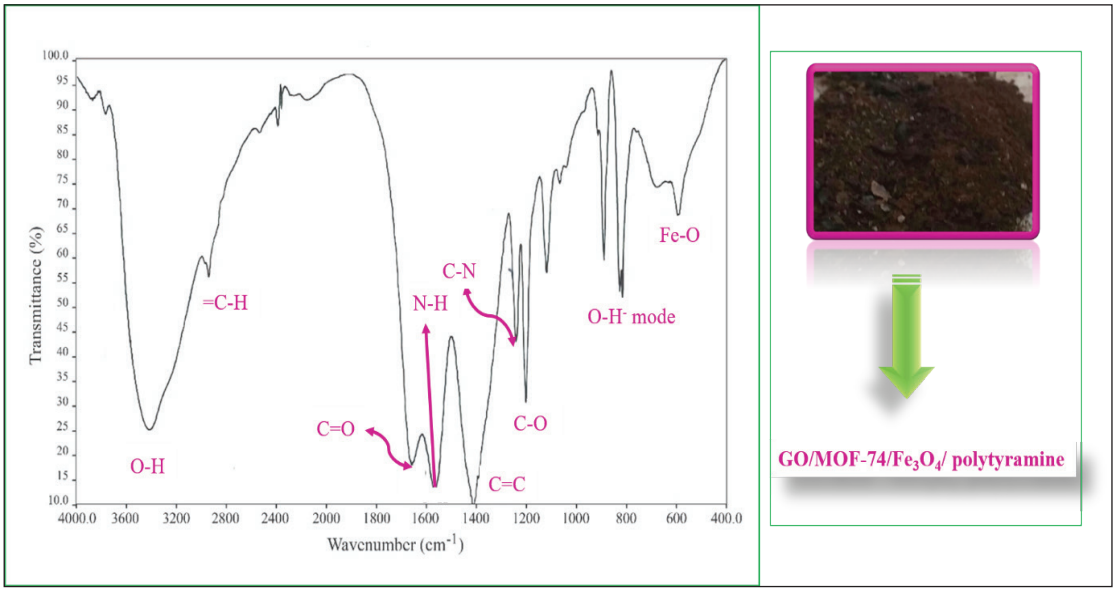

Fig. 2. The FT-IR spectrum of GO/MOF-74/Fe_3O_4/PTy nonporous composite

cm^{-1} assigns to hydroxyl groups with stretching vibrations in the structure of GO. Oxygen-containing functional groups in the composition of this sorbent include epoxy C-O and C=O stretching vibrations with absorption peaks in the range of 1100-1200 cm^{-1} and 1650-1680 cm^{-1}, respectively. The absorption peaks corresponding with aromatic absorption bonds with C=C stretching vibrations are located in the range of 1410-1450 cm^{-1}. Due to the adjusted attachment of magnetic Fe_3O_4 on the surface of GO, a peak is observed at 500-580 cm^{-1}, which attributes to the stretching vibrations of Fe-O. µ-hydroxo groups can also be identified in the corner-sharing hexagonal units of MOF-74 with two sharp peaks at 850-950 cm^{-1} [48]. Other peaks placed in the range of 1210-1250 cm^{-1} are related to N-H and C-N vibrations, respectively.

In the XRD spectrum (Fig. 3), the peaks associated with GO, GO/MOF-74/Fe_3O_4, and GO/MOF-74/Fe_3O_4/PTy are meticulously compared with each other. The XRD pattern with diffraction peak assigned to (101) at 2θ=11.281˚, which was shown in Figure 3a, confirms the GO structure. As Figure 3b and 3c, the MOF structure is clearly exhibited in the XRD pattern that confirms its unique crystal structure according to the x-ray reflection indexed to (110) to (300) and diffraction peaks at 2θ=7˚ and 12˚. Also, Fe_3O_4 can be found in the structure of the nanocomposite sorbent due to the following data: the corresponding x-ray diffraction peaks assigned to (220), (311), (400) at 2θ =30.3˚, 43.3˚, 57.3˚, and 62.9˚ can be seen in the XRD patterns of Figure 3b and 3c, endorsing the presence of Fe_3O_4. Since Fe_2O_3 is also integrated into the fabricated nano-hybrid sorbent, other diffraction peaks at 33.2˚, 40.8˚, and 35.6˚ related to (104), (110), (113) plates can be identified, manifesting the presence of Fe_2O_3 in the sorbent as well as Fe_3O_4. Moreover, the grain size and morphology and of nanoporous composite was evaluated by SEM images of GO (d), GO/MOF-74/Fe_3O_4 (e) and GO/MOF-74/Fe_3O_4/PTy (f) in Figure 3. As illustrated in Figure 3d, GO nanosheets were stacked in condensed layers within the lamellar morphological components. Moreover, it shows that wrinkles and folds were observed in robust agglomeration of graphene sheets, which consists of multiple agglomerated layers of graphene, with a strong tendency to stack due to the high surface energy caused by strong interactions of surface groups on the graphene layer. Figure 3e exhibits the crystal growth mechanism and evolution of MOF-74 and Fe_3O_4 particles over the GO nanosheet that resulted in development of sphere-like morphologies, appropriately distributed over GO surface. In Figure 3f, SEM image of GO/MOF-

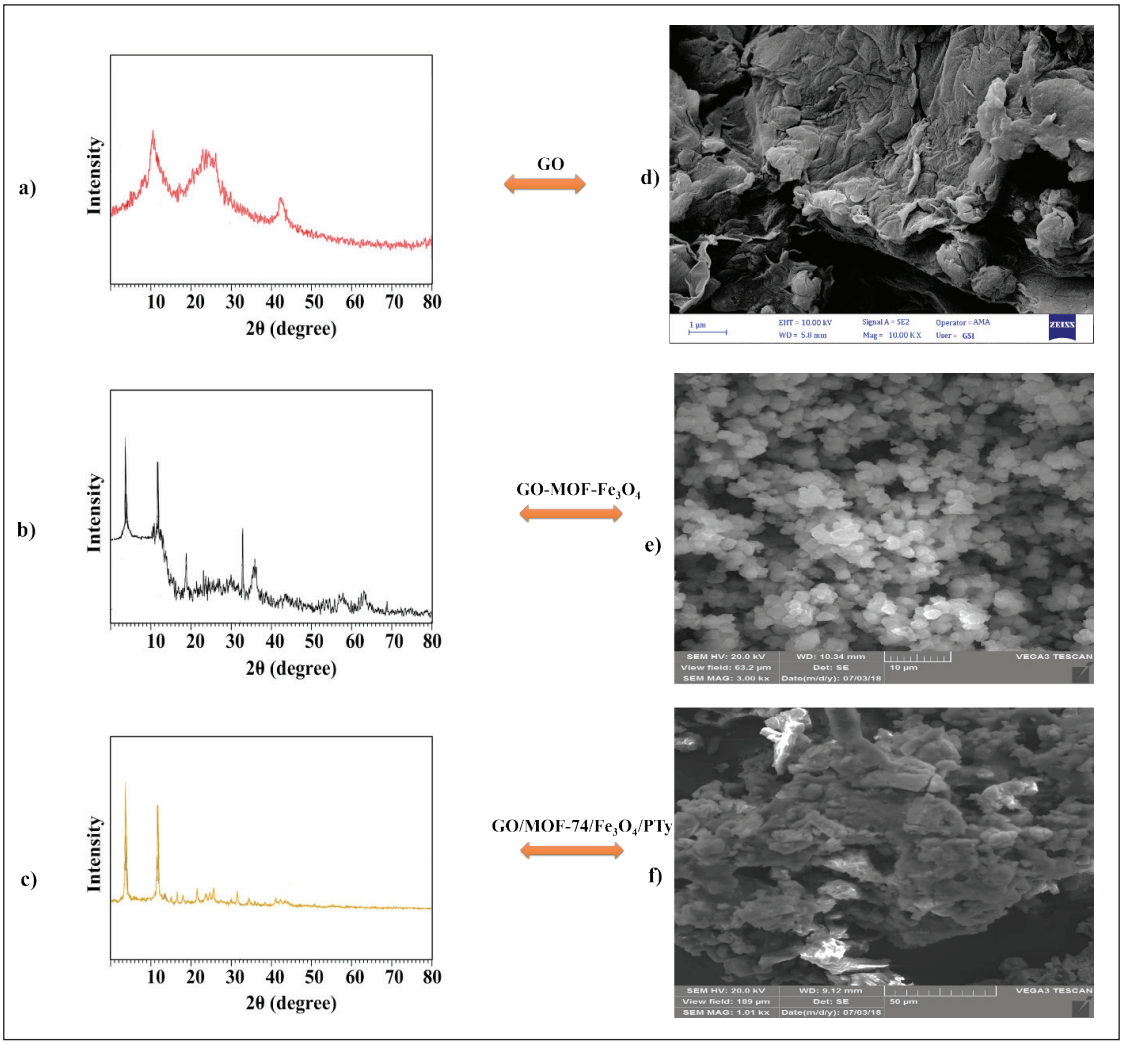

Fig. 3. XRD patterns of GO (a), GO/MOF-74/Fe_3O_4 (b) and GO/MOF-74/Fe_3O_4/PTy (c); SEM images of GO (d), and GO/MOF-74/Fe_3O_4 (e) and GO/MOF-74/Fe_3O_4/PTy (f)

74/Fe_3O_4/ PTy obviously shows the modification process of GO with the layers of target polymer. As it can be seen, PTy layers have grown on the surface of GO and formed significant coating sheets, demonstrating prosperous synthesis of the final nanoscale extractor.

When crystalline MOF-74 particles in Figure 4a are evenly dispersed on the surface of GO sheets, MOF-74 would adhere to GO (Fig. 4b). SEM image of MOF-74 seems to be very similar when compared to GO/MOF-74 image in Figure 4a and 4b. Hence, by referring to EDX spectra of MOF-74 and GO/MOF-74, it could be possible to determine the successful immobilization of MOF-74 on the surface of GO (Fig. 5). The current data exhibit the homogeneous distribution of the contents of MOF-74 such as Ni, C and O elements in both groups, confirming the effective attachment of MOF-74 blocks with GO layers. For more evidences, an increase in mass percent of carbon material from 31.2 to 49.2% proves the presence of GO in GO/MOF-74 composite, which firmly demonstrates well dispersion of target MOF on the GO sheets.

In Figure 5, the EDX spectrum of GO confirms the existence of C and O elements, with weight percent of 77.1% and 18.5%, respectively. Since MOF-74 is obtained from the reaction between of nickel cation and ligand 2,5-dihydroxybenzene-1,4-dicarboxylate, Ni, C, and O appear at 39.8%,

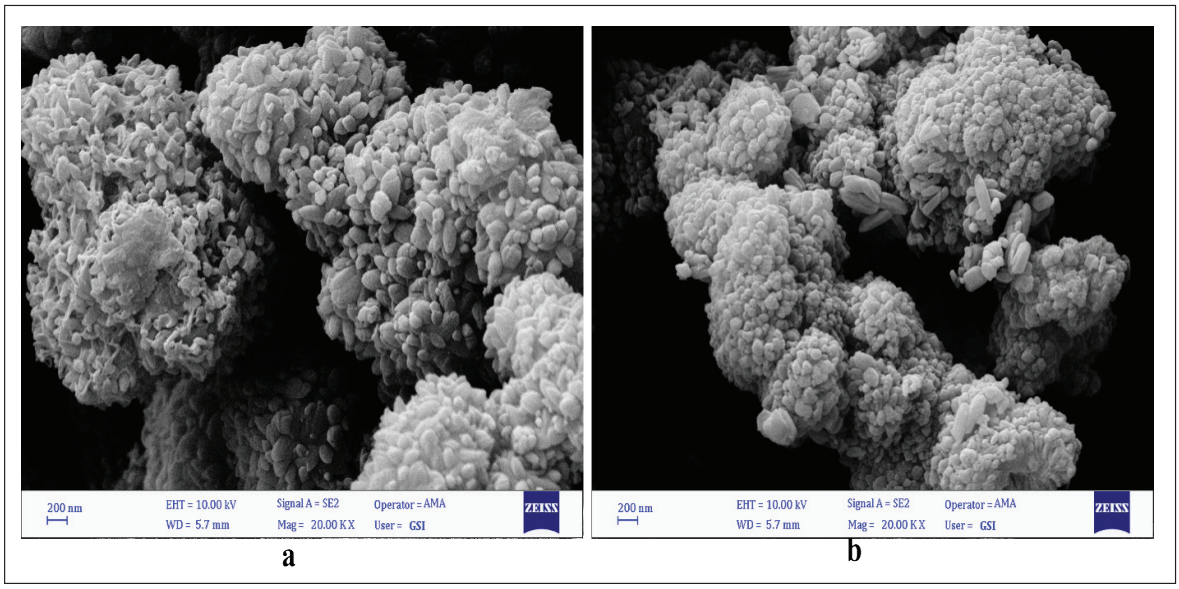

Fig. 4. SEM images of MOF-74(a), GO/MOF-74 (b)

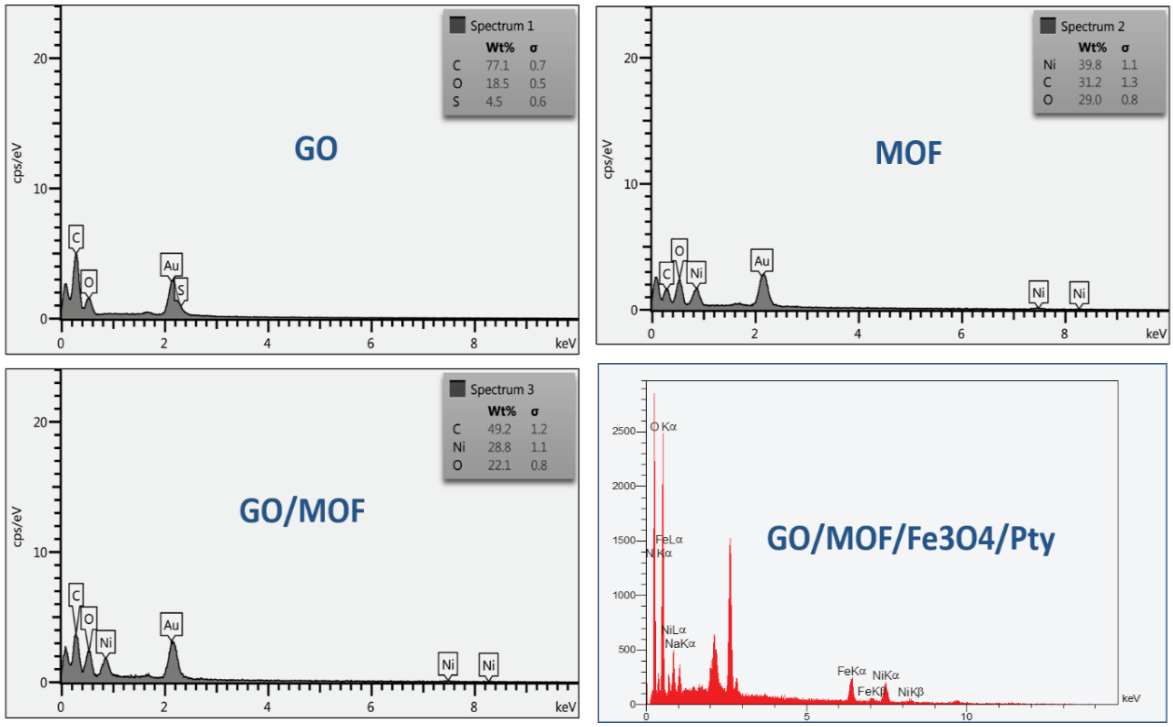

Fig. 5. EDX spectrum of GO, MOF-74, GO/MOF-74 and GO/MOF-74/Fe_3O_4/Pty

31.2%, and 29%, respectively. When MOF is bonded to GO, the carbon content increased from 31.2% to 49.2%, designating the proper adjustment of MOF-74 on the GO surface. In the EDX spectrum of GO/MOF-74/ Fe_3O_4/PTy, Fe and N, associated with Fe_3O_4 and PTy, respectively, can be recognized in addition to previous components.

3.2. Influence of nanosorbent dosage

In the enrichment protocols based on nanoporous sorbents, the amount of extractor is an important factor which effects both reproducibility and sensitivity features [49]. To achieve the best performance of the extraction method for analysis of FQs, various amounts of the fabricated

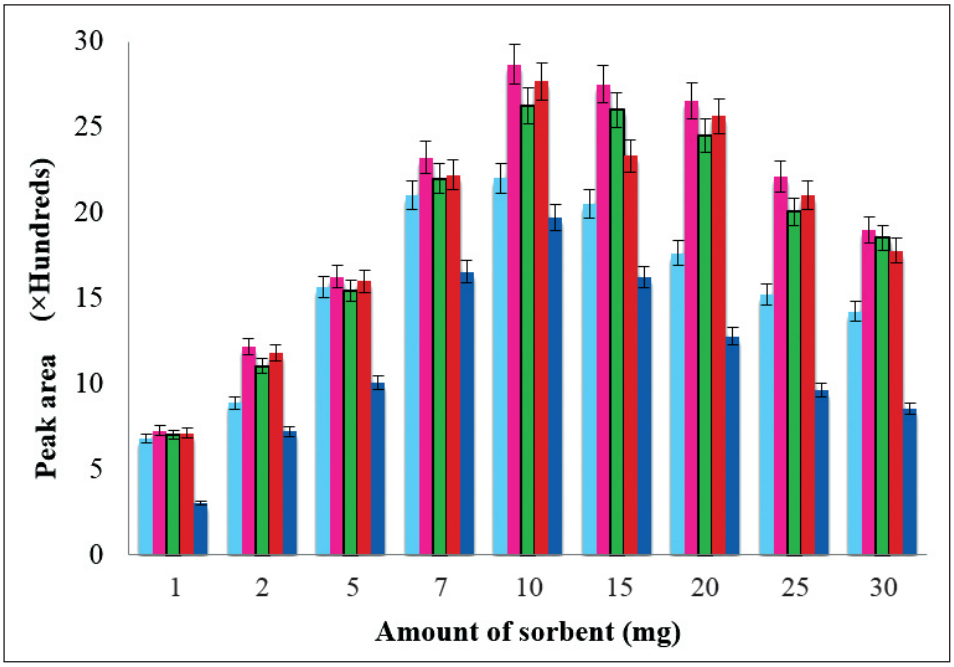

Fig. 6. Influence of GO/MOF-74/Fe3O4/PTy composite amount, other conditions: concentration of each FQs 20.0 ng mL^{-1}; pH 5.0; extraction time 10 min; eluting solvent acetonitrile; desorption time 2 min.

nanocomposite within the range of 1.0-30.0 mg were investigated in detail. As Figure 6 shows, there is a significant and direct relationship between peak area of FOs and amounts of nanosorbent from 1.0 to 10.0 mg. GO/MOF-74/Fe_3O_4/PTy has high surface area-to-volume ratio resulting the maximum analytical sensitivity is attainable at a relatively low amount of sorbent (10.0 mg), which can be considered as a prominent advantage of the new designed extractor. But after the value of 10.0 mg, a decrease in signal was observed, which was due to this fact that at higher amounts of sorbent, the separation of analytes from the extractor using the magnet could not be performed effectively and a certain amount of FQs remains in sample. Hence, 10.0 mg of GO/MOF-74/Fe_3O_4/PTy was operative enough to obtain a compromise between analytical sensitivity and repeatability of data, so this value was utilized for the rest of the work.

3.3. Influence of pH

Owing to the presence of carboxyl and amino groups in FQ structures, FQs exist as ionized or neural forms depending on the pH of the aqueous media, while the reported pK_a values for these compounds are as follow: (5-5.5) for pK_{a1}, (6.2-6.4) for pK_{a2}, and (8.9-9) for pK_{a3}[5]. pH of the sample media plays a meaningful role on the type of interactions between sorbent and FQs controlling the adsorption phenomena of analytes and the subsequent extraction yields. The impact of pH solution on the determination of FQs was evaluated in the range of 1.0-12.0 by applying 0.01 M HCl and NaOH. As it can be revealed in Figure 7, the best quantification condition was obtained at pH 5.0, which the following explanations exhibit the probable reason: according to the pK_a values of all FQs, at pH 5 the neutral forms (uncharged forms) of drugs are dominant and due to the hydrophobic property of GO/MOF-74/Fe_3O_4/PTy, the hydrophobic-hydrophobic interactions between analytes and sorbent become prevalent at this pH resulting higher recovery values. Hence, pH 5.0 was chosen as the optimum in all enrichment steps, in order to achieve the best performance of the method in the trace monitoring of FQs.

3.4. Influence of ultrasonic irradiation and extraction time

It is well-known that application of ultrasonic

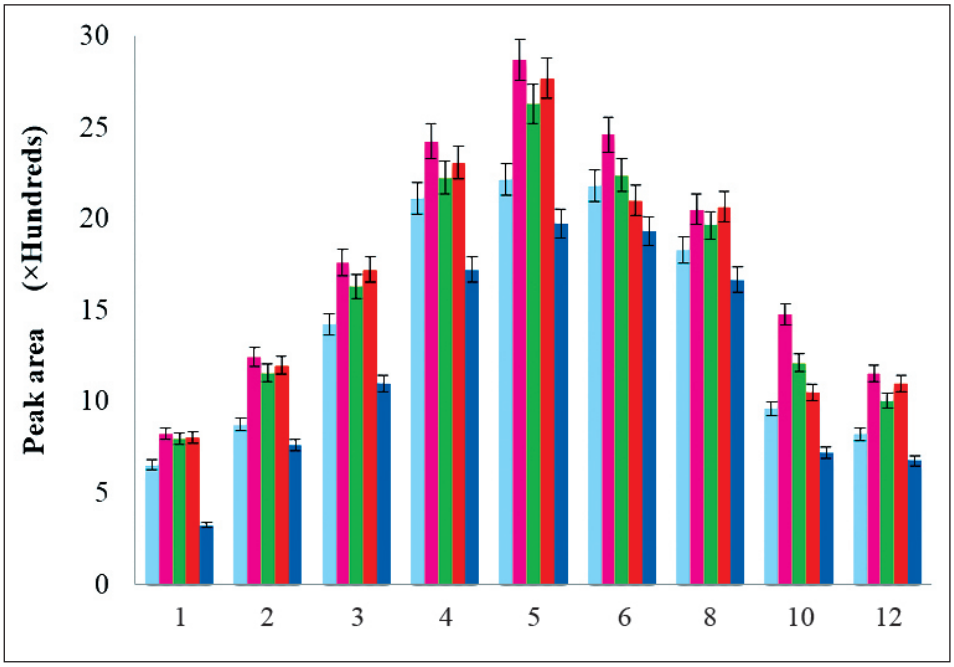

Fig. 7. Influence of sample pH, other conditions: concentration of each FQs 20.0 ng mL^{-1}; sorbent amount 10.0 mg; extraction time 5 min; eluting solvent acetonitrile; desorption time 2 min.

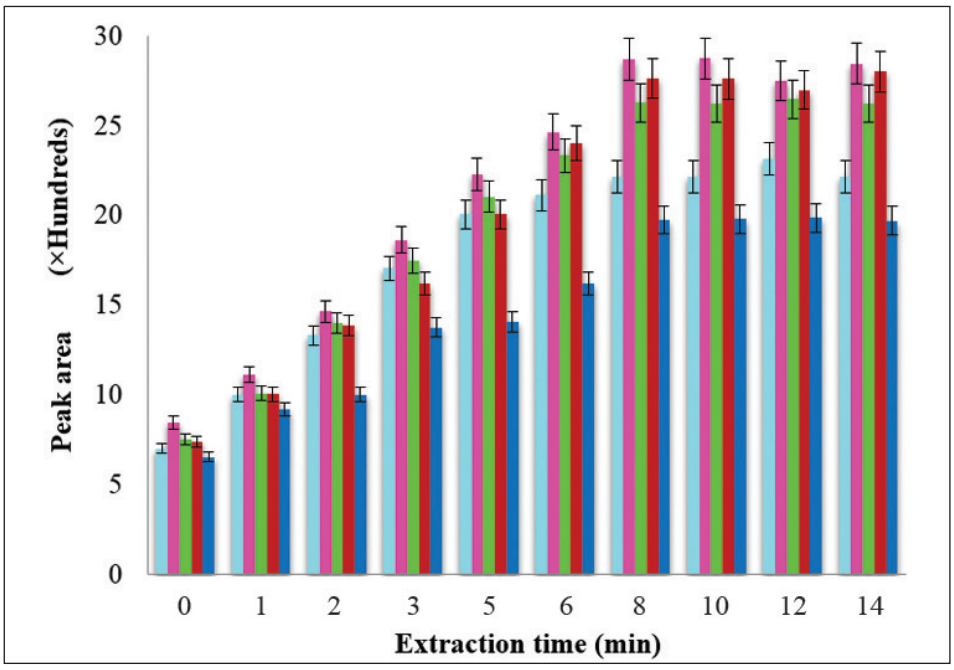

Fig. 8. Influence of extraction time, other conditions: concentration of each FQs 20.0 ng mL^{-1}; sorbent amount 10.0 mg; pH 5.0; eluting solvent acetonitrile; desorption time 2 min.

irradiation has reasonable potential for dispersing the sorbent into the whole sample while the time of irradiation either plays a significant role on a successful extraction process. The time of irradiation is considered as the extraction time which a desirable value causes better mass transfer and more sensitive signals [50]. The influence of extraction time on analytical signals was examined from 0 to 14 min and the obtained data are shown in Figure 8. Stable and sensitive results were obtained at 10 min revealing a relatively rapid isolation of drugs have been happened, which is due to the high

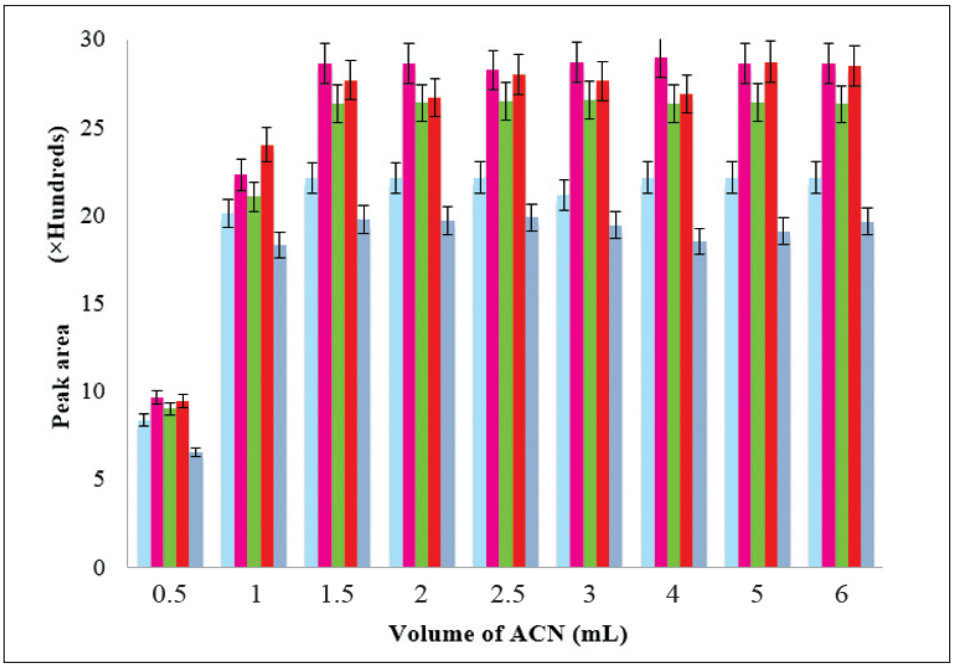

Fig. 9. Influence of acetonitrile volume, other condition: concentration of each FQs 20.0 ng mL^{-1}; sorbent amount 10.0 mg; pH 5.0; extraction time 10 min; desorption time 2 min.

porosity of the sorbent. After 10.0 min the analytical signals slowly decrease owing to this fact that at higher time values, FQs are separated from the sorbent and re-entered to the solution. According to these criteria, 10.0 min was good enough to cover all necessities associated to quantification features and this value was selected in all experiments.

3.5. Desorption condition

To evaluate the best desorption condition, different kinds of organic solvents such as methanol, acetonitrile and acetone as eluting agents with different volumes were tested. The volume and kind of eluting agents significantly affect the enrichment and isolation of target drugs so it is essential to carefully evaluate these parameters in detail. Acetonitrile exhibited individual and more practical desorbing ability in comparison with other solvents. After selecting the kind of solvent, its volume should be taken to the account, hence various volume of acetonitrile from 0.5 to 6.0 mL were subjected to the extraction protocol and as it can be seen in Figure 9, 2.5 mL of this solvent was adequate to deal with all necessary issues and provide reproducible and sensitive data.

3.6. The influence of salt concentration

In analytical chemistry there is a well-known phenomenon termed salting out effect which is based on non-electrolyte-electrolyte interactions. Non-electrolytes are less soluble in water at high values of salt and as a result the adsorption process could be prevalent. Thus, in this study different samples containing NaCl from concentration levels from 0 to 10% w/v were studied to evaluate the salting out effect on the extraction of FQs. It was expected by adding salt, the solubility of analytes in aqueous phase decreases due to an increase in polarity of the aqueous medium, and thus, the extraction performance improves [51, 52] But as it is clear in Figure 10, the analytical sensitivities have been missed by increasing the salt level. The latter happening can be explained as follows: at higher concentrations of NaCl, the sample become more viscose and make the mass transfer of FQs so difficult that results a meaningful decline in analytical signals. Finally, in order to obtain better condition, no electrolyte was used in all evaluations.

3.7. Evaluation of Reusability

To evaluate the reusability of GO/MOF-74/Fe_3O_4/

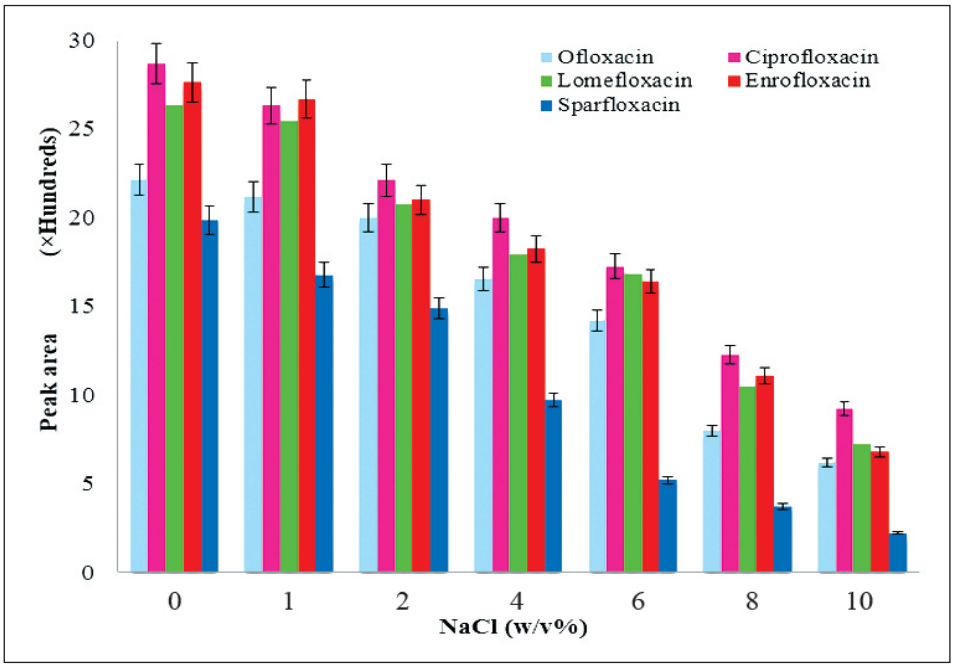

Fig. 10. Influence of ionic strength, other conditions: concentration of each FQs 20.0 ng mL^{-1}; sorbent amount 10.0 mg; pH 5.0; extraction time 10 min; eluting solvent acetonitrile; desorption time 2 min.

PTy, the number of adsorption-desorption cycles must be examined. Reusability is considered an essential characteristic of nanoscale sorbents, in order to reduce the cost of analyses and provide reliable data. To study this capability of magnetic sorbent, after extraction process it was washed with 1.5 mL deionized water and 1.5 mL acetonitrile during the application of ultrasonic for 6 min. Then, the magnetic nanosorbent was allowed to be dried at room temperature and reused for other subsequent extractions. It was found that after 15 adsorption-desorption cycles, the recovery values decreased around 13%.

3.8. Analytical figures of merit

Analytical aspects of the presented MD-μ-SPE-HPLC-UV were evaluated and main features are as follow: calibration curves revealed satisfactory linearity ($0.992 \leq r^2 \leq 0.997$) in the range of 1.0-475.0, 0.5-350.0, 0.5-350.0, 0.5-375.0 and 1.5-300.0 ng mL^{-1} with limit of detections (LODs, S/N=3) of 0.3, 0.1, 0.2, 0.1 and 0.4 ng mL^{-1} and limit of quantifications (LOQs, S/N=10) of 1.0, 0.5, 0.5, 0.5 and 1.5 ng mL^{-1} for ofloxacin, ciprofloxacin, lomefloxacin, enrofloxacin and sperfloxacin, respectively. The mentioned analytical figures of merit along with calibration curve equation, extraction recovery (ER) and enrichment factor are summarized in Table 1. EF value of each FQ was defined as the ratio of the calibration curve slope before and after extraction method. ER values were calculated using the equation (I):

$$ER\% = EF \times (V_{Final\ volume}/V_{Initial\ volume}) \times 100 \quad \text{(Eq. I)}$$

Figure 11 shows the HPLC chromatograms for blank sample and egg sample with different spiked level of FQs. The obtained chromatogram exhibits other contaminants existing in the egg samples have no notable effect on the recording of data and subsequent measurements.

3.9. Evaluation of precision and accuracy

Intra-day (within one day) and inter-day (within three days) precisions along with related accuracies were studied and estimated through the analyses of various quality control (QC) samples in the concentration levels of 10, 150 and 350 ng ml^{-1}. Each QC sample was obtained from spiking the drug under study into

Table 1. Various analytical figures of merit of MD-μ-SPE-HPLC-UV.

Analyte	LDR (ng mL^{-1})	Linear equation	r^2	LOD (ng mL^{-1})	LOQ (ng mL^{-1})	EF	ER% (n=3)
Ofloxacin	1.0-475.0	Y=106X + 93	0.992	0.3	1.0	43.6	87.2
Ciprofloxacin	0.5-350.0	Y=137X + 128	0.996	0.1	0.5	45.0	90.0
Lomefloxacin	0.5-350.0	Y=126X + 114	0.995	0.2	0.5	43.4	86.8
Enrofloxacin	0.5-375.0	Y=128X + 205	0.997	0.1	0.5	45.6	91.3
Sparfloxacin	1.5-300.0	Y=95X + 89	0.995	0.4	1.5	44.2	88.5

LDR: Linear dynamic range; r^2: Correlation coefficient; LOD: Limit of detection; LOQ: Limit of quantification; EF: Enrichment factor; ER: Extraction recovery

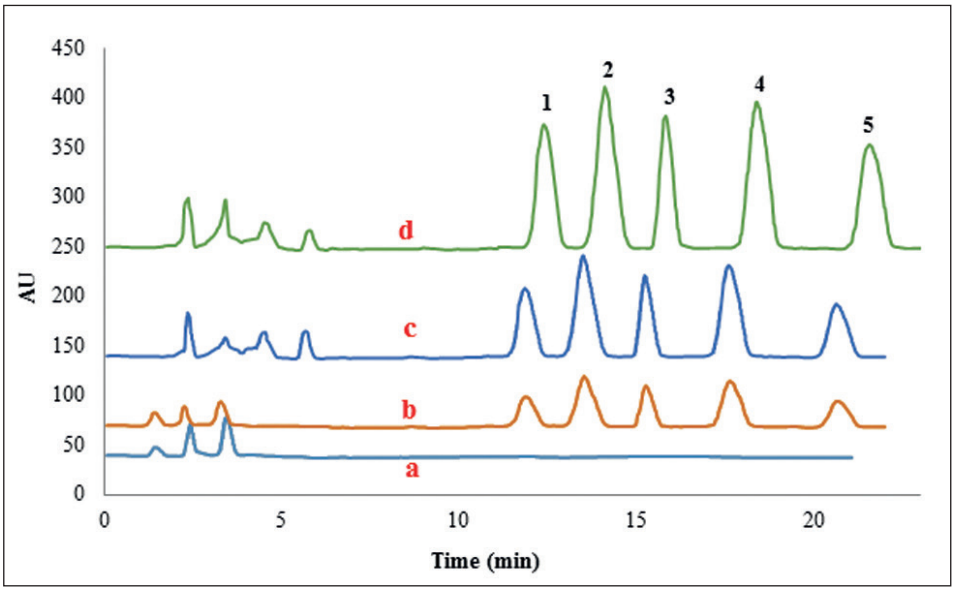

Fig. 11. Various HPLC-UV chromatograms of ofloxacin, ciprofloxacin, lomefloxacin, enrofloxacin, sparfloxacin after enrichment protocol: egg sample as the blank after applying MD-μ-SPE (a); Spiked egg samples after applying MD-μ-SPE with concentration level of each FQs at (b) 25.0 ng mL^{-1}, (c) 50.0 ng mL^{-1}, and (d) 150.0 ng mL^{-1}. (1) ofloxacin, (2) ciprofloxacin, (3) lomefloxacin, (4) enrofloxacin, (5) sparfloxacin.

Table 2. Intra-day and inter-day precisions along with corresponding accuracies for trace measument of ofloxacin, ciprofloxacin, lomefloxacin, enrofloxacin, sparfloxacin in spiked egg samples.

Drug	Conc. (ng mL^{-1})	Intra-day, n = 9			Inter-day, n = 9		
		Found (ng mL^{-1})	RSD (%)	Accuracy (%)	Found (ng mL^{-1})	RSD (%)	Accuracy (%)
Ofloxacin	10.0	10.6 ± 0.4	3.8	6.0	9.3 ± 0.5	5.4	-7.0
	150.0	143.9 ± 7.1	4.9	-4.1	141.0 ± 8.0	5.7	-6.0
	350.0	329.5 ± 16.8	5.1	-5.9	371.8 ± 15.6	4.2	6.0
Ciprofloxacin	10.0	9.6 ± 0.4	4.2	-4.0	10.5 ± 0.8	7.6	5.0
	150.0	159.5 ± 8.6	5.4	6.3	162.0 ± 9.0	5.5	8.0
	350.0	362.0 ± 14.4	4.0	3.4	379.3 ± 22.0	5.8	8.4
Lomefloxacin	10.0	10.3 ± 0.6	5.8	3.0	9.4 ± 0.7	7.4	-6.0
	150.0	140.6 ± 5.7	4.0	-6.3	138.5 ± 9.1	6.6	-7.6
	350.0	322.5 ± 15.3	4.7	-7.9	322.4 ± 17.3	5.4	-7.8
Enrofloxacin	10.0	10.6 ± 0.6	5.7	6.0	9.1 ± 0.7	7.7	-9.0
	150.0	155.5 ± 8.2	5.3	3.7	137.0 ± 7.9	5.8	-8.6
	350.0	324.1 ± 22.7	7.0	-7.4	370.4 ± 26.6	7.1	5.8
Sparfloxacin	10.0	10.4 ± 0.5	4.8	4.0	9.3 ± 0.8	8.6	-7.0
	150.0	156.4 ± 7.7	4.9	4.3	140.3 ± 8.3	5.7	-6.5
	350.0	325.9 ± 18.1	5.5	-6.9	321.0 ± 20.4	6.3	-8.3

RSD (%) values are determined as 100 × SD/mean; Accuracy (%) values were defined as (mean level found – known level)/(known level); Three independent analyses were obtained for every concentration of target FQs.

the egg sample, in order to examine the developed method in the analysis of real matrix. The results of the recent experiments are completely shown in Table 2. As it can be seen, reasonable intra-assay (≤7.7%, n = 9), inter-assay (≤7.0%, n = 9) as well as accuracy values (<9.0%) were obtained which all demonstrate the reliability of the method for simultaneous trace screening of FQs in real samples.

3.10. Application of the method to egg sample analysis

To check the validity of the MD-μ-SPE-HPLC-UV for simultaneous trace monitoring of FQs in complicated matrices, it was applied for analyzing target drugs in egg samples. The egg samples from hens which had been fed the drug per day with 7 days were subjected the extraction protocols and the obtained results are summarized in Table 3. Furthermore, egg samples were spiked with different amounts of FQs and after analyzing the samples, the recovery values in three independent measurements were calculated. The recovery values for all FQs varied from 91.0 to 106.8% and relative standard deviations (RSDs%) were in the range of 3.3-7.2% which demonstrate the validity of the method in analysis of complicated real matrices like egg samples.

Table 3. Simultaneous monitoring of ofloxacin, ciprofloxacin, lomefloxacin, enrofloxacin, sparfloxacin in egg samples by the developed method.

Analytes	Added (ng mL^{-1})	Found (ng mL^{-1})	RSD (%, n=3)	Recovery (%)
Ofloxacin	-	5.8	5.3	-
	5	10.1	4.9	93.5
	25	28.0	6.0	91.0
	50	59.6	5.9	106.8
Ciprofloxacin	-	3.7	4.8	-
	2	5.3	6.0	93.0
	25	26.6	5.5	93.9
	50	50.7	5.4	94.4
Lomefloxacin	-	3.1	5.1	-
	2	4.7	7.2	92.2
	25	29.5	4.3	105.0
	50	49.7	4.0	93.6
Enrofloxacin	-	14.5	3.3	-
	2	15.2	4.9	92.1
	25	37.0	4.4	93.7
	50	59.7	5.0	92.6
Sparfloxacin	0	8.2	4.8	-
	5	12.3	5.2	93.2
	25	31.2	6.8	94.0
	50	53.8	6.0	92.4

Three independent measurements were carried out for each concentration level and mean values were calculated.

3.11. Comparison with other methods

To highlight the robustness of the method, major analytical figures of merit including RSD, LOD, LOQ, correlation coefficient (r^2) along with some extraction features were compared with previously reported methods in literature. The results of the current investigation are summarized in Table 4. As it can be seen, the developed protocol exhibits notable improvements in approximately all analytical features besides a comparable extraction time over other reported procedure. Furthermore, the MD-μ-SPE-HPLC-UV reveal some worthy advantages like a reduction in the usage of toxic solvent in comparison with conventional SPE methods, opportune magnetic separation with the no need of individual device, easy-to-recycle the magnetic nanosorbent that can be used more than 14 times along with the possibility of trace simultaneous screening of target drugs with the least interferences.

4. Conclusions

A four-part magnetic nanoporous GO/MOF-74/Fe_3O_4/PTy was effectively fabricated and employed as a capable sorbent for MD-μ-SPE. Surface immobilization of GO with modifier agents including MOF-74, PTy and iron oxide significantly improved the merits of the hybrid materials and provided notable advantages like improvement of aromatic-aromatic interactions, high mass transfer, desired porosity, worthy reusability, easy-to-recycle the magnetic nanosorbent and reasonable recovery values. The results exhibited that MD-μ-SPE in combination with HPLC-UV is a valid protocol of enrichment and simultaneous trace level quantification of fluoroquinolones in real media like egg samples. The satisfactory sensitivity and reproducibility along with acceptable accuracy without considerable interferences form contaminants in egg matrices demonstrated the reliability of the method for trace screening purposes, and according to these criteria it possesses

Table 4. Comparison of MD-µ-SPE-HPLC-UV with other reported methods in literature for quantitation of different fluoroquinolones in eggs.

Extraction Method	Extraction Phase	LOD (µg L^{-1})	LOQ (µg L^{-1})	r^2	Extraction time(min)	RSD (%)	Detection system	Ref.
MSPE	C_{18}	0.5-5	0.7-17	0.9990-7	12	<5	HPLC-UV	[11]
SPME	C_{18}	*3-10	*10-30	0.986-7	10	NR	**LC	[46]
DSPE	C_{18}	[a]0.1-2.6	[a]0.4-8.6	0.9996-9	10	1-7	HPLC	[47]
SPE	[b]ENVI-18 disk	0.7, 2	2, 6	0.9994-7	5	<10	HPLC	[6]
SFE	C_{18}	<10	NR	>0.995	50	NR	HPLC-F	[53]
PLE	C_8-silica	0.4-33.5	0.2-19.8	NR	>54	<23	HPLC-F	[54]
MSPE	[C]PA	[d]0.4-1.4	[d]1.1-4.5	0.9974-1	2	3.6-17.6	HPLC	[55]
MD-µ-SPE	GO/MOF/Fe_3O_4/PTy	0.1-0.4	0.5-1.5	0.992-7	10	3.3-7.2	HPLC-UV	This work

*µg/kg,** LC-FLC-TMS, [a] µg/ g , [b] polystyrene-divinylbenzene copolymer disk,[C] PA:One-dimensional polyanilines, [d] ng/g,
MSPE: magnetic solid phase extraction
SPME: solid-phase microextraction
DSPE: dispersive solid phase extraction
PLE: pressurized liquid extraction
NR: not reported
RP-HPLC/UV: Reversed phase high performance liquid chromatography
RP-HPLC-F: reversed phase high-performance liquid chromatography with fluorescence detection
HPLC-UV: high performance liquid chromatography with UV detection
DMIP: dummy molecularly imprinted polymers

appreciable potential to be employed in the other applications related to the food aspects.

5. Acknowledgements

The authors appreciate Islamic Azad University South Tehran Branch for provided grant and we also thank Miss Zahra Shojaei and Mr Sajad Arzbin for cooperating to perform the HPLC measurements.

6. References

[1] H. Wu, Y. Liu, J. Chang, B. Zhao, Y. Huo, Zh. Wang, Y. Shi, Extraction of Five Fluoroquinolones in Eggs by Magnetic Solid-Phase Extraction with Fe_3O_4–MoS_2 and Determination by HPLC-UV, Food Anal. Methods, 12 (2019)712-721.

[2] Wm. Scheld, Maintaining fluoroquinolone class efficacy: review of Influencing factors, Emerg. Infect. Dis., 9 (2003)1-9.

[3] H. Yan, F. Qiao, KH. Row, Molecularly imprinted-matrix solid-phase dispersion for selective extraction of five fluoroquinolones in eggs and tissue, Anal. Chem., 79 (2007) 8242-8248.

[4] A. Gajda, A. Posyniak, J. Zmudzki, M. Gbylik, T. Bladek, Determination of (fluoro) quinolones in eggs by liquid chromatography with fluorescence detection and confirmation by liquid chromatography–tandem mass spectrometry, food chem., 135 (2012) 430-439.

[5] JF. Huang,B. Lin, QW. Yu, YQ. Feng, Determination of fluoroquinolones in eggs using in-tubensolid-phase microextraction coupled to high-performance liquid chromatography, Anal. Bioanal. Chem., 384 (2006) 1228–1235.

[6] M. Sturini, A. Speltini, L. Pretali, E. Fasani, A. Profumo, Solid-phase extraction and HPLC determination of fluoroquinolones in surface waters, J. Sep. Sci., 32 (2009) 3020-3028.

[7] IS. Ibarra, JA. Rodriguez, CA. Galán-Vidal, A. Cepeda, JA. Miranda, Magnetic solid phase extraction applied to food analysis, J. Chem., 8 (2015) 1-13.

[8] ShV. Gopalan, AN. Hasanah, MI-SPE, M-SPE

AND M-SPD recent application on solid phase extraction for compound extraction of complex matrices, Int. J. App. Pharm., 11 (2019)16-25.

[9] L. Reis, L. Lorena Vidal, A. Canals, Determination of siloxanes in water samples employing graphene oxide/Fe_3O_4 nanocomposite as sorbent for magnetic solid-phase extraction prior to gas chromatography-mass spectrometry, J. Sci. Food Agric., 41 (2018) 4177-4184.

[10] A. Issa, Kh. Al Saad, A. S. Luyt, Magnetic solid phase extraction for chromatographic separation of carbamates, J. Sci. Food Agric., 101 (2017) 2038-2049.

[11] T. Khezeli, A. Daneshfar, Development of dispersive micro-solid phase extraction based on micro and nano sorbents, Trends Anal. Chem., 89 (2017) 99-118.

[12] M. Zeeb, H. Farahani, Graphene oxide/Fe3O4@polythionine nanocomposite as an efficient sorbent for magnetic solid-phase extraction followed by high-performance liquid chromatography for the determination of duloxetine in human plasma, Chem. Paper, 72 (2018) 15-27.

[13] N. Li, HL. Jiang, X. Wang, X. Wang, Gu. Xu, B. Zhang, L. Wang, RS. Zhao, JM. Lin, Recent advances in graphene-based magnetic composites for magnetic solid-phase extraction, Trends Anal. Chem., 102 (2018) 60-74.

[14] A. Roostaie, Mohammadiazar, H. Bargozin, S. Ehteshami, A modified nanoporous silica aerogel as a new sorbent for needle trap extraction of chlorobenzenes from water samples, Chromatogra., 81 (2018) 649-655.

[15] Ch. Xu, X. Wang, J. Zhu, Graphene-metal particle nanocomposites, J. Phys. Chem. C, 112 (2008) 19841–19845.

[16] NM. El-Shafai, ME. El-Khouly, M. El-Kemary, MS. Ramadana, MS. Masoud, Graphene oxide–metal oxide nanocomposites: fabrication, characterization and removal of cationic rhodamine B dye, RSC Adv., 8 (2018) 13323-13332.

[17] Xu. XubiaoLuo, Ch. Wang, Sh. Luo, R. Dong, X. Tu, Gu. Zeng, Adsorption of As (III) and As (V) from water using magnetite Fe_3O_4-reduced graphite oxide MnO_2 nanocomposites, Chem. Eng. J., 187 (2012) 45-52.

[18] WK. Chee, H. Lim, HN. Ming, I. Harrison, Nanocomposites of graphene/polymers: a review, RSC Adv., 5 (2015) 68014-68051.

[19] F. Xu, Y. Yu, J. Yan, Q. Xia, H. Wang, J. Li, Zh. Li, Ultrafast room temperature synthesis of GrO@HKUST-1 composites with high CO_2 adsorption capacity and CO_2/N_2 adsorption selectivity, Chem. Eng. J., 303 (2016) 231-237.

[20] A. Amiri, F. Ghaemi, B. Maleki, Hybrid nanocomposites prepared from a metal-organic framework of type MOF-199(Cu) and graphene or fullerene as sorbents for dispersive solid phase extraction of polycyclic aromatic hydrocarbons, Microchim. Acta, 3 (2019) 131-139.

[21] I. Ahmed, NA. Khan, SH. Jhung, Graphite oxide/metal−organic framework (MIL-101): remarkable performance in the adsorptive denitrogenation of model fuels, Inorg. Chem., 24 (2013)14155-14161.

[22] JR. Li, RJ. Kuppler, HC. Zhou, Selective gas adsorption and separation in metal–organic frameworks, Chem. Soc. Rev., 38 (2009) 1477-1504.

[23] J. An, SJ. Geib, NL. Rosi, High and selective CO_2 uptake in a cobalt adeninate metal−organic framework exhibiting pyrimidine- and amino-decorated pores, Am. Chem. Soc., 132 (2010) 38-39.

[24] D. Britt, H. Furukawa, B. Wang, TG. Glover, OM. Yaghi, Highly efficient separation of carbon dioxide by a metal-organic framework replete with open metal sites, Nat. Acad. Sci. U. S. A., 106 (2009) 20637-20640.

[25] YS. Bae, AM. Spokoyny, OK. Farha, RQ. Snurr, JT. Hupp, CA. Mirkin, Separation of gas mixtures using Co(II) carborane-based porous coordination polymers, Chem. Commun., 46 (2010) 3478-3480.

[26] H. Li, K. Wang, Y. Sun, ChT. Lollar, J. Li,

HC. Zhou, Recent advances in gas storage and separation using metal–organic frameworks, Mater. today, 21 (2018) 108-121.

[27] H. Li, L. Li, RB. Lin, W. Zhou, Zh. Zhang, Sh. Xiang, B. Chen, Porous metal-organic frameworks for gas storage and separation: Status and challenges, Energy Chem., 1 (2019) 100006-100049.

[28] A. Chowdhury, The applications of metal-organic-frameworks in controlled release of drugs, Rev. J. Chem., 7 (2017) 1-22.

[29] H. Zhou, X. Liu, J. Zhang, X. Yan, Y. Liu, Yua, Enhanced room-temperature hydrogen storage capacity in Pt-loaded graphene oxide/HKUST-1composites, Int. J. Hydrog. Energy, 39 (2014) 2160-2167.

[30] X. Liu, H. Zhou, Y. Zhang, Y. Liu, A. Yuan, Syntheses, Characterizations and adsorption properties of MIL 101/graphene oxide composites, Chin. J. Chem., 30 (2012) 2563-2566.

[31] LCh. Lin, D. Paik, J. Kim, Understanding gas adsorption in MOF-5/graphene oxide composite materials, Phys. Chem. Chem. Phys., 19 (2017) 11639-11644.

[32] P. Peipei Yang P, Q. Liu, J. Liu, H. Zhang, Zh. Li, R. Li, L. Liu, J. Wang, Interfacial growth of metal organic framework (UiO-66) on the functionalization of graphene oxide (GO) as a suitable seawater sorbent for extraction of uranium(VI), J. Mater. Chem. A, 5 (2017) 17933-17942.

[33] C. Petit, TJ. Bandosz, Synthesis, Characterization, and ammonia adsorption properties of mesoporous metal–organic framework (MIL(Fe))–graphite oxide composites: exploring the limits of materials fabrication, Adv. Funct. Mater., 21 (2011) 2108–2117.

[34] Ad. Oliveira, GFd. Lima, HAD. Abreu, Structural and electronic properties of M-MOF-74 (M = Mg, Co or Mn), Chem. Phys. Lett., 691 (2018) 283–290.

[35] M. Díaz-García, A. Mayoral, I. Díaz, M. Sánchez-Sánchez, Nanoscaled M-MOF-74 materials prepared at room temperature, Cryst. Growth Des., 14 (2014) 2479−2487.

[36] TG. Glover, GW. Peterson, BJ. Schindler, D. Britt, O. Yaghi, MOF-74 building unit has a direct impact on toxic gas adsorption, Chem. Eng. Sci., 66 (2011) 163-170.

[37] S. Patra, E. Roy, R. Madhuri, PK. Sharma, Fast selective preconcentration of europium from wastewater and coal soil by graphene oxide/silane@Fe_3O_4 dendritic nanostructure, Sci. Technol., 49 (2015) 6117-6126.

[38] O Metin, S. Aydoğan, K. Meral, A new route for the synthesis of graphene oxide-Fe_3O_4 (GO–Fe_3O_4) nanocomposites and their schottky diode applications, J. Alloy Compd., 585 (2013) 681-688.

[39] BS. Rodríguez, JH. Borges, AV. Herrera-Herrera, M. Rodríguez-Delgado M, Multiresidue analysis of oestrogenic compounds in cow, goat, sheep and human milk using core-shell polydopamine coated magnetic nanoparticles as extraction sorbent in micro-dispersive solid-phase extraction followed by ultra-high-performance liquid chromatography tandem mass spectrometry, Anal. Bioanal. Chem., 410 (2018) 2031-2042.

[40] A. Mehdinia, N. Khodaee, A. Jabbari, Fabrication of graphene/Fe_3O_4@polythiophene nanocomposite and its application in the magnetic solid-phase extraction of polycyclic aromatic hydrocarbons from environmental water samples, Anal. Chim. Acta, 868 (2015) 1–9.

[41] GR. Lopes, DC. Pinto, AMS. Silva, Horseradish peroxidase (HRP) as a tool in green chemistry, RSC Adv., 4 (2014) 37244-37265.

[42] NC. Veitch, Horseradish peroxidase: a modern view of a classic enzyme. Phytochem., 65 (2004) 249–259.

[43] H. Kawakita, K. Hamamoto, K. Ohto, Kb. Inoue, Polyphenol polymerization by horseradish peroxidase for metal adsorption studies, Ind. Eng. Chem. Res., 48 (2009) 4440–4444.

[44] F. Pourbahman, M. Zeeb, A. Monzavi, SS.

Homami, Simultaneous trace monitoring of prokinetic drugs in human plasma using magnetic dispersive micro-solid phase extraction based on a new graphene oxide/metal–organic framework-74/Fe3O4/polytyramine nanoporous composite in combination with HPLC, Chem. Papers, 73 (2019) 3135-3150.

[45] J. Song, X. Wang, ChT. Chang ChT, Preparation and characterization of graphene oxide, J. Nanometer., 4 (2014) 1-6.

[46] SK. Kimitoshi, JG. Li, H. Kamiya, T. Ishigaki, Ultrasonic dispersion of TiO_2 nanoparticles in aqueous suspension, J. Am. Ceram., Soc., 91 (2008) 2481–2487.

[47] AK. Adhikari, K. Lin, Synthesis, fine structural characterization, and CO, Nanosci. Nanotech., 13 (2013) 1–9.

[48] DW. Wang, YQ. Li, QH. Wang, Nanostructured Fe_2O_3–graphene composite as a novel electrode material for supercapacitors, J. Solid State Electrochem., 16 (2012) 2095–2102

[49] Zh. Li, B. Yu, H. Cong, H. Hua Yuan, Q. Peng, Recent development and application of solid phase extraction materials, Rev. Adv. Mater. Sci., 48 (2017) 87-111.

[50] E. Tahmasebi, MY. Masoomi, Y. Yamini, A. Morsali, Application of a Zn(II) based metal-organic framework as an efficient solid-phase extraction sorbent for preconcentration of plasticizer compounds, J. Name., 00 (2013) 1-3.

[51] M.A. Farajzadeh, A. Yadeghari, M. Abbaspour, Dispersive solid phase extraction using magnetic nanoparticles performed in a narrow-bored tube for extraction of atorvastatin, losartan, and valsartan in plasma, Adv. Pharm. Bull., 9 (2019) 138-146.

[52] A. babaeia, M. Zeeb, A. Es-haghi, Magnetic dispersive solid-phase extraction based on graphene oxide/Fe3O4@polythionine nanocomposite followed by atomic absorption spectrometry for zinc monitoring in water, flour, celery and egg, J. Sci. Food Agric., 98 (2018) 3571-3579.

[53] JH. Shim, MH. Lee, MR. Kim, CJ. Lee, IS. Kim, Simultaneous measurement of fluoroquinolones in eggs by a combination of supercritical fluid extraction and high pressure liquid chromatography, Biosci. Biotechnol. Biochem., 67 (2014) 1342–1348.

[54] V. Jimenez, R. Companyo, J. Guiteras, Validation of a method for the analysis of nine quinolones in eggs by pressurized liquid extraction and liquid chromatography with fluorescence detection, Talanta, 85 (2011) 596–606.

Anal. Methods Environ. Chem. J. 4 (2) (2021) 25-33

AMECJ

Research Article, Issue 2
Analytical Methods in Environmental Chemistry Journal
Journal home page: www.amecj.com/ir

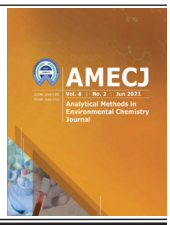

A rapid cadmium determination based on ion selective membrane potentiometric sensor by bis (salicylaldehydo) ethylenediimine as carrier

Mahdiyeh Ghazizadeh[a,*] and Hamideh Asadollahzadeh[a]
[a] *Department of Chemistry, Kerman branch, Islamic Azad University, Kerman, Iran, P. O. Box 7635131-167*

ARTICLE INFO:
Received 24 Feb 2021
Revised form 29 Apr 2021
Accepted 17 May 2021
Available online 27 Jun 2021

Keywords:
Cadmium,
Ion selective electrode,
Membrane sensor,
Potentiometry,
Salen,
Water samples

ABSTRACT
An ion selective potentiometric electrode (IPE) was prepared based on salen material (bis(salicylaldehydo)ethylenediimine) as a suitable carrier for determination of cadmium ions. An acceptable response for cadmium ions obtained over a linear range 8×10^{-7} to 1.0×10^{-2} M with a slope of 29.8 ± 0.8 mv per decade of activity and a detection limit of 3.2×10^{-7} M for Cd (II) ions in water and liquid samples. It has a response time less than 10 s and can be used for at least 2.5 months without any measurable divergence in potential. The ion selective electrode can be used based on potential and potential changes in the pH range 3.5 to 6.5, so, the cadmium determination was obtained at independent pH. Moreover, the selectivity of proposed method in presence of interference ions was studied. The results showed that the other cations do not interfere significantly in response electrode at optimized pH. This electrode was successfully used for the determination of cadmium ions in aqueous samples. The validation was obtained based on ICP analyzer and certified reference material in water samples (CRM, NIST).

1. Introduction

Due to recently reported by WHO, NIOSH and ACGIHA organizations, the heavy metals such as cadmium belong to harmful material for animals and humans. Heavy metals exist in different matrixes such as, food, tobacco smoke, air and water samples and have toxic effect in human cells. It may cause some serious diseases in humans such as renal failure, pancreatic/ liver cancers and accelerate tumor growth in human body [1] and some organs such as liver, kidneys or lungs may be hurt seriously [2]. So, the removal, separation and determination of heavy metals in blood serum, water and food samples is necessary. Cadmium has carcinogenesis effect in humans which was enter to human cells by the inhalation, food, waters [3]. Cadmium concentrations in natural waters are less than 1 µg L^{-1}. The tissues kidneys and livers can be concentrated cadmium. Levels in fruit and vegetables are below 10-1000 µg kg^{-1} in liver and in kidney. Cadmium determined by atomic absorption spectroscopy (ETAAS, FAAS) using aspiration water samples into a flame or injection to graphite tube of furnace spectrometric technique (ET-AAS) [4,5]. The LOD is 10 µgL^{-1} with the GBC spectrometer of F-AAS and 0.1 µg L^{-1} with ET-AAS was obtained. Cadmium can be determined by chemical vapor generation atomic fluorescence spectrometry(CVG-AFS)

*Corresponding Author: Mahdiyeh Ghazizadeh
Email: ghazizadeh1385@gmail.com
https://doi.org/10.24200/amecj.v4.i02.136

and carbon paste ion selective electrode(CP-IS) [6,7].The potentiometric method and chemical sensors are the reproducible and rapid methods for cadmium determination in liquid phases. In recent years, the design of chemical sensors as interested method based on highly selective carriers and ion-selective electrodes (ISEs) was reported by researchers for determination of various ionic species such as Pb, Cd, V and Hg. The potentiometric sensors act based on ion-selective electrodes (ISEs) and the electrochemical response is usually controlled by one ionic species presented in the solution. Numerous applications of these potentiometric selective electrodes have been reported. Biochemical applications and environmental applications are two important examples for this propose [8]. The Schiff base ligands were easily prepared from the condensation of a ketone or an aldehyde compounds with an amine groups. Ionophores include antibiotics and use to shift ruminal fermentation patterns. Many ionophores are lipid-soluble entities that transport ions across the cell membrane. They are suitable ionophore to form effective ion-selective electrodes, because of affinity toward metal ions [9, 10]. The Schiff bases are ligands with mixed O,N-donor atoms which bonds to some transition metal ions, such as Mn(II), Fe(III), Cu(II), Pb(II), Cd(II). The Schiff base ligands are so important for their various applications in dye and plastic industries, liquid crystal technology, biochemistry and physiology [11]. They are also use in development of photonic devices and have potential applications such as metallomesogens [12]. However, despite extensive applications of these ligands and many reports on synthesis and characterization of the Schiff base ligands and their complexes, there are a few reports on their ion-selective studies [13-16]. Moreover, it seems that Schiff base ligands are suitable ionophores for preparation ion selective electrodes and determination of many metal ions [17, 18]. Among Schiff bases, salens are tetradentate ligands that derived from salicylaldehyde and could be formed to stable complexes with transition metal ions. For these reasons, we used the salen compound as carrier in ion selective membrane for determination of Cd (II).

2. Experimental

2.1. Materials

Ethanol, methanol, acetone, sodium tetraphenylborate (NaTPB), dibutyl phthalate (DBP) and tetrahydrofuran with high purify (99%) were purchased from Merck chemical company. High relative molecular weight polyvinyl chloride (PVC) was purchased from sigma chemical company. Reagent grade nitrate salts of the used cations (all from Merck) were of the highest purity available and were used without any further purification. Aqueous solutions were prepared with doubly distilled water. Sodium hydroxide (0.1 M) and nitric acid (0.1 M) were used for pH control. The target Schiff base was synthesized from salicylaldehyde and ethylene diamine and purified as described elsewhere.

2.2. Instruments

Control of pH was achieved by a digital pH meter (inoLab 7110, Germany). The reference calomel electrode (RCE) has reaction between elemental mercury and mercury(I) chloride. However, the calomel electrode has a reputation of being more robust. The liquid phase in contact with the Hg/ HgCl in a saturated solution of KCl. The electrode is normally linked via a porous frit to the solution as a salt bridge. Finally, all of potentiometric measurements were made with a pH/mV meter (Zag Chimi, Iran) using calomel electrode (Azar electrode, Iran). The electrode of system to act as a reference against which potential measurements can be made and potentiometric methods was obtained based on measurements of the potential of electrochemical cells in the absence of appreciable currents and basic components such as reference electrode (gives reference for potential measurement), the indicator electrode and salt bridge and potential measuring device were used as Schema 1.

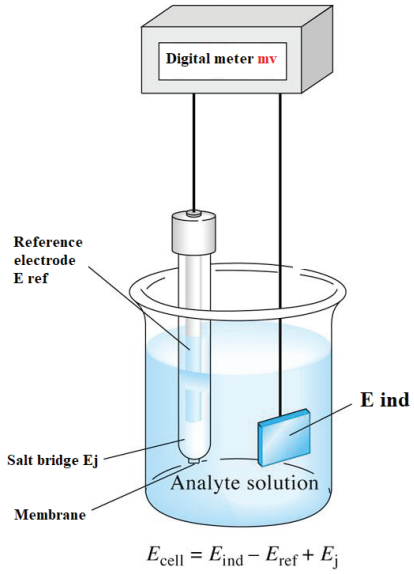

Schema 1. The potentiometric methods based on measurements of the potential of electrochemical cells

2.3. Electrode preparation

Preparation of the PVC membrane achieved by mixing thoroughly 61 mg of powdered PVC, 134.6 mg of plasticizer DBP, 2 mg of NaTBP and 6.12 mg of ionophore (Fig. 1) in 10 mL of THF. The mixture was transferred into a glass dish of 2 cm diameter. The solvent was evaporated in room temperature during 5-6 hours until an oily concentrated mixture was left. A Pyrex tube was dipped into the oily mixture for a few seconds, so that a non-transparent film was formed. Then the tube was pulled out from the mixture and kept at room temperature for 48 hours to produce a dry membrane. After that the tube was filled with an internal 1.0×10^{-3} M solution of $Cd(NO_3)_2.4H_2O$. The electrode was finally conditioned for 24 h by soaking in a solution of 1.0×10^{-2} M $Cd(NO_3)_2.4H_2O$.

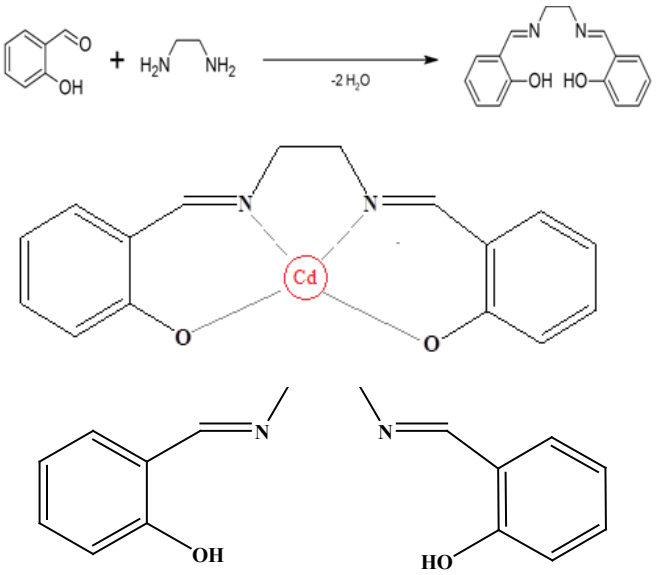

Fig. 1. The synthesis and structure of salen as ionophore and complexation with cadmium

2.4. Emf measurements

All emf measurements were done with the following assembly:

Hg/Hg_2Cl_2 (sat'd), KCl (sat'd) | internal solution, $Cd(NO_3)_2.4H_2O$ (1.0×10^{-3} M) | PVC membrane | sample solution | Hg/Hg_2Cl_2 (sat'd), KCl (sat'd)

All emf measurements were carried out in a 50 mL of double walled glass cell with a constant magnetic stirring of the test solution. Activities were calculated according to Debye-Huckel procedure about solutions of electrolytes and plasmas. Debye-Huckel procedure provides a starting point for modern treatments of non-ideality of electrolyte solutions based on 2-dimensional section of electrolyte solution. The ions have as spheres with unit negative and positive charges. The EMF of the cell for varying the concentrations of one participating electrolyte (HCl) will be measured. This measurement verifies the Debye–Huckel limiting Law and to determine the mean activity coefficient of the electrolyte.

3. Results and Discussion

3.1. Potentiometric response of the prepared sensor

At first, membrane electrodes were prepared based on PVC by using of salen as ionophore. Then potentiometric responses of sensors to the different metal ions were investigated under the same conditions. It is obvious that the best response to the metal ions belongs to cadmium ion (Fig. 2).

3.2. Effect of the membrane composition

It is obvious that the electrode response depends on the nature and the amount of the electrode's components. The data clearly show that the electrode response does not improve by increasing of the ionophore's amount. This divergence in electrode response in higher concentration of the ionophore caused the less selectivity and enhanced interference of the lipophilic counter ions of the test solution as assumed in the phase boundary potential model of carrier based ISEs. Plasticizer also plays an important role in electrode responses and influences the detection limits [19, 20], the sensitivity and selectivity [21] of the electrodes. Moreover, the nature of the additive may have significant effect on the sensitivity and selectivity [22-24]. Thus, cadmium selective electrodes prepared with different amounts of ionophore and the aspects of membrane preparation based on salen for Cd^{2+} were optimized and the results are reported in Table 1. It indicates that membrane no. 9 with an optimized composition of 66% DBP, 30%

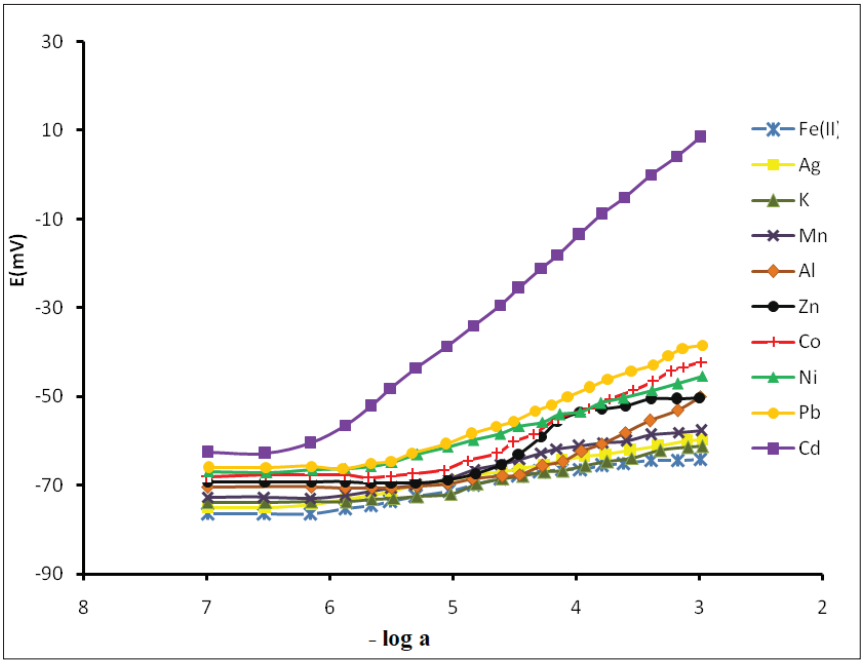

Fig 2. The responses of different ion selective electrodes

PVC, 3% ionophore and 1% NaTBP due to the best sensitivity. It has a Nernstian slope of 29.8 ± 0.8 mV decade^{-1} activity of Cd^{2+} ions with an extensive dynamic range.

3.3. Effect of pH

The effect of pH on the responses of cadmium-selective electrode was investigated by adjusting pH over a range of 2.0–9.0. It was achieved by using small drops of nitric acid (0.1 M) or sodium hydroxide (0.1 M) and 1.0×10^{-3} M Cd^{2+} solution. The Figure 3 showed that potential is constant over a pH range of 3.5–6.5. Thus pH was adjusted at 5 for all experiments. The observed decreasing of electrode potential at higher pH values could be due to the interference of hydroxide ion. Acidic solutions can also cause the less potential at low pH because of protonating of ionophore and interference of H^+ ions.

Table 1. Composition and optimization of the membranes ingredients.

Numbers	ionophore(%)	NaTBP)(%)	DBP(%)	PVC(%)	Slope (mV decade^{-1})
1	4.5	2.5	63	30	24.6±0.9
2	5	2	63	30	21.8±0.4
3	3.5	2.5	64	30	22.3±0.6
4	3	0	67	30	27.7±0.5
5	0	5	65	30	18.8±0.3
6	4	1	65	30	25.7±0.7
7	2	3	65	30	23.8±0.9
8	5.5	2.5	62	30	20.2±0.3
9	3	1	66	30	29.8±0.8
10	7	3	60	30	21.6±0.4

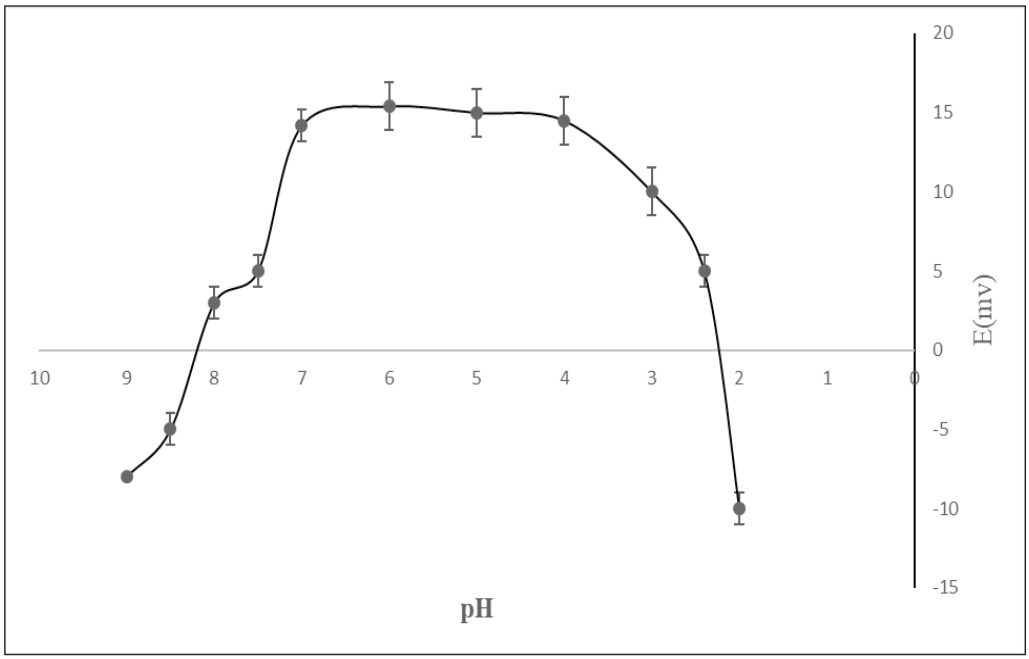

Fig. 3. Influence of pH on the potential response of cadmium selective electrode (1.0×10^{-3}M Cd^{2+})

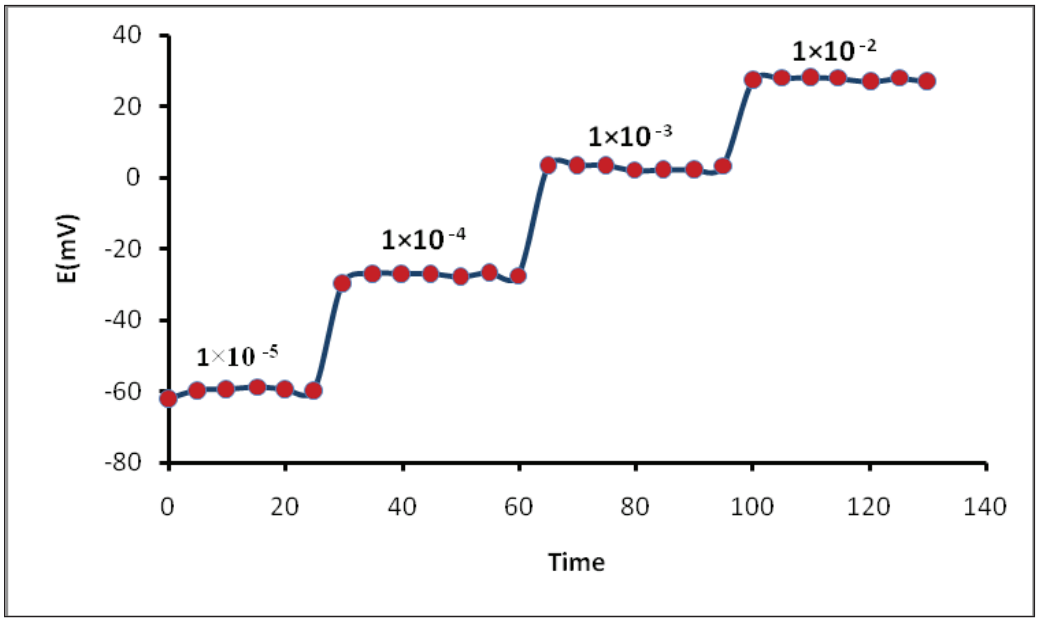

Fig. 4. Response time of cadmium selective electrode

3.4. Response time

An important factor for all ionic selective electrodes is dynamic response time. In this research, the practical response time was measured by changing the Cd^{2+} concentration from 1.0×10^{-2} to 1.0×10^{-5} M in solution. The response time was about 10 s did not change by varying Cd^{2+}concentration (Fig. 4). This is most probably result in the fast exchanging of complexation–decomplexation of Cd^{2+} ion with the ionophore (salen) at the test solution–membrane interface.

3.5. Effect of internal solution

The effect of internal solution concentration on the potentiometric responses of cadmium ion selective electrode was investigated. There was no considerable change in the potentiometric responses by using different concentrations of internal solution in the range of 1.0×10^{-4} to 1.0×10^{-1} M. Therefore 1.0×10^{-3} M was chosen for the concentration of internal solution.

3.6. Effect of non-aqueous solutions

The potentiometric responses of cadmium-selective electrode were studied in non-aqueous solutions by using several mixtures such as water/methanol,

Table 2. Effect of non-aqueous solutions on the slope and linear range of the prepared electrode

Non-aqueous solution (V/V%)	Linear range (M)	Slope (mV decade^{-1})
0	$1.0 \times 10^{-2} - 3.8 \times 10^{-6}$	29.1 ± 0.4
Ethanol 10%	$1.0 \times 10^{-2} - 3.0 \times 10^{-6}$	29.0 ± 0.5
Ethanol 15%	$1.0 \times 10^{-2} - 3.0 \times 10^{-6}$	28.9 ±0.5
Ethanol 20%	$1.0 \times 10^{-2} - 1.1 \times 10^{-6}$	26.3 ± 0.6
Ethanol 25%	$1.0 \times 10^{-3} - 1.3 \times 10^{-5}$	24.5 ± 0.7
Methanol 10%	$1.0 \times 10^{-2} - 3.0 \times 10^{-6}$	29.1 ± 0.6
Methanol 15%	$1.0 \times 10^{-2} - 3.0 \times 10^{-6}$	29.0 ± 0.5
Methanol 20%	$1.0 \times 10^{-2} - 4.1 \times 10^{-6}$	27.1 ± 0.6
Methanol 25%	$1.0 \times 10^{-2} - 4.1 \times 10^{-6}$	25.4 ± 0.5
Acetone 10%	$1.0 \times 10^{-2} - 3.0 \times 10^{-6}$	29.1 ± 0.6
Acetone 15%	$1.0 \times 10^{-2} - 3.0 \times 10^{-6}$	28.5 ± 0.7
Acetone 20%	$1.0 \times 10^{-2} - 2.1 \times 10^{-6}$	24.1 ± 0.7
Acetone 25%	$1.0 \times 10^{-2} - 1.3 \times 10^{-5}$	19.0 ± 0.8

water/ethanol and water/acetone with 10, 15, 20 and 25 volume percent of non-aqueous part (Table 2). The results indicated a slope decreasing when the volume percent of non-aqueous solution was more than 15%.

3.7. Potentiometric selectivity

The effect of interfering ions on the potentiometric behavior of Cadmium ion selective electrode, known as potentiometric selectivity coefficients, was studied. The results showed the other ions do not interfere in potentiometric responses of the prepared electrode based on salen as ionophore (Table 3). Therefore, Cd-selective electrode has high selectivity for cadmium ions.

3.8. Calibration curve and statistical data

Optimized equilibrium time for membrane electrode is 24 h. After that the potentiometric responses of electrode was defined according to IUPAC. The potential response of the electrode to different concentration of Cd(II) ion in the range of 8×10^{-7} to 1.0×10^{-2} M at pH = 5 (Fig. 5) indicates a linear response and the slope of calibration curve was 29.8 ± 0.8 mV/decade of concentration of Cd^{2+} at room temperature. The standard deviation of 5 replicate measurements is ±0.5 mV. The detection limit as determined from the crossing of the two extrapolated parts of the calibration curve was 3.2×10^{-7} M. The PVC membrane electrode could be applied for at least 2.5 months without any measurable change.

Table 3. Potentiometric selectivity coefficients of various interfering cations.

Cation	$K_{Cd(II),J}$
Ni^{2+}	2.4×10^{-3}
Co^{2+}	2.5×10^{-3}
Pb^{2+}	6.8×10^{-3}
Cr^{3+}	1.1×10^{-3}
Al^{3+}	3.3×10^{-3}
Na^{+}	3.1×10^{-3}
K^{+}	1.8×10^{-3}

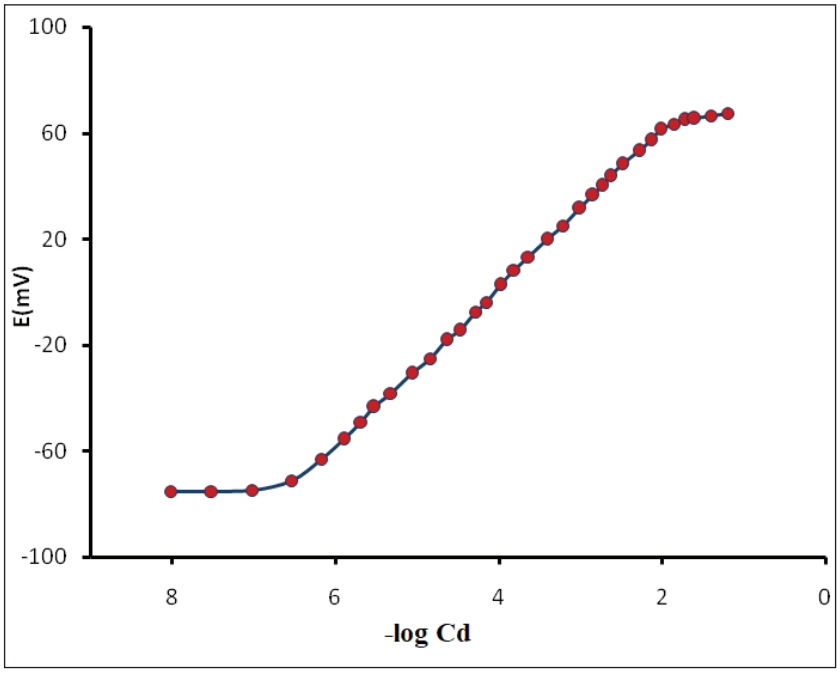

Fig. 5. Potentiometric response of the Cd^{2+} ion selective electrode to cadmium concentration using the optimized membrane electrode.

Table 4. Determination of Cd^{2+} by the new ion selective electrode and recovery.

Sample	Cd^{2+} added (mol L^{-1})			Cd^{2+} found[a] (mol L^{-1})			Recovery (%)		
	Sample I	Sample II	Sample III	Sample I	Sample II	Sample III	Sample I	Sample II	Sample III
Ground water	---	5.5×10^{-5}	1.0×10^{-4}	<LOD	$(5.7\pm0.05)\times10^{-5}$	$(1.04\pm0.03)\times10^{-5}$	---	103	104
River water	---	5.5×10^{-5}	1.0×10^{-4}	<LOD	$(5.6\pm0.06)\times10^{-5}$	$(9.7\pm0.08)\times10^{-5}$	---	101	97

[a] Mean value ± standard deviation (three determination)

3.9. Analytical applications at real sample

The prepared cadmium selective ion electrode based on salen was successfully applied for determination of cadmium ions concentration in the samples of water. The results are shown in Table 4.

4. Conclusions

Rapid response, low detection limit and high selectivity, make ion selective electrodes suitable for measuring the concentration of metal ions. Salen was easily synthesized and used as ionophore in preparing an ion selective electrode for direct determination of cadmium. The prepared electrode showed high selectivity and low detection limit. This electrode also applied successfully for Cd ions determination in the samples of water.

5. Acknowledgement

The authors are gratefull to Islamic Azad University, Kerman Branch, for financial assistance of this work.

6. References

[1] F. Zheng, B. Hu, Thermo-responsive polymer coated fiber-in-tube capillary microextraction and its application to on-line determination of Co, Ni and Cd by inductively coupled plasma mass spectrometry (ICP-MS), Talanta, 85 (2011) 1166-1173.

[2] P. Wu, Ch. Li, J. Chen, Ch. Zheng, X. Hou, Determination of cadmium in biological samples: An update from 2006 to 2011, Appl. Spectrosc. Rev., 47 (2012) 327-370.

[3] G. Adani, T. Filippini, Dietary intake of acrylamide and risk of breast, endometrial and ovarian cancers: A systematic review and dose-response meta-analysis, Cancer Epidemiol. Biomarkers Prev., 29 (2020) 1095-1106.

[4] L.A. Meira, D.F. de Souza, Application of constrained mixture design and Doehlert matrix in the optimization of dispersive liquid-liquid microextraction assisted by ultrasound for preconcentration and determination of cadmium in sediment and water samples by FAAS, Microchem. J., 130 (2017) 56–63.

[5] M. Naghizadeh, M.A. Taher, M. Behzadi, F.H. Moghaddam, Preparation a novel magnetic natural nano zeolite for preconcentration of cadmium and its determination by ETAAS, Environ. Nanotechnol. Monit. Manag., 8 (2017) 261–267.

[6] J. Zhang, J. Fang, X. Duan, Determination of cadmium in water samples by fast pyrolysis–chemical vapor generation atomic fluorescence spectrometry, Spectrochim. Acta Part B , 122 (2016) 52–55.

[7] M.R. Ganjali, H. Khoshsafar, F. Faridbod, A. Shirzadmehr, M. Javanbakht, P. Norouzi, Room temperature ionic liquids (RTILs) and multiwalled carbon nanotubes (MWCNTs) as modifiers for improvement of carbon paste ion selective electrode response; a comparison study with PVC membrane, Electroanal. Int. J., 21(2009) 2175–98.

[8] R. Yan, Sh. Qiu, L. Tong, Y. Qian, Review of progresses on clinical applications of ion selective electrodes for electrolytic ion tests: from conventional ISEs to graphene-based ISEs, Chem. Speciat. Bioavailab., 28 (2016) 72-77.

[9] W.A. Zoubi, N.A. Mohanna, Membrane sensors based on Schiff bases as chelating ionophores - A review, Spectrochim. Acta A Mol. Biomol. Spectrosc., 132 (2014) 854-870.

[10] C. Mohan, K. Sharma, S. Chandra, Cd(II) ion-selective electrode based on 2–acetylthiophene semicarbazone in polymeric membrane, Anal. Bioanal. Electrochem., 9 (2017) 35-46.

[11] A. Xavier1, N. Srividhya, Synthesis and study of Schiff base ligands, IOSR-J. Appl. Chem., 7 (2014) 6-15.

[12] C. Cretu, L. Caseh, B.J. Tang, V. Badea, E.I. Szerb, G. Mehi, S. Shova, O. Cosistor, Mononuclear Cu(II) complexes of novel salicylidene Schiff bases: synthesis and mesogenic properties, Liq. Cryst., 42 (2015) 1139-1147.

[13] A. Vijayalakshmi, J. Thamarai Selvi, Calcium ion selective electrode based on Schiff base as an electro active material-Its preparation and analytical application, Int. J. Curr. Res., 5 (2013) 2176-2178.

[14] Y.H. Ma, R. Yuan, Y.Q. Chai, X. Wu, W. Zhou, X.L. Liu, F. Deng, New Ni(II) ion-selective electrode based on the N-S Schiff base ligand as neutral carrier in PVC matrix, Anal. Lett., 42 (2009) 2411-2429.

[15] S. Suman, R. Sighn, Thiophene-based Schiff base ligand as ionophore for Ni(II)-selective polyvinyl chloride membrane electrode, J. Polym. Eng., 40 (2020) 481–485.

[16] T. Tamoradi, H. Goudarziafshar, S. Rashki, F. Katouzian, F. Chalabian, Synthesis of new Schiff base ligand and its complexes in the presence of some transition metal ion and evaluation of their antibacterial properties, Med. Lab. Sci., 11 (2017) 5-10.

[17] K.R. Bandi, A.K. Singh, A. Upadhyay, Biologically active Schiff bases as potentiometric sensor for the selective determination of Nd^{3+} ion, Electrochim. Acta, 105 (2013) 654-664.

[18] A.Q. Alorabi, M. Abdelbaset, S.A. Zabin, Colorimetric detection of multiple metal ions using Schiff base 1-(2-Thiophenylimino)-4-(N-dimethyl)benzene, Chemosensors, 8 (2020) 1-10.

[19] H.M. Abu Shawish, N. Abu Ghalwa, A.R. Al-Dalou, F.R. Zaggout, S.M. Saadeh, A.A. Abou Assi, Effect of plasticizers and ion-exchangers on the detection limit of tramadol-PVC membrane electrodes, Eurasian J. Anal. Chem., 6 (2011) 70–83.

[20] P. Adhikari, L. Alderson, F. Bender, A.J. Ricco, F. Josse, Investigation of polymer-plasticizer blends as SH-SAW sensor coatings for detection of benzene in water with high sensitivity and long-term stability, ACS Sens., 2 (2017) 157-164.

[21] C. Carey, Plasticizer effects in the PVC membrane of the dibasic phosphate selective electrode, Chemosensors, 3 (2015) 284-294.

[22] A.R. Fakhari, M. Shamsipour, Kh. Ghanbari, Zn(II)-selective membrane electrode based on tetra(2-aminophenyl) porphyrin, Anal. Chim. Acta, 460 (2002) 177–183.

[23] A.R. Fakhari, M. Alaghemand, M. Shamsipur, Iron(III)-selectivemembranepotentiometricsensor basedon5,10,15,20-tetrakis(pentafluorophenyl)-21H,23H-porphyrin, Anal. Lett., 34 (2001) 1097–1106.

[24] A.R. Fakhari, T. Ahmad Raji, H. Naeimi, Copper-selective PVC membrane electrodes based on salens as carriers, Sens. Actuators B Chem., 104 (2005) 317–323.

Anal. Methods Environ. Chem. J. 4 (2) (2021) 34-46

AMECJ

Research Article, Issue 2
Analytical Methods in Environmental Chemistry Journal
Journal home page: www.amecj.com/ir

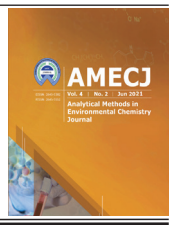

Development of electrodeposited nanostructural poly (o-aminophenol) coating as a solid phase microextraction fiber for determination of bisphenol A

Mohammad Saraji[a], Bahman Farajmand*[,b] and Esmaeil Heydari Bafrouei[c]
[a] *Department of Chemistry, Isfahan University of Technology, Isfahan, Iran.*
[b] *Department of Chemistry, Faculty of Science, University of Zanjan, Zanjan, Iran.*
[C] *Department of Chemistry, Vali-Asr University of Rafsanjan, Rafsanjan, Iran.*

ARTICLE INFO:
Received 10 Mar 2021
Revised form 28 Apr 2021
Accepted 25 May 2021
Available online 28 Jun 2021

Keywords:
Poly (o-aminophenol),
Nanostructure,
Bisphenol A,
Solid phase microextraction,
Gas chromatography-flame ionization detector

ABSTRACT
In this research nanostructural poly (o-aminophenol) was synthesized by electropolymerization and used for solid phase microextraction fiber procedure (SPME). Thin film of Poly (o-aminophenol) (4 µm thickness) was shaped by sweep potential for 45 min on the surface of stainless steel wire. Polymer was synthesized by potentiostat procedure too. Prepared polymer by sweep potential procedure showed nanostructures on the surface. Acetic anhydride was employed for derivatization of bisphenol A (BPh-A) and analysis of acetylated BPh-A was utilized by gas chromatography-flame ionization detector (GC-FID). Affecting parameters on derivatization and extraction such as amount of acetic anhydride, stirring rate, temperature, ionic strength and extraction time were optimized. The limit of detection (LOD) and relative standard divisions (RSDs%) were achieved 0.6 $\mu g L^{-1}$ and less than 6.8%, respectively under optimized conditions. Finally proposed method was used for extraction of bisphenol A from leaching of baby and drinking water bottles. Relative recovery was achieved 98% for leaching from drinking bottle. In leaching from plastic baby bottle, bisphenol A (BPh-A) was detected in the range 5–15 $\mu g\ L^{-1}$.

1. Introduction

Solid phase microextraction (SPME) is a simple, solvent free and green sample preparation technique which includes the employing of a small amount of polymeric sorbent coated on a thin fiber for extraction [1]. Nowadays, commercial SPME fibers are available. The important disadvantages of commercial SPME fibers are high cost, frangibility of the fibers and weakness of sorbents for extraction of polar compounds. For domination of these drawbacks, conductive polymers (CPs) such as polyaniline (PANI) and polypyrole (PPy), coated on the surface of metallic fiber, are good choices [2] but thermal instability of these CPs is a problem when gas chromatography is applied for followed analysis. Many solutions such as changing of counter ion [3] or doping carbon nanotube [4] and nanosilica [5] in the matrix of polymer, have been suggested for modifying of thermal stability and other properties of PANI and PPy. Application of other new CPs with multi-functional groups can be an alternative way for modifying of thermal stability, selectivity and extraction efficiency of SPME fibers.

*Corresponding Author: Bahman Farajmand
Email: farajmand@znu.ac.ir
https://doi.org/10.24200/amecj.v4.i02.142

Poly (o-aminophenol) (POAP) has been an interesting polymer during three past decades. Many of researches have been performed about its synthesis, structure and application in sensor, biosensor and corrosion protection [6]. The POAP is formed by electrochemical oxidation of o-aminophenol (o-AP) on the surface of different electrode in aqueous solution. o-AP can be polymerized electrochemically in alkaline, neutral and acidic media. However, while a conducting polymer film is only produced in acidic media, POAP prepared in neutral and alkaline media leads to a nonconducting polymer film so, the polymer thickness of POAP synthesized in basic and natural media is limited within 10–100 nm due to a self-limiting growth [7]. The o-AP is containing –OH and $–NH_2$ groups in ortho position on a phenyl ring. Polymerization of the o-AP can be performed by both groups therefore a ladder structure could be formed which has better thermal stability rather than PANI [8]. POAP has been employed to build biosensors, because it has been showed permselective properties so the interference from different electroactive species can be significantly reduced during the analysis of biological samples by utilizing a biosensor based on POAP. Moreover, as both hydroxyl and amino groups are involved in the electropolymerization process of o-aminophenol, large amounts of biological macromolecules such as glucose oxidase [9,10] or horseradish peroxidase [11] could be immobilized in poly(o-aminophenol), which results in higher sensitivity of the sensor as compared with sensors based on other polymers. on the other hands the presence of POAP as a sensing material can decrease the oxidation overpotential of some molecules, so it has shown the electrocatalytic behavior [12]. A hybrid modified electrode was also prepared by electropolymerization of o–AP in the presence of sulfonated nickel phtalocyanine. The modified electrode could electrocatalyze NO oxidation and has been employed as NO sensor [13]. The copolymer poly(aniline-co-o-aminophenol) has been exhibited favorable properties to its application in sensors, electrocatalysis, analytic determinations and rechargeable batteries [14,15]. The pH dependence of the electroactivity of the copolymer is much better than that of PANI. Poly(aniline-co-oaminophenol) has been employed as sensor of catechol [16] and ascorbic acid [17]. POAP has been applied as a molecular imprinting polymer for sensor preparation. In this regard, an electrochemical sensor for nicotine based on the electropolymerization of o-PA as monomer and nicotine as template was proposed by Zhaoyang et al. [18]. Compared with nicotine imprinting membranes, the POAP film, was homogeneous, had nanometric thickness and its synthesis was easy. Other application of POAP film was reviewed by Tucerri [6].

Bisphenol A, (BPh-A), 2,2-bis(4-hydroxyphenyl) propane, is one of the highest volume chemicals in the world. It was applied for production of polycarbonate with the second largest outlet being epoxy resins [19]. A broad variety of food contact materials stand out among their uses, mainly derived from polycarbonates (infant feeding bottles, storage containers, tableware, returnable water, milk bottles and water pipes) and epoxy resins (internal protective lining for food and beverage cans, coating on metal lids for glass jars and bottles and drinking water storage tanks) [19]. The BPh-A has shown estrogenic activity so it acts as an endocrine disruptor. Furthermore, researches also has been indicated the potential of BPh-A to disrupt thyroid hormone action [20], to cause proliferation of human prostate cancer cells [21] and to block testosterone synthesis [22] at very low part-per-trillion doses So, there are needs for introducing of new analytical procedures particularly application of modern sample preparation methods (such as microextraction techniques) in order to have reliable tools for control of human exposure to BPh-A. SPME with commercial fibers was utilized for extraction of BPh-A frequently [23–27]. Molecularly imprinted polymeric fiber was employed for selective extraction of BPh-A from complex matrix which was shown by Tan et al. [28].

The POAP, as a multi-functional group compound, can be a remarkable sorbent for extraction of different analytes so, in this paper, nanostructural POAP coated on the stainless steel wire has been prepared by electropolymerization under cyclic voltametry and finally the polymeric coating was used as a SPME fiber for extraction of BPh-A from aqueous matrix. Different effective parameters on derivatization and extraction of BPh-A have been evaluated and optimized and finally the method has been applied for determination of BPh-A in leaching from drinking and plastic baby bottle that are made from polycarbonate.

2. Experimental

2.1. Materials

Bisphenol A was obtained from Sigma & Aldrich (St. Louis, USA) and dissolved in methanol to make stock solution at the concentration of 500 mg L^{-1}. Intermediate standard solution was prepared at concentration 10 mg L^{-1}. More diluted working solutions used in optimization studies were prepared daily by diluting different amounts of the intermediate standard solution with pure water. All solutions were stored at 4 °C prior to use. HPLC grade methanol was purchased from Merck (Darmstadt, Germany). Sodium dodecyl sulfate (SDS), sulfuric acid, sodium chloride, sodium sulfate and o-aminophenol were purchased from Merck (Darmstadt, Germany). Sodium carbonate and acetic anhydride for derivatization of BPH-A was obtained from Merck too. Pure water was prepared by OES (Overseas Equipment & Services) water purification system (OK, USA). The surgical grade stainless steel plunger of a disposable spinal needle (27G, Bartar Co., Tehran, Iran) was used as the substrate of the SPME fibers.

2.2. Instrumentation

The SPME device was purchased from Supelco (Bellefonte, PA, USA) and used for SPME experiments with commercial fibers (85 µm PA and 65 µm PDMS/DVB). A homemade SPME holder was assembled and used to perform extraction with the fibers produced in the present work. A piece of stainless steel wire (3 cm) was mounted into the SPME device and used as a working electrode to make the SPME fiber. Electrochemical polymerization was carried out with a potentiastat/galvanostat AutoLab (Echo Chemie, Netherlands). A SP-3420A gas chromatograph equipped with a split/splitless injector and a flame ionization detector (BFRL, Beijing, China) was employed for all experiments. The injector was equipped with a low-volume insert designed for the analysis by SPME (Restek, Bellefonte, PA, USA). Nitrogen (99.999%) was used as carrier and make-up gas. The carrier and make-up gas flow rate was set at 1.7 and 30 mL min^{-1}, respectively. The chromatographic separation was performed using a DB-35ms, 10 m×0.25 mm, fused silica capillary column with a 0.15 µm stationary phase thickness (Supelco, Bellefonte, PA, USA). The injector and detector temperatures were set at 260 and 280 °C, respectively. The column temperature was initially maintained at 100 °C for 1 min; subsequently, the temperature was increased to 250 °C (at a rate of 30 °C min^{-1}) and held for 10 min. Surface characteristic studies of the poly (o-aminophenol) coating was performed using field emission-scanning electron microscopy (FE-SEM) (Hitachi, S-4160, Japan). Chemical bonding characterization of the coating was investigated using Fourier transform infrared spectroscopy (FT-IR-350, Jasco Co., Tokyo, Japan). Thermogravimetric analysis (TGA) was performed using a Rheometric Scientific TGA 1500 instrument.

2.3. Preparation of SPME coating

Poly(o-aminophenol) film was prepared according to work of Kunimura et al [29] with some modification. Polymerization was performed with a potential-sweep electrolysis by using a standard three-electrode cell. Stainless steel wire (o.d. 0.2 mm) and platinum electrode were used as working and counter electrodes. A length of 1 cm from the end part of stainless steel wire was

immersed into the polymerization solution. The electrode potential was cycled between 0 and 1.3 V versus an Ag/AgCl electrode at 50 mV s^{-1} in a 0.5 M Na_2S0_4 solution (pH 1.0) containing 100 mM o-aminophenol and 0.05 mM SDS (as the counter ion and catalyst). Solution was stirred magnetically by a 1 cm stir bar at 800 rpm. For the comparison purpose, polymer was synthesis at a constant potential of 1.3 V for 45 min too. To make the coating adhere firmly to the surface of the wire, the wire surface was first roughened by a smooth sand paper and then washed in methanol while sonicating. After polymerization, prepared fiber was thoroughly rinsed with distillated water and thermally conditioned before use. Thermal conditioning of the fibers was carried out by heating at 150 °C for 20 min, then at 200 °C for 20 min, and finally at 290 °C for 20 h in a GC injector port under a nitrogen atmosphere.

2.4. Derivatization and SPME procedure

A 3.0 mL standard solution of BPH-A containing 0.05 mol L^{-1} of sodium carbonate was transferred into a 7-mL glass vial from Supelco (14 mm i.d.). A 13 mm×3 mm Teflon coated stir bar was used in the vial for stirring the solution. For derivatization step, amount of 25 µL acetic anhydride was added to the vial. The vial was caped and reaction was performed for 5 min at 300 rpm and room temperature. After the reaction, 0.6 g of sodium chloride was added to the solution and magnetically stirred until dissolving. For extraction step, the SPME fiber was immersed into the sample solution under optimum stirring rate (600 rpm) at room temperature. After 30 min, the fiber was retracted into the needle and immediately introduced into the GC injection port (260 °C). Injection was made in splitless mode and desorption time obtained at 3 min.

3. Results and discussion

3.1. Characterization of POAP coating

The morphological structures of POAP coating were investigated with FE-SEM and have been shown in Figure 1. POAP coating prepared by sweep potential showed granular structures which were contained the large number of nanoparticles (o.d. 50 nm or smaller) attached to each other (Fig. 1a and b). However, in some places, nanoparticles were placed beside each other without any granular structure (Fig. 1d). The thickness of the coating was obtained about 4 µm (Fig. 1c). It seems low conductivity of polymer causes the thickness does not increase in the period of electropolymerization [29]. Figure 1e and f demonstrate surface morphology of POAP prepared by constant potential. As can be seen, polymer film is uniform and flat and there is no granular structure. Application of the fiber prepared by constant potential shows 4 times weaker result than the one prepared by sweep potential. It seems the higher surface area of the polymer film prepared by sweep potential plays important role in extraction of analyte.

For gas chromatography applications, SPME fibers must be have efficient thermal stability. The TGA curve of the POAP coating under argon atmosphere at a heating rate of 10 °C min^{-1} has been shown in Figure 2a. This film was found to start a slow loss of weight around 300 °C. The weight loss was at most 4% at this temperature which could be attributed to the evaporation of water moisture trapped in the pores of the film. So the present SPME fiber coating is stable at temperatures below 300 °C due to ladder chemical structure [29]. Then the fiber is suitable for gas chromatographic analysis.

Investigation of infrared spectroscopy of POAP was carried out by many researchers and more chemical structures have been proposed. o-AP has two functional groups which contains –OH and $–NH_2$ sites. Polymerization of o-AP can be performed by both sites. Due to spectroscopic measurements, different structures have been proposed for POAP. Besides a completely ring-closed or ladder structure with phenoxazine units [8,30–32], other two structures, a partially ring opened and another partially hydrolyzed, have been considered for POAP. In-situ Raman spectroscopy measurements propose

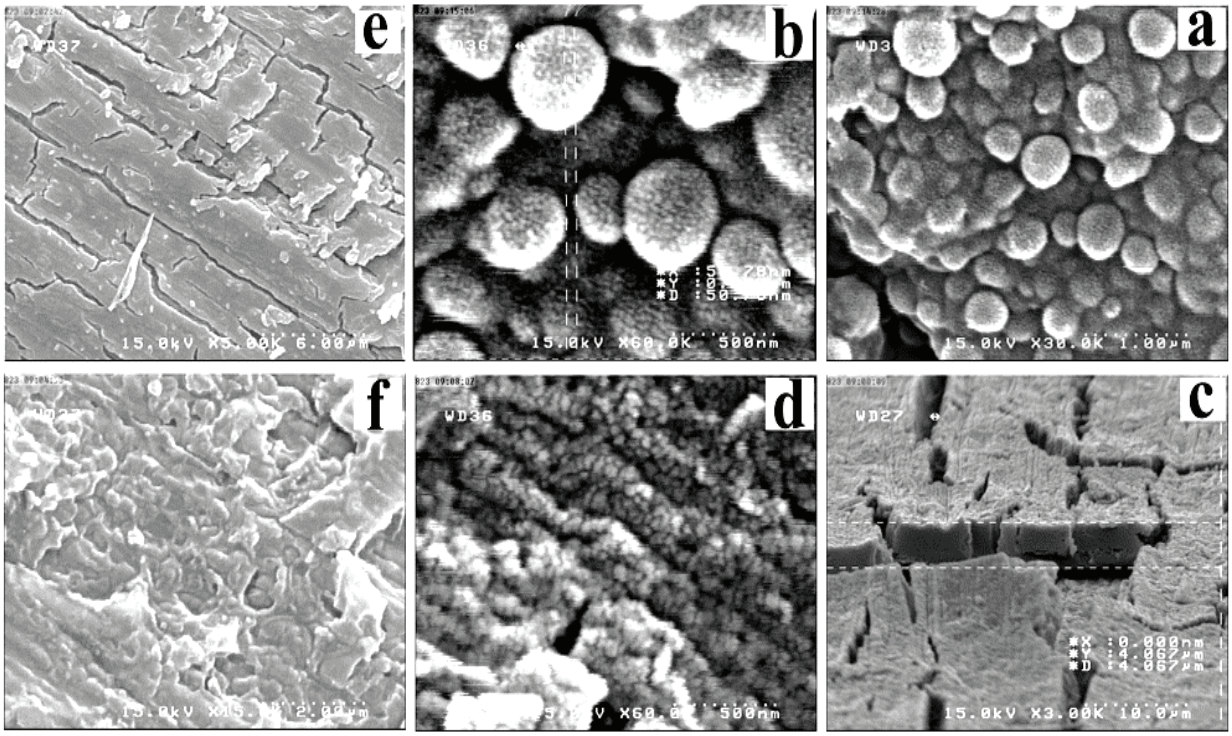

Fig. 1. FE-SEM images from POAP coated on the surface of stainless steel wire at (a, b, c & d) cyclic potential between 0 and 1.3 V with 50 mV/s rate; (e & f) constant potential at 1.3 V.

that the POAP medium contains alternating oxidized (quinonoid) and reduced (N-phenyl-p-phenylenediamine) repeating units [33,34]. Zhang et al. introduced 1,4-substituted molecular structure for POAP [33,34] allows explaining the interaction of the polymer with metal ions. The cation capturing process by POAP was certified to simultaneous presence of -OH and $–NH_2$ groups of the polymeric backbone, in which the lone-pair electrons are available to form metal complex. IR studies have been indicated that the POAP film-growing process in alkaline media involves the deprotonation of the aminophenol molecule, which is probably chemisorbed at the metal surface, followed by oxidation and electropolymerization reactions. In this whole process, the polymerization affects the –OH group by the formation of C–O–C bond while the $–NH_2$ groups are preserved [35].

In this study Fourier transform infrared spectroscopy (FT-IR) was used to investigate the functional groups of the polymer. Spectrum has been revealed in Figure 2b. Broad peak between 3000 and 4000 cm^{-1} assigned to the symmetric stretching of NH and OH in aromatic system. Strong peaks at 1582 and 1379 cm^{-1} are belonging to C-N stretching vibrations for quinoide structure or combination band for protonated aromatic amine [36]. Strong peak at 1460 cm^{-1} can be assigned for NH scissoring vibrations. Weak peak at 1037 cm^{-1} is belonging to C-C stretching vibrations in benzene ring [36]. Consequently, a blend of structures could be considered for POAP film. A weak peak at 2926 cm^{-1} assigned to stretching of CH in aliphatic system which can be considered for dodecyl sulfate counter ion. SDS plays two roles for preparation of POAP. At first it acts as a catalyst and oxidation potential of o-AP was shifted to less positive potentials (almost 0.075V) and the oxidation current increased, as compared with the process in the absence of SDS. The rate of polymerization also increased considerably in the presence of SDS [37] on the other hands dodecyl sulfate has been used as a frequent counter ion in conductive polymer preparation that used for microextraction process because it increases thermal stability of polymeric film [38].

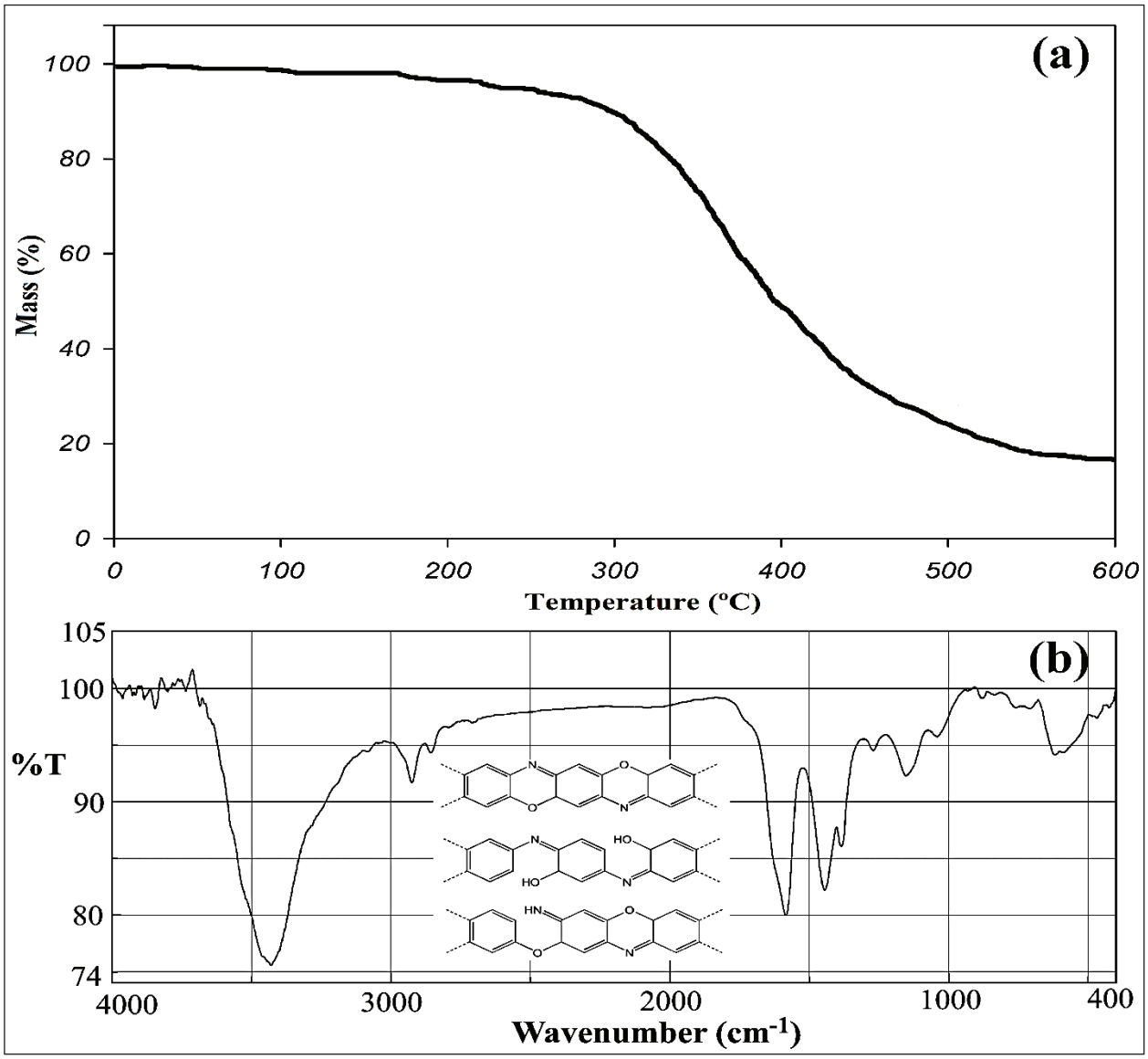

Fig. 2. Thermal gravimetric analysis (a) and FT-IR spectra of POAP coating prepared by sweep potential.

3.2. Optimization of conditions

For evaluation of POAP film as a solid phase microextraction fiber, effects of various parameters that can probably influence the performance of the derivatization and extraction of BPH-A, including amounts of acetic anhydride and sodium carbonat, salt concentration, stirring rate, extraction time and temperature were investigated. All experiments were performed three times.

3.2.1. Optimization of derivatization conditions

Derivatization can reduce the polarity of some analytes and can improve the extraction efficiency and also it leads to better peak shape, and higher sensitivity. Acetic anhydride is a common derivatization reagent that has been applied for blocking of hydroxyl group of phenolic compounds frequently [23,39,40]. The derivatization with acetic anhydride was performed in situ. Consequently, the experimental variables affecting to both the extraction and derivatization processes were studied together. Derivatization of bisphenol A with acetic anhydride performs in basic condition. Sodium carbonate usually has been used for adjustment of sample pH hence in this research effect of different concentration of sodium carbonate was investigated. Figure 3a show the consequences. The concentrations of 0.05 and 0.1

mol L^{-1} reveal maximum derivatization efficiency, Therefore, 0.05 mol L^{-1} of sodium carbonate was applied for adjustment of pH. Under optimized pH, the amount of acetic anhydride was evaluated for the best derivatization efficiency. Effect of different amount of acetic anhydride on extraction efficiency was summarized in Figure 3b. As can be seen, concentration more than 0.75% (V/V) has not significant effect on derivatization efficiency therefore this concentration was selected as an optimum point. Acetylation of phenolic compounds usually is completed at a short time nonetheless in this research the reaction time was studied too. The results satisfy that the times more than 5 min have not considerable effect on the reaction recovery (the curve has not shown).

3.2.2. Optimization of extraction conditions

Effective parameters such as ion strength, stirring rate, extraction temperature and time were evaluated and optimized. The ion strength of the sample solution was studied by spiking a series of NaCl concentrations of 0–0.3 g L^{-1}. The response increases with the increase of ion strength; however, the extraction efficiency slightly decreases under the high salt content (Fig. 4a). A salt level of 0.2 g mL^{-1} of NaCl was used in the following experiments. The fiber is directly immersed in the liquid samples, and partitions between the sample matrix and the stationary phase were happened. Agitation of the sample is often carried out with a small stirring bar to decrease the time necessary for equilibrium and to decrease the tension of the static aqueous film. The stirring bar is of dimension 10 mm × 3 mm. The effect of the stirring rate on the responses was tested from 250 to 1000 rpm. At a higher stirring rate of 600 rpm, a significant decrease in the area response was observed (Fig. 4b). Moreover, better result was obtained at a relatively medium stirring rate than at the lower and higher ones. Thus, a stirring rate of 600 rpm was chosen for further experiments. Temperature has kinetic and thermodynamic effects on extraction recovery. On the other hands, solubility of analyte in water increases at high temperature, so, effect of temperature in the range of 10 to 45 °C (Fig. 5a). Best results were achieved at 15 °C but for simplicity room temperature was applied as an optimal temperature. The extraction time was studied from 10 min to 60 min (Fig. 5b). The result shows that the equilibrium time is reached until 40 min when a further increase of the extraction time does not result in a significant increase in the detector response but for shortening the analysis time, an extraction time of 30 min was established in all the experiments.

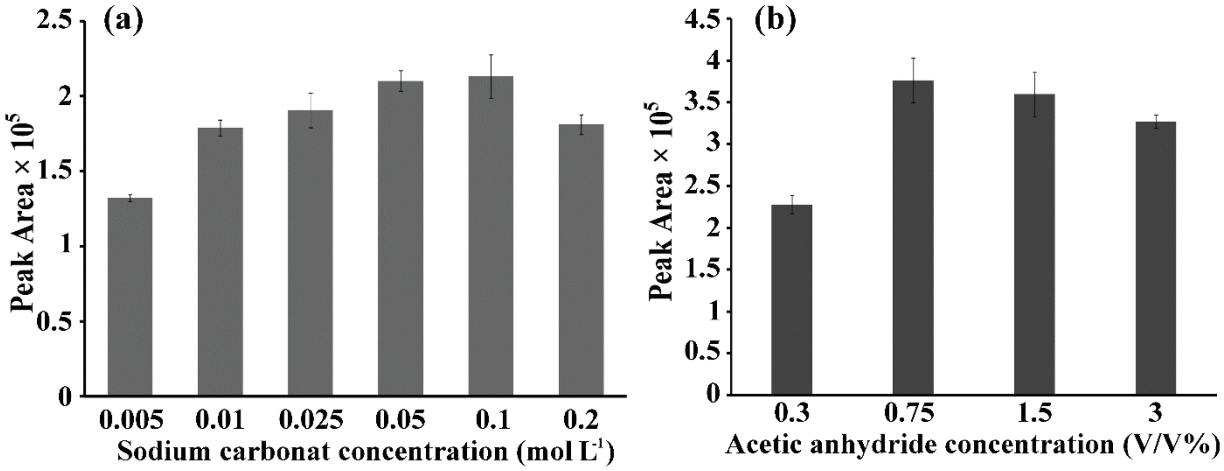

Fig. 3. (a) Effect of sodium carbonate concentration and (b) effect of acetic anhydride amount on the derivatization efficiency of bisphenol A (sample volume, 3 mL; concentration of analyte, 200 µg L^{-1}; amount of acetic anhydride (for (a)), 10 µL; amount of sodium carbonat (for (b)), 0.05 mol L^{-1}; reaction time, 5 min; salt addition, 0.1 g mL^{-1}; stirring rate, 400 rpm; extraction time, 30 min).

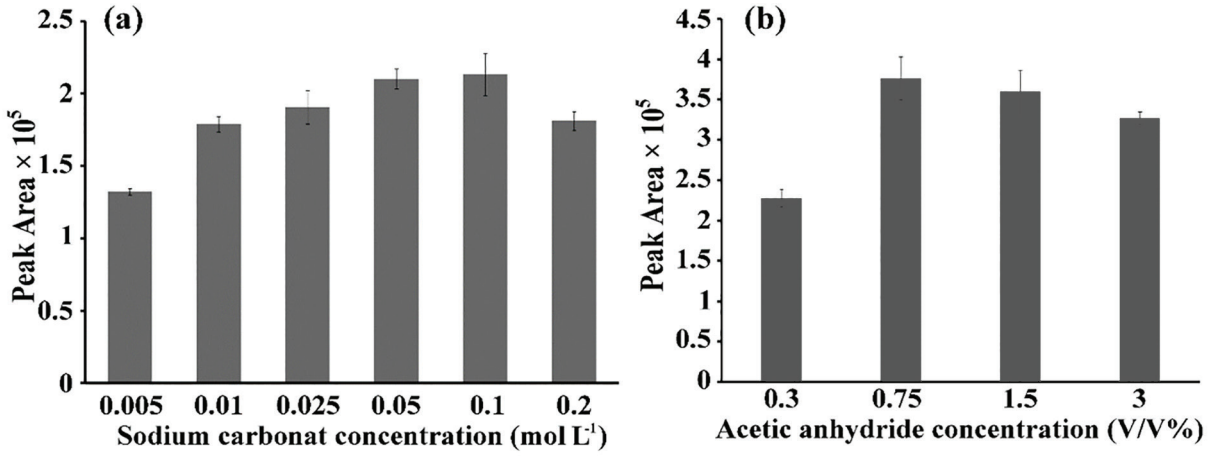

Fig. 4. (a) Effect of salt addition and (b) stirring rate on extraction of bisphenol A (sample volume, 3 mL; analyte concentration, 200 µg L^{-1}; 0.05 mol L^{-1} sodium carbonate; amount of acetic anhydride, 25 µL; reaction time, 5 min; stirring rate (for (a)), 400 rpm; salt addition (for (b)), 0.3 g mL^{-1}; extraction time, 30 min at room temperature).

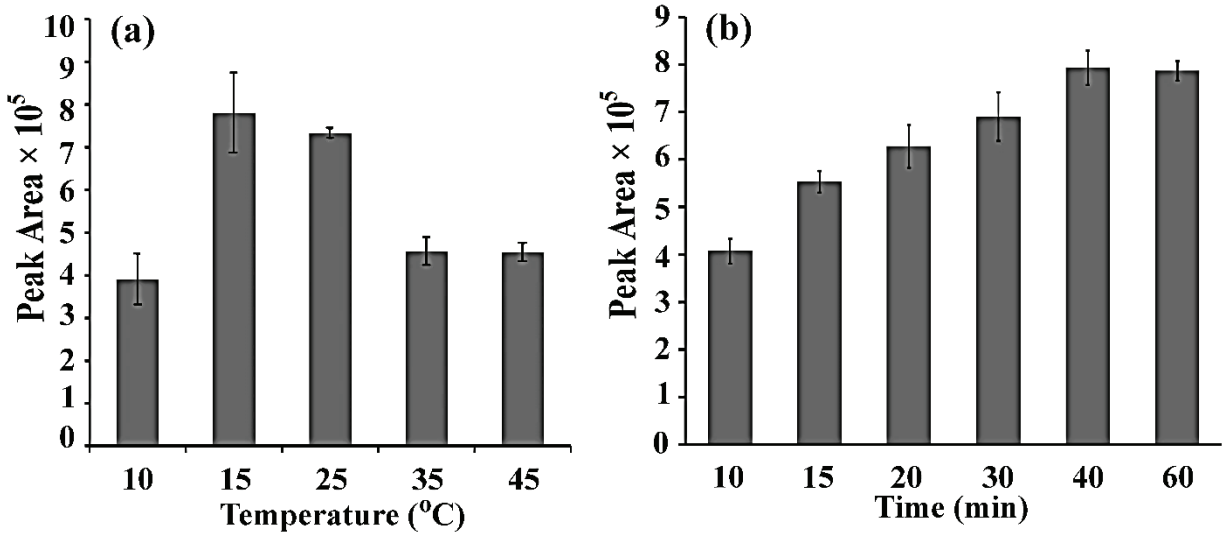

Fig. 5. (a) Effect of temperature and time on extraction of bisphenol A (sample volume, 3 mL; analyte concentration, 200 µg L^{-1}; 0.05 mol L^{-1} sodium carbonate; amount of acetic anhydride, 25 µL; reaction time, 5 min; stirring rate, 600 rpm; salt addition, 0.3 g mL^{-1}; extraction time (for a), 30 min at room temperature (for b).

3.3. Method validation

The linearity, the repeatability and the detection limits of the proposed method were investigated. The correlation coefficient (0.9981) indicated a good linearity between 2 - 500 µg L^{-1}. Under optimal conditions, LOD was achieved 0.6 µg L^{-1}. Relative standard deviation for intra- and inter day were 4.0 and 6.1%, respectively. The amount of 6.8% was attained for fiber-to-fiber relative standard deviation too. On the other hands, extraction capability of the POAP coated fiber was compared with commercial SPME fibers. Poly acrylate (PA) and poly dimethylsiloxane/divinylbenzen (PDMS/DVB) commercial fiber were chosen for this comparison. Figure 6 shows the results. POAP coated fiber revealed better capacity for extraction of bisphenol A. It seems the chemical composition and surface configurations of coating are two effective factors for this investigation. POAP has more chemical functional groups compared to PA and PDMS/DVB coating. On the other side, POAP nanostructure morphology can help for more and fast extraction.

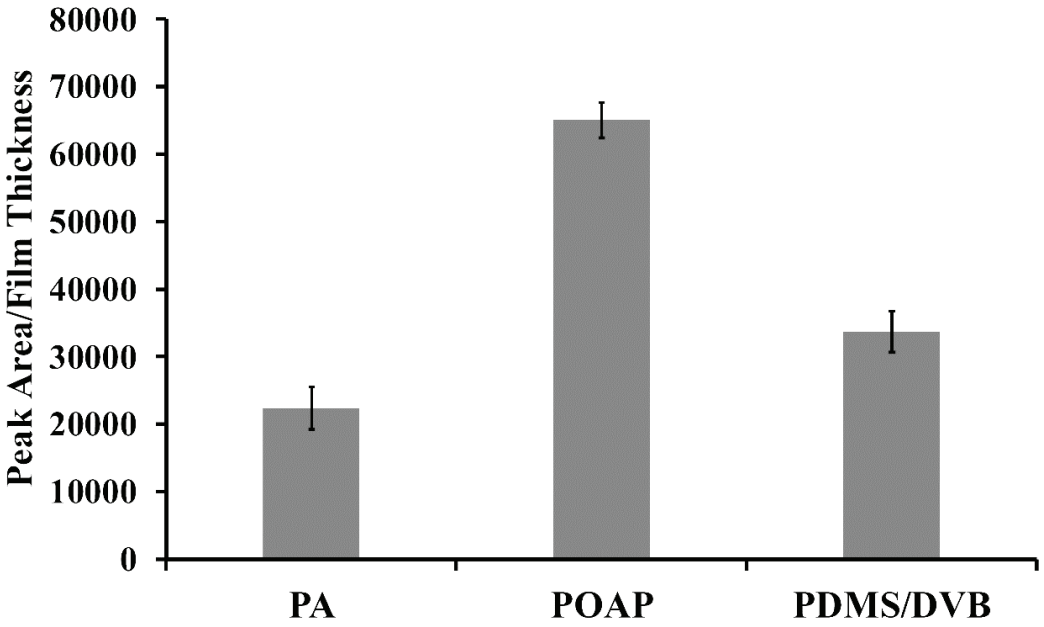

Fig. 6. Comparison of POAP coated SPME fiber with PA & PDMS/DVB commercial fiber (sample volume, 3 mL; analyte concentration, 50 µg L^{-1}; 0.05 mol L^{-1} sodium carbonate; amount of acetic anhydride, 25 µL; reaction time, 5 min; stirring rate, 600 rpm; salt addition, 0.3 g/mL; extraction time, 30 min at room temperature).

3.4. Real sample analysis

To examine the feasibility of the method, new SPME fiber was applied for analysis of bisphenol A released from milk and drinking water bottle. All the leachate samples were collected from the containers that had been filled with 50 mL of boiling hot water. Bisphenol A was below the LOD for drinking water bottle but was detected in the range 5–15 µg L^{-1} in leaching from plastic baby bottle. Relative recovery was attained 98±3% for leaching from drinking bottle. Relative recoveries were reported in Table 1. Figure 7 shows the chromatograms from the leaching of baby bottle with and without spiking of bisphenol A. Releasing of bisphenol A from plastic baby bottle was investigated in four time reusing and the results were summarized in Figure 8. As can be seen, bisphenol A exists in the consecutive leaching but the amount of it reduces.

Table 1. Relative recoveries of bisphenol A in different real samples (µg L^{-1})

Added	Drinking water bottle		Plastic baby bottle (1st leachate)	
	Found	Relative Recovery (%)	Found	Relative Recovery (%)
0.0	ND*	-	15.1	-
10.0	9.7	97	25.4	103
20.0	20.6	103	35.3	101
50.0	51.0	102	64.1	98
100.0	94.1	94	109.1	94

* Not detected.

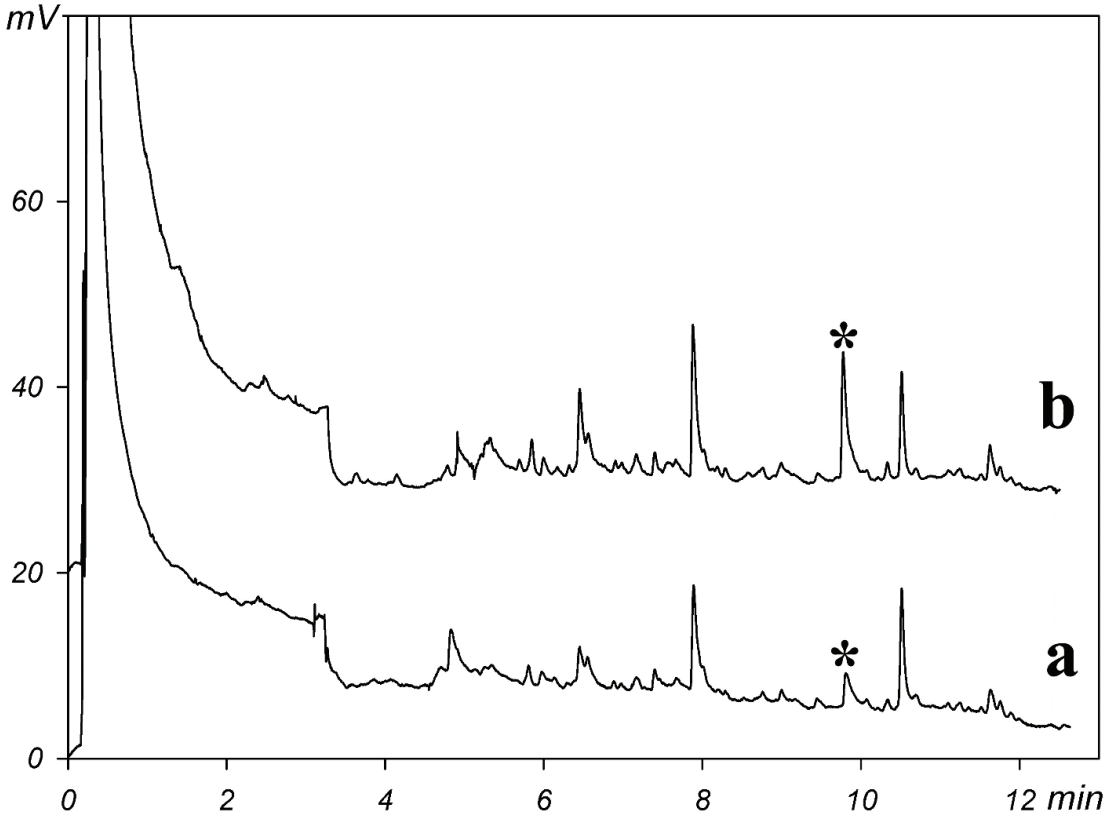

Fig. 7. GC-FID chromatograms after SPME of non-spiked (a) and spiked (b) leaching from plastic baby bottle with 10 µg L^{-1} of bisphenol A.

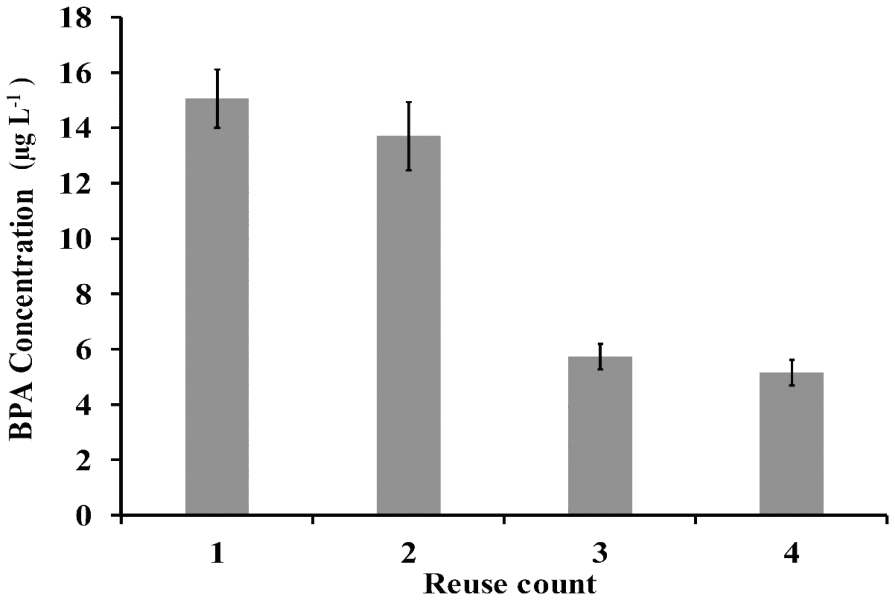

Fig. 8. Determined concentration of bisphenol A (BPH-A) in leaching from plastic baby bottle after four time reusing.

Conclusions

This study shows application of nanostructural poly (o-aminophenol) as a new SPME fiber combined with GC–FID is a precise method for reproducibly analyzing trace bisphenol A from aqueous samples. Better chromatographic shape and sensitivity were obtained by derivatization of bisphenol A using acetic anhydride. Different effective parameters were studied and optimized. The figures of merit belonged to the method were favorable. The dynamic range was achieved in the ranges of 2 - 500 µg L^{-1}. The limits of detection and RSD were 0.6 µg L^{-1} and <6.8% respectively. The feasibility of using the SPME–GC–FID system to measure the amount of bisphenol A in leaching from plastic baby and drinking water bottle was tested. Bisphenol A was detected in the range 5–15 µg L^{-1}.

5.Acknowledgment

The authors are grateful to the Research Council of Isfahan University of Technology (IUT) and the Center of Excellence for Sensor and Green Chemistry for their support of this project.

6. References

[1] A. Spietelun, Ł. Marcinkowski, M. De, J. Namie, Recent developments and future trends in solid phase microextraction techniques towards green analytical chemistry, J. Chromatogr. A, 1321 (2013) 1–13.

[2] M. Lashgari, Y. Yamini, An overview of the most common lab-made coating materials in solid phase microextraction, Talanta, 191 (2019) 283-306.

[3] A. Mollahosseini, E. Noroozian, Polyphosphate-doped polypyrrole coated on steel fiber for the solid-phase microextraction of organochlorine pesticides in water, Anal. Chim. Acta, 638 (2009) 169–174.

[4] W. Du, F. Zhao, B. Zeng, Novel multiwalled carbon nanotubes – polyaniline composite film coated platinum wire for headspace solid-phase microextraction and gas chromatographic determination of phenolic compounds, J. Chromatogr. A, 1216 (2009) 3751–3757.

[5] H. Bagheri, A. Roostaie, Aniline – silica nanocomposite as a novel solid phase microextraction fiber coating, J. Chromatogr. A, 1238 (2012) 22–29.

[6] R. Tucceri, Poly (o-aminophenol) film electrodes, Springer International Publishing Switzerland, 2013.

[7] R. Tucceri, P. Arnal, A. Scian, Electrosynthesis and spectroscopic characterization of poly (o-aminophenol) film electrodes, ISRN Polym. Sci., 2012 (2012) 1–26.

[8] C. Barbero, J.J. Silber, L. Sereno, Formation of a novel electroactive film by electropolymerization of ortho-aminophenol, Study of its chemical structure and formation mechanism, Electropolymerization of analogous compounds, J. Electroanal. Chem., 263 (1989) 333–352.

[9] X. Chen, J. Chen, C. Deng, C. Xiao, Y. Yang, Z. Nie, et al., Amperometric glucose biosensor based on boron-doped carbon nanotubes modified electrode, Talanta, 76 (2008) 763–767.

[10] D. Pan, J. Chen, S. Yao, W. Tao, L. Nie, An amperometric glucose biosensor based on glucose oxidase immobilized in electropolymerized poly (o-aminophenol) and carbon nanotubes composite film on a gold electrode, Anal. Sci., 21 (2005) 367–371.

[11] M.A.V. Garcia, P.T. Blancoa, A. Ivaska, A poly (o-aminophenol) modified electrode as an amperometric hydrogen peroxide biosensor, Electrochim. Acta, 43 (1998) 3533–3539.

[12] N. Kumar, R. N. Goyal, Simultaneous determination of melatonin and 5-hydroxytrptophan at the disposable poly-(melamine)/poly-(o-aminophenol) composite modified screen printed sensor, J. Electroanal. Chem., 874 (2020) 114458.

[13] M.C. Miras, A. Badano, M.M. Bruno, C. Barbero, Nitric oxide electrochemical sensors based on hybrid films of conducting polymers and metal phtalocyanines, Port. Electrochim. Acta, 21 (2003) 235–243.

[14] L. Liu, H. Cui, H. An, J. Zhai, Y. Pan, Electrochemical detection of aqueous nitrite based on poly(aniline-co-o-aminophenol)-modified glassy carbon electrode, Ionics, 23 (2017) 1517-1523.

[15] A. B. Slimane, A. F. Al-Hossainy, M. S. Zoromba, Synthesis and optoelectronic properties of conductive nanostructured poly(aniline-co-o-aminophenol) thin film, J. Mater. Sci.: Mater. Electron., 29 (2018) 8431-8445.

[16] S. Mu, Catechol sensor using poly (aniline-co- o-aminophenol) as an electron transfer mediator, Biosens. Bioelectron., 21 (2006) 1237–1243.

[17] L. Zhang, J. Lian, Electrochemical synthesis of copolymer of aniline and o-aminophenol and its use to the electrocatalytic oxidation of ascorbic acid, J. Electroanal. Chem., 611 (2007) 51–59.

[18] W. Zhaoyang, Z. Xiaolei, Y. Yunhui, S. Guoli, Y. Ruqin, A sensitive nicotine sensor based on molecularly imprinted electropolymer of o-aminophenol, Front. Chem. China, 32 (2006) 183–187.

[19] A. Ballesteros-gómez, S. Rubio, D. Pérez-bendito, Analytical methods for the determination of bisphenol A in food, J. Chromatogr. A, 1216 (2009) 449–469.

[20] R.T. Zoeller, R. Bansal, C. Parris, Bisphenol-A , an environmental contaminant that acts as a thyroid hormone receptor antagonist in vitro , increases serum thyroxine , and alters RC3 / neurogranin expression in the developing rat brain, Endocrinology, 146 (2004) 607–612.

[21] Y.B. Wetherill, C.E. Petre, K.R. Monk, A. Puga, K.E. Knudsen, The xenoestrogen bisphenol A induces inappropriate androgen receptor activation and mitogenesis in prostatic adenocarcinoma cells 1, Mol. Cancer Ther., 13 (2002) 515–524.

[22] B.T. Akingbemi, C.M. Sottas, A.I. Koulova, G.R. Klinefelter, M.P. Hardy, Inhibition of testicular steroidogenesis by the xenoestrogen bisphenol A is associated with reduced pituitary luteinizing hormone secretion and decreased steroidogenic enzyme gene expression in rat leydig cells, Endocrinology, 145 (2004) 592–603.

[23] P. Viñas, N. Campillo, Comparison of two derivatization-based methods for solid-phase microextraction – gas chromatography – mass spectrometric determination of bisphenol A , bisphenol S and biphenol migrated from food cans, Anal. Bioanal. Chem., 397 (2010) 115–125.

[24] M.K.R. Mudiam, R. Jain, V.K. Dua, A.K. Singh, V.P. Sharma, Application of ethyl chloroformate derivatization for solid-phase microextraction– gas chromatography-mass spectrometric determination of bisphenol-A in water and milk samples, Anal. Bioanal. Chem., 401 (2011) 1695–1701.

[25] W. Gao, J. Cheng, X. Yuan, Y. Tian, Covalent organic framework-graphene oxide composite: A superior adsorption material for solid phase microextraction of bisphenol A, Talanta, 222 (2021) 121501.

[26] Y. H. Pang, Y. Y. Huang, X. F. Shen, Y. Y. Wang, Electro-enhanced solid-phase microextraction with covalent organic framework modified stainless steel fiber for efficient adsorption of bisphenol A, Anal. Chim. Acta, 1142 (2021) 99-107.

[27] N. Mohammadnezhad, A. A. Matin, N. Samadi, A. Shomali, H. Valizadeh, Ionic liquid-bonded fused silica as a new solid-phase microextraction fiber for the liquid chromatographic determination of bisphenol A as an endocrine disruptor, J. AOAC Int., 100 (2017) 218–223.

[28] Y. Liu, Y. Liu, Z. Liu, F. Du, G. Qin, G. Li, X. Hu, Z. Xu, Z. Cai, Supramolecularly imprinted polymeric solid phase microextraction coatings for synergetic recognition nitrophenols and bisphenol A, J. Hazard. Mater., 368 (2019) 358–364

[29] S. Kunimura, T. Ohsaka, N. Oyama, Preparation of thin polymeric films on electrode surfaces by electropolymerization of

o-aminophenol, Macromolecules, 21 (1988) 894–900.
[30] J.M. Ortega, Conducting potential range for poly (o-aminophenol), Thin Solid Films, 371 (2000) 28–35.
[31] D. Gonc, R.C. Faria, M. Yonashiro, L.O.S. Bulhoes, Electrochemical oxidation of o-aminophenol in aqueous acidic medium: formation of film and soluble products, J. Electroanal. Chem., 487 (2000) 90–99.
[32] A.A. Shah, R. Holze, Poly (o-aminophenol) with two redox processes: A spectroelectrochemical study, J. Electroanal. Chem., 597 (2006) 95–102.
[33] A.Q. Zhang, C.Q. Cui, Y.Z. Chen, J.Y. Lee, Synthesis and electrochromic properties of poly-o-aminophenol, J. Electroanal. Chem., 373 (1994) 115–121.
[34] A.Q. Zhang, C.Q. Cui, J.Y. Lee, Metal-polymer interactions in the Ag+ -poly-o-aminophenol system, J. Electroanal. Chem., 413 (1996) 143–151.
[35] A. Guenbour, A. Kacemi, A. Benbachir, L. Aries, Electropolymerization of 2-aminophenol Electrochemical and spectroscopic studies, Prog. Org. Coat., 38 (2000) 121–126.
[36] S.M. Sayyah, M.M. El-Rabiey, S.S.A. El-rehim, R.E. Azooz, Electropolymerization kinetics of o-aminophenol and characterization of the obtained polymer films, J. Appl. Polym. Sci., 99 (2006) 3093–3109.
[37] R. Ojani, J. Raoof, S. Fathi, Poly (o-aminophenol) film prepared in the presence of sodium dodecyl sulfate : Application for nickel ion dispersion and the electrocatalytic oxidation of methanol and ethylene glycol, Electrochim. Acta, 54 (2009) 2190–2196.
[38] A. Mohammadi, Y. Yamini, N. Alizadeh, Dodecylsulfate-doped polypyrrole film prepared by electrochemical fiber coating technique for headspace solid-phase microextraction of polycyclic aromatic hydrocarbons, J. Chromatogr. A, 1063 (2005) 1–8.
[39] N. De Coensel, F. David, P. Sandra, Study on the migration of bisphenol-A from baby bottles by stir bar sorptive extraction- thermal desorption-capillary GC-MS, J. Sep. Sci., 32 (2009) 3829–3836.
[40] N. Rastkari, R. Ahmadkhaniha, M. Yunesian, L.J. Baleh, A. Mesdaghinia, Sensitive determination of bisphenol A and bisphenol F in canned food using a solid-phase microextraction fibre coated with single-walled carbon nanotubes before GC/MS, Food Addit. Contam., 27 (2010) 1460–1468.

Anal. Methods Environ. Chem. J. 4 (2) (2021) 47-59

AMECJ

Research Article, Issue 2
Analytical Methods in Environmental Chemistry Journal
Journal home page: www.amecj.com/ir

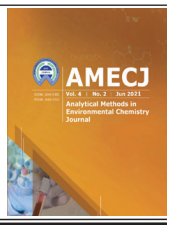

Evaluation and determination of occupational and environmental exposure of lead in workplace air and human workers based dispersive ionic liquid solid phase micro extraction in battery manufacturing factories from Iran

Somayeh Mirza[a,*] and Azadeh Yahya Meymandi[b]

[a] *Ph.D in Environment Chemistry and Management, Department of Environmental Management, Faculty of Natural resources and Environment, Science and Research branch, Islamic Azad University, Tehran, Iran.*
[b] *Faculty of Science, Department of chemistry, University of Birjand, Birjand, Iran*

ARTICLE INFO:

Received 5 Mar 2021
Revised form 19 May 2021
Accepted 3 Jun 2021
Available online 29 Jun 2021

Keywords:
Lead,
Human whole blood,
Workplace air,
Nanotechnology,
Dispersive ionic liquid solid phase micro extraction,
Battery manufacturing factories

ABSTRACT

The exposure of lead in workplace air and human workers of battery manufacturing factory was evaluated determined by nanotechnology since 2019-2020. Human whole blood (HWB) for subject and healthy peoples (25-55, Men, 40 N) and workplace air (40N) was prepared based on NIOSH sampling. 10 mL of HWB samples added to 20 mg of mixture ionic liquid/ ligand ([HMIM][PF_6]/APDC) modified on graphene oxide nanostructures(GONs) at pH=6. After sonication, the lead ions separated/extracted by dispersive ionic liquid solid phase micro extraction (DIL-SPME) and determined by flame atomic absorption spectrometry (F-AAS). All air samples in workplace were analyzed based on NIOSH process. The results showed us the negative correlation between Pb concentration in human blood subject and healthy peoples (r=0.24). The range concentrations of lead in human subject, healthy peoples and workplace air were obtained 193.4-543.7 µg L^{-1}, 85.6-175.9 µgL^{-1} and 44.7-81.5 µgm^{-3}, respectively. The LOD, linear rang, enrichment factor(EF) and RSD% were achieved 1.25 µg L^{-1}, 5.0- 310 µg L^{-1}, 19.6 and less than 5% by procedure. The method was validated by standard reference material (SRM), the electrothermal atomic absorption spectrometry (ET-AAS) and ICP-MS analyzer for human samples.

1. Introduction

Heavy metals have toxic effects in environmental and human health which it causes main problem in many human organs such as brain. Lead (Pb) with dangerous properties in human consider as a hazardous chemical [1]. The battery and chemical factories use the lead in their products. The lead enters in environment by various sources such as, water, soil, the medical industries, air dust, water and gas pipes, paint factories and chemical products [2-5]. Lead causes many problem in human organs such as, the nervous central system (insomnia, delirium, cognitive deficits and tremor), kidney, liver, gastrointestinal and bone disorders [6,7]. Also, an acute poisoning of lead cause to neurological defect include, pain, muscle weakness and numbness. In biochemistry, the lead can be seen in various of proteins and amino acids. Also, lead bonded to sulfur groups of aminoacids such as cysteine (Cys) and a homoleptic and hemidirectic (SR)3 complex [8,9]. Moreover,

*Corresponding Author: Somayeh Mirza
Email: somayeh.mirza@gmail.com
https://doi.org/10.24200/amecj.v4.i02.143

lead can be complexed to copper/ zinc and caused brain problems. Therefore, the lead determination in the human biological samples (blood, serum and urine) with accurate and precise method must be considered. The environmental protection agency (EPA), NIOSH , OSHA, the National toxicology program (NTP) and food and drug administration (FDA) reported that the lead concentration in water, air and human blood samples are between 0.01-0.1 mg L^{-1}, less than 50 µg m^{-3} and 250 µg L^{-1}, respectively [10-12]. Recently, many researchers reported the different lead analysis in water and human blood samples [13]. The various techniques such as flame atomic absorption spectrometry (F-AAS) [14,15], the electrothermal atomic absorption spectrometry (ET-AAS) [16], the inductively coupled plasma mass spectrometry(ICP-MS), the microwave plasma atomic emission spectrometry(MP-AES) [17, 18], the gas chromatography mass spectrometry GC-MS [19] and laser-induced breakdown spectroscopy (LIBS)[20] were used for lead determination in different matrixes. Due to difficulty of matrixes and interferences, the extraction/preconcentration method for lead determination in blood samples is used. Various methodology such as, solid-phase extraction (SPE)[21], the magnetic-SPE [22], the dispersive liquid–liquid microextraction (DLLME) [23], the cloud point extraction (CPE) [24], the dispersive solid phase extraction (D-SPE), the ultrasound-assisted dispersive micro solid phase extraction (USA-µ-SPE) [25], and the emulsification microextraction using a ionic liquid (IL-EME) [26] were reported. Recently, the dispersive ionic liquid solid phase micro extraction (DIL-SPME) for separation/ determination of heavy metals in liquid phases was used. The DIL-SPME method has many advantages such as high efficiency/recovery and easy to use in short time. The various sorbents include, the carbon nanotubes (CNTs) [27], the silica gel functionalized with thiosalicylic acid [28], and graphene/graphene oxide [29] was used for extraction/removal of heavy metals from solutions by scientists. The Ionic liquids were used for the separation of heavy metals from samples. Currently, safety, health and environmental assessments in factories can help manage pollutants in industry and pollutants are reduced in the long run after analysis [30].

In this study, the mixture of ionic liquid/ ligand ([HMIM][PF_6]/APDC) modified on graphene oxide(NGO) was used for lead extraction from blood samples at pH=6. The speciation of lead was achieved based on IL/APDC/NGO adsorbent before the DIL-SPME procedure. The method was validated in blood and water samples by spiking samples and ICP-MS analyzer.

2. Experimental

2.1. Apparatus

The GBC atomic absorption spectrophotometer equipped with flame and graphite tube (electrical furnace) were used for the determination of lead in blood and serum samples (F-AAS, ET-AAS, GBC 932 plus, Australia). The Pal GF3000 as auto sampler accessory for ET-AAS was used as a low volume of samples for lead determination by injecting 1-100 µL of sample to graphite tube (wavelength 283.3 nm, slit 0.5 nm, lamp current 5.0 mA). Also, the auto sampler accessory for flame technique was used (0.5-5 mL). After atomization process in flame or graphite tube, the ppm and ppb concentration of lead was determined in liquid samples, respectively (Table 1). The ICP-MS analyzer with high sensitivity was used for as ultra-trace lead determination in human blood samples (Perkin Elmer, USA, 1100 W; 14 L min^{-1}; 1.2 sec per mass; auxiliary gas 1.1 L min^{-1}). The pH meter was used for measuring pH in blood samples (Metrohm, E-744, Switzerland). The shacking of samples was achieved by 300 rpm speeds by vortex mixer (Thermo, USA) and samples centrifuged with Falcon accessory (4000 rpm, 5-30 mL of polypropylene conical tubes, USA). An ultrasonic bath was used for dispersing of solid phase in blood samples with the temperature controlling accessory between 10-100°C (HB120, USA). The X-ray diffraction (XRD) based on a Panalytical X'Pert PRO X-ray diffractometer was used. The scanning electron microscopy (SEM) images were obtained using a Tescan Mira, Field Emission Scanning Electron Microscope (FEG-SEM).

Table 1. The AT-F-AAS and ET-AAS conditions for lead (Pb) determination

Features	AT-F-AAS	ET-AAS
Linear range	0.1-6.2 (mg L^{-1})	5-145 (µg L^{-1})
Wavelength	283.3 nm	283.3 nm
Lamp current	5.0 mA	5.0 mA
Slit	0.5 nm	0.5 nm
Mode	Peak Area	Peak Area
Atomization	Air-Acetylene	Electrical
Auto Sampler	0.5-5.0(mL)	1-100(µL)
LOD	0.03(mg L^{-1})	1.2(µg L^{-1})
R^2	0.9998	0.9995

2.2. Reagents

The standard solution of lead (Pb^{2+}) was purchased from Merck with a concentration of 1000 mg L^{-1} in 1 % HNO_3 (CAS N: 119776, 1 Li, Germany). The calibration standard of lead between 0.5-60 µg L^{-1} was daily prepared by diluting of lead stock. Ammonium pyrrolidinedithiocarbamate as ligand (APDC, CAS N.: 169209-63-6) was prepared from Merck. Germany. Ultrapure water was purchased from Millipore Company (USA) for dilution of solutions or standards. The hydrophobic ionic liquid of 1-Hexyl-3-methylimidazolium hexafluorophosphate was prepared from Sigma Aldrich (CAS N: 304680-35). The pH of 6 was adjusted by sodium phosphate buffer solution (Merck, Germany, (Na_2HPO_4/NaH_2PO_4). The polyoxyethylene octyl phenyl ether (TX-100), HNO_3, HCl, acetone, and butanol were purchased from Sigma Aldrich, Germany.

2.3. Human and air sample

For preparation of blood samples, the glass mixed in nitric acid (1 M) for 24 h and washed with DW for 8 times. The low concentrations of lead in blood samples (<250 µg L^{-1}), caused to the effect on accurate results. So, the process of blood sampling was carefully done based on standard methods. The 5 mL of blood samples were prepared from battery workers from Iran (40 Men, 25-55 age) due to world medical association declaration of Helsinki and dilution with DW up to 10 mL. Clean tubes and syringes with plastic needles were purchased for Merck, Germany for blood sampling. The 10 µL heparin (pure metals) was added to human blood sample. The blood samples were maintained frozen in refrigerator below -4°C.

The air sampling for lead was prepared based on Filter (0.8 µm cellulose ester membrane) by 7082 NIOSH method. The flowrate adjusted 1 to 4 L min^{-1} and ashing process with 6 mL of HNO_3, 1 mL of H_2O_2 (30%) at 140 °C was achieved. The working standards covering the range 0.25 -20 µg mL^{-1} of Pb used for calibration method (2.5-200 µg lead per sample). The lead concentration in workplace air was determined by F-AAS and D_2 or H_2 continuum or Zeeman background correction used to control flame or molecular absorption. The working range between 0.05 -1 mg m^{-3} for a 200 L of air sample was selected. In addition, the flow rate between 1.0 - 4.0 L min^{-1} for 8 h was used by personal pump.

2.4. Synthesis of IL/GONPs

The mixture ionic liquid with ligand ([HMIM][PF_6]/APDC) modified on graphene oxide nanostructures(GONs) and used as adsorbent for lead extraction. The synthesis of graphene oxide (GO) was followed by the modified Hummers method [31-33]. First, 10 g of graphite powder was mixed with 500 mL of H_2SO_4 and stirred for one day. Then, $KMnO_4$ (48 g) was mixed to the above mixture at 55 °C. Next, the mixture was moved into a beaker with 1000 mL of ice. Also, 100 mL of H_2O_2 in 1000 mL of DW was added to the mixture up to create a yellow color. The product was washed with deionized water and HCl for many times and dried at 70 °C. Then, 0.1 g of APDC mixed with 0.25 g

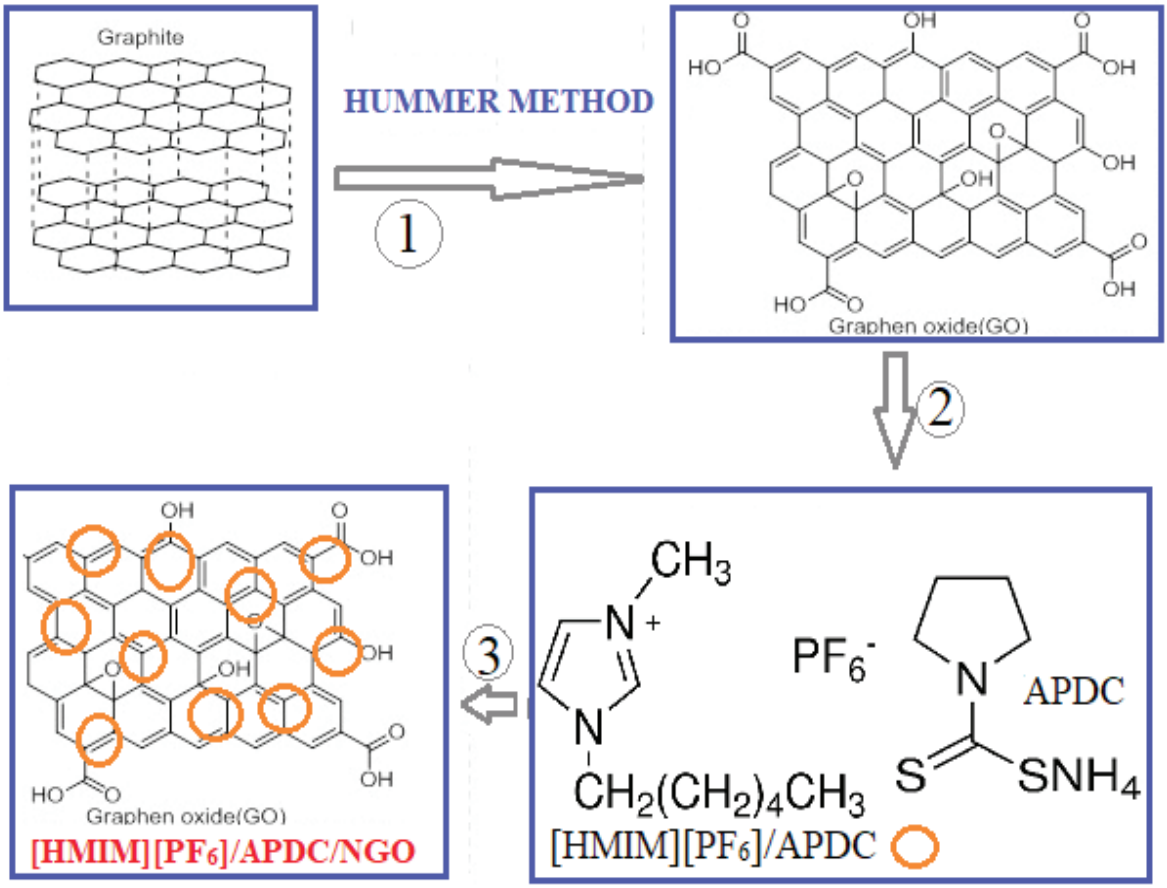

Fig.1. Synthesis of ([HMIM][PF_6]/APDC) modified on graphene oxide

of IL in presence of 2 mL of acetone and 0.2 g of GO. After increasing temperature up to 50°C, the mixture of IL/APDC were uniformly modified on Go (Fig.1). Finally, 20 mg of adsorbent selected for lead extraction in blood samples.

2.5. Extraction Procedure

In the DIL-SPME method, 10 mL of blood samples were used for extraction and determination of lead ions at pH 6.0. By procedure, 20 mg of IL/APDC modified on GO were injected to human blood samples and standard solution (5 - 310 µg L^{-1}) at pH=6.0 (Fig.2). After sonication of samples for 3.0 min, the lead separated and extracted with the APDC on adsorbent as sulfur coordination bonding in liquid phase (Pb^{2+}→: APDC/IL-GONPs). By centrifuging (5 min; 4000 rpm), the solid phase trapped in [HMIM][PF_6] phase and collected from the samples in the end of the conical tube. The liquid phase was set aside and the lead ions back-extracted from ([HMIM][PF_6]/APDC)/NGO adsorbent in pH=2 (HNO_3, 0.5 M, 200 µL) and diluted with 300 µL of DW before determined by F-AAS. In addition, On the other hand, the 10 mL of standard solution was used based on the DIL-SPME procedure by the same conditions at pH=6.0. A blank run without any lead ions was used for ten times. The calibration curve for lead in standards solutions was prepared. The analytical procedure was showed in Table 2. Validation was followed by CRM of lead and real samples, which was analyzed by ETAAS and ICP-MS analyzer. The concentration lead in work place air was achieved based on 7082 NIOSH method for 40 workers and the mean concentration in air were obtained 65.6 µgm^{-3} for TWA measurements. The recovery of lead procedure in blood samples based on APDC/IL-GONPs was obtained by the equation 1. The C_i is the primary concentrations and C_f is the secondary concentration of Pb(II), which was determined by APDC/IL-GONPs coupled DIL-SPME procedure (n=8).

$$R\% = (C_i - C_f)/C_i \times 100 \qquad \text{(Eq.1)}$$

For workplace air, after determination lead in filter, the concentrations (C_s, µg mL^{-1}) of lead in the sample air was achieved by NIOSH method (The average blank, C_b). The concentration in air calculated based on equation 2, the volumes (mL) of the sample and media blanks is V_s and V_b, respectively. Finally, the C (mg m^{-3}), of lead showed the concentration lead in air where the air volume sampled was V (L).

$$C = \frac{C_s V_s - C_b V_b}{V} \qquad \text{(Eq. 2)}$$

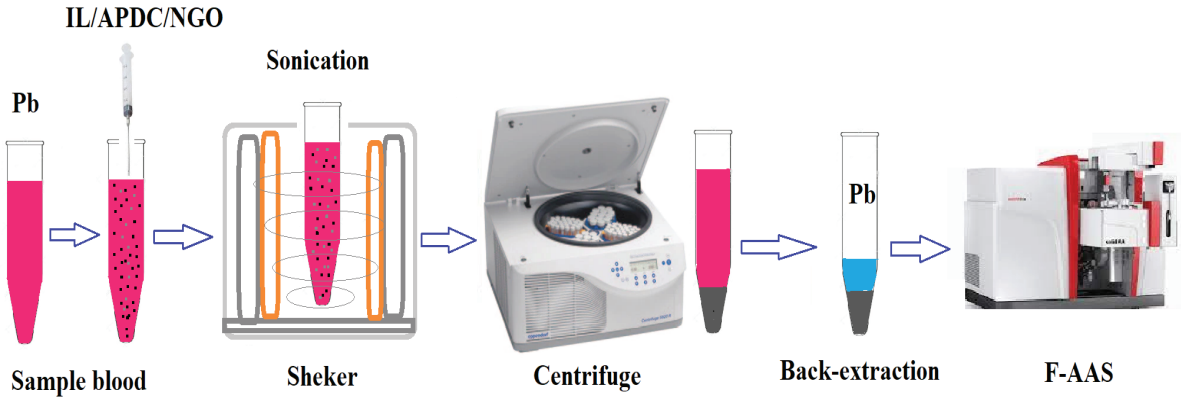

Fig.2. Lead extraction based on APDC/IL/NGO coupled to DIL-SPME procedure

Table 2. The analytical features for determination lead in human blood samples by DIL-SPME procedure

Features	value
pH	6.0
Amount of APDC/IL modified on GONPs (mg)	20.0
Sample volume of blood, serum (mL)	10 .0
Volume of sample injection	0.5 mL
Linear range for blood	5-310 µg L^{-1}
Mean RSD %, n=8	4.6
LOD for blood	1.25 µg L^{-1}
Enrichment factor for blood	19.6
Volume and concentration of HNO_3	0.2 mL,0.5 M
Shaking/Centrifuging time	3.0 min, 5 min
Correlation coefficient	$R^2 = 0.9995$

3. Results and discussion

3.1. Characterization

XRD patterns of GO and APDC/IL/GO are similar and shown in Figure 3. Graphene oxide exhibits the sole main diffraction peak at 2θ = 12° corresponding to the oxygen functional groups which are intercalated between graphene sheets in the course of oxidation. The peaks at 2θ = 12° and 42.58° are related to the diffraction planes of (002) and (100) respectively, which can be observed in the XRD patterns of both GO and APDC/IL/GO. However, existence of this peak at about 2θ = 12° agrees well with the modification of graphene oxide with APDC and IL.

The morphology of GO and APDC/IL/GO are evaluated by scanning electron microscope (SEM) (Fig. 4). According to the SEM images (Fig. 4I and 4II), Comparison between the SEM images of GO and APDC/IL/GO revealed that, the modification of GO had no prominent effect on the morphology of the graphene sheets.

3.2. Optimization of proposed procedure

The DIL-SPME procedure with new IL/APDC/NGO was applied for the extraction and separation of lead ions in human blood samples. The high recovery for lead extraction was obtained by optimizing of parameters.

3.2.1. The pH optimization

The pH is the main factor for lead extraction in human blood samples by APDC ligand which was mixed with IL and modified on NGO. The various pH for lead extraction in blood samples was used and studied between 2-12. The results showed, the IL/APDC/NGO had highly lead extraction at pH of 5.5-6.5 (<95%). The complexation of lead with APDC were decreased at pH less than 5 and

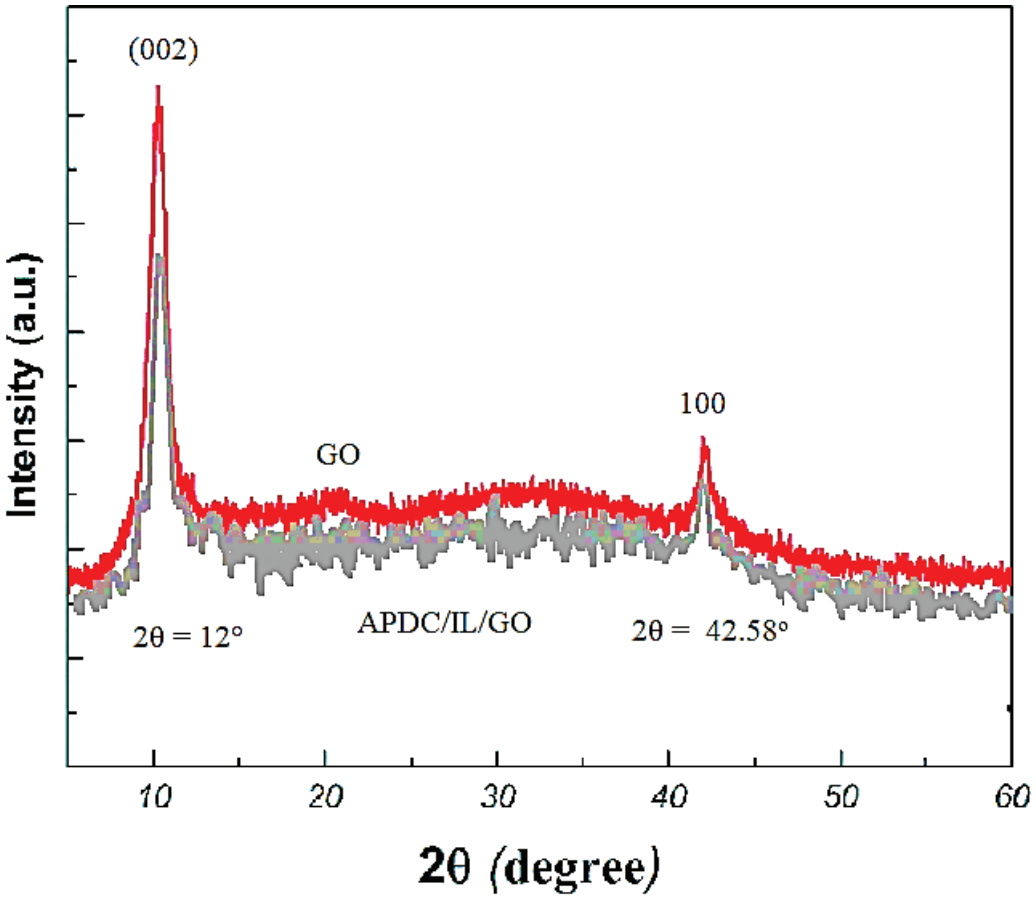

Fig.3. XRD of NGO and IL/APDC/NGO

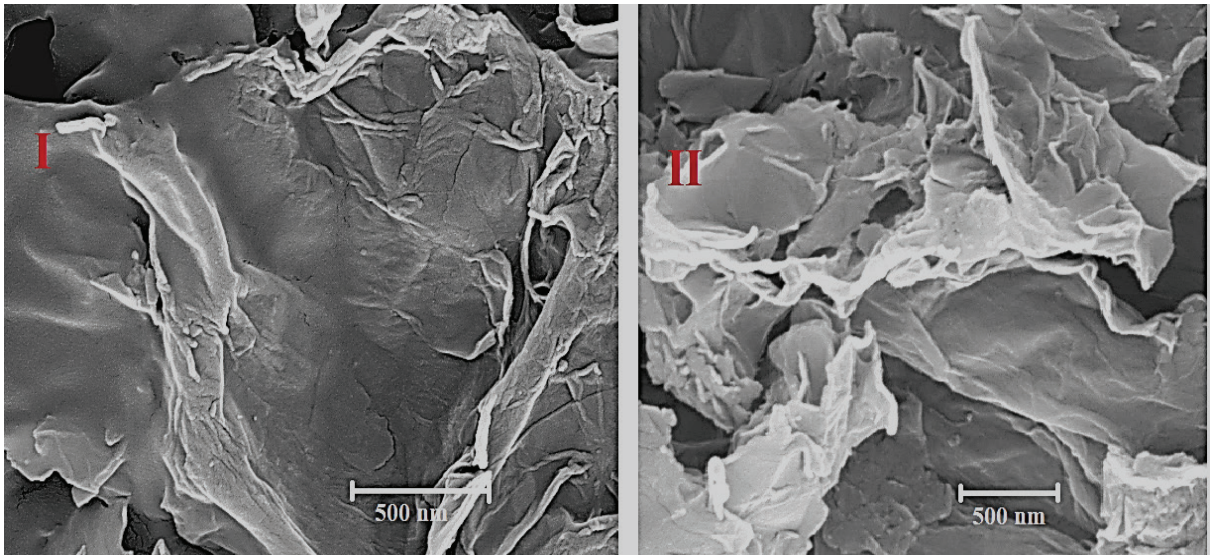

Fig.4. I (SEM of NGO II) SEM of IL/APDC/NGO

pH more than 6.5. So, the pH=6 was selected as optimum pH for lead extraction in blood samples (Fig. 5). The mechanism of lead extraction depended on sulfur group in APDC which was created a dative bond with Pb ions in liquid phase (Pb^{2+}→:S….APDC/IL/NGO-GO). At lower pH the surface of adsorbent had positive-charge (S+) and extraction decreased due to similarity charges law. At pH of 6.0, the surface of APDC/IL/NGO have negatively charged (S─) and Pb (+) complexed by sulfur groups. Moreover, the lead participated in liquid phase ($Pb(OH)_2$) and the extraction efficiency was decreased at more than pH of 7. Therefore, the pH=6 used for further studies in blood samples.

3.2.2. Optimization of APDC/IL/NGO mass

The high extraction was achieved based on APDC/IL/NGO mass which was depended to sulfur group of APDC as complexation. So, the mass of APDC/IL/NGO must be optimized conditions. The amounts of APDC/IL/NGO between 2-50 mg in human blood samples and standard solution were studied for lead extraction by DIL-SPME procedure. As Figure 6, the maximum recoveries were achieved for Pb extraction by 20 mg of APDC/IL/NGO in human blood samples. So, 20 mg of APDC/IL/NGO was selected for experimental run by DIL-SPME procedure. The extraction efficiency of lead had constant rate for more than 20 mg of APDC/IL/NGO in blood samples.

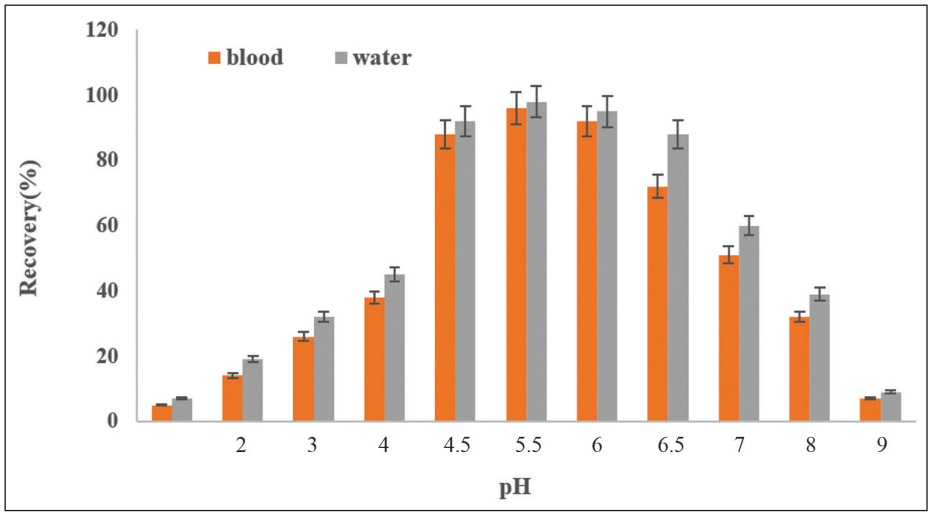

Fig.5. The effect of pH on lead extraction based on APDC/IL/NGO by DIL-SPME procedure

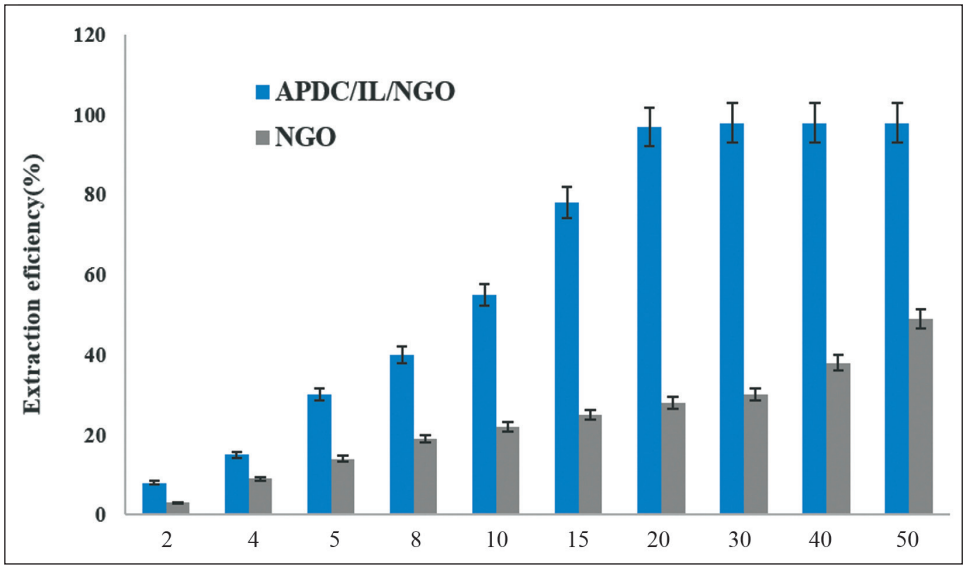

Fig.6. The effect of amount of APDC/IL/NGO on lead extraction based on APDC/IL/NGO by DIL-SPME procedure

3.2.3.Optimization of sample volume and eluent

The volume and concentration of eluents such as acid or bases is important for back extraction Pb ions from APDC/IL/NGO were studied. The low/ high pH caused to dissociate the sulfur-Pb covalent bonds and released the Pb ions from adsorbent. So, the different reagents (HCl, HNO_3, CH_3COOH, H_2SO_4, H_2CO_3) were used for the back-extraction of lead from APDC/IL/NGO to liquid solutions. The 0.1-1.0 molar of various eluents with different volumes from 0.1 to 0.7 mL was studied. Due to Figure 7, the efficient recovery obtained by 0.2 mL of HNO_3 (0.5 M). In addition, the volume of blood and standard solutions for lead extraction based on APDC/IL/NGO adsorbent was optimized from 1.0 mL to 20.0 mL for LLOQ and ULLOQ concentration of Pb(II) (5.0-310 µg L^{-1}). The results showed that the best recovery was achieved less than 10 mL for in blood samples at pH=6. therefore, the 10 mL of blood or standard solution was used for further work (Fig. 8).

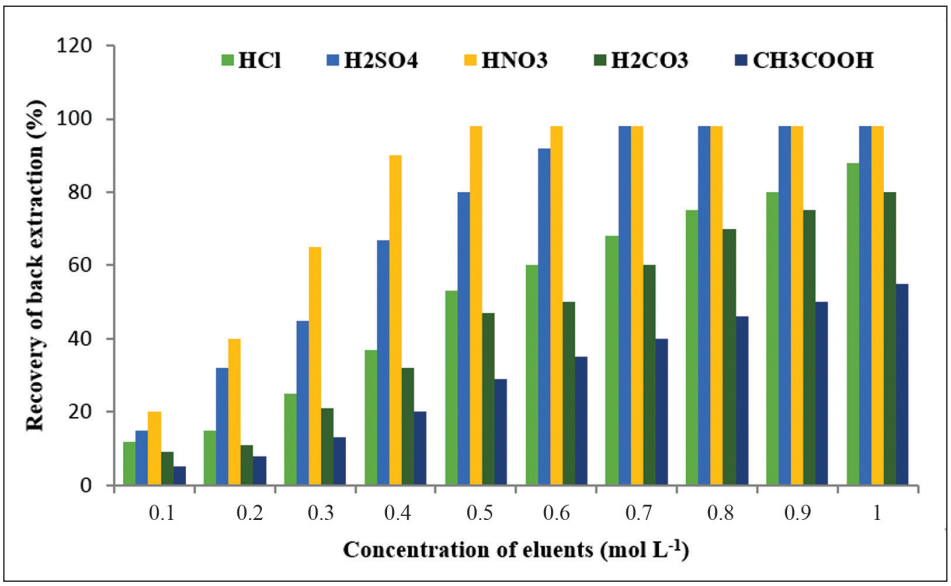

Fig.7. The effect of eluents on lead extraction based on APDC/IL/NGO by DIL-SPME procedure

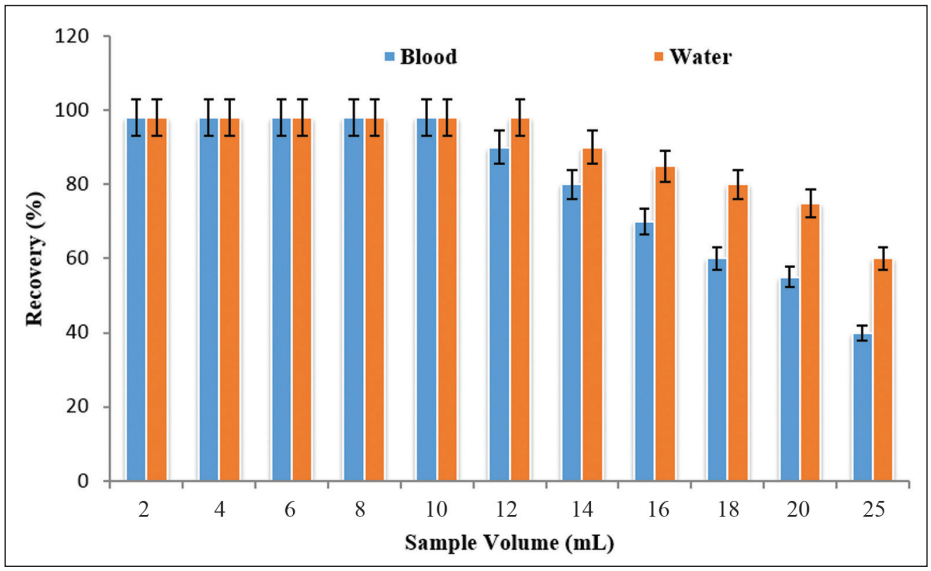

Fig.8. The effect of sample volume on lead extraction based on APDC/IL/NGO by DIL-SPME procedure

3.2.4.Optimization of time, reusability and absorption capacity

The time dispersion of APDC/IL/NGO adsorbent in blood or standard samples had a main factor for efficient extraction of lead. Moreover, the mass-transference between APDC/IL/NGO and Pb ions was occurred at pH=6 by DIL-SPME procedure. In optimized conditions, the sonication time was evaluated between 1 - 8 min. the results showed that the sonication time of 3.0 min has maximum extraction of lead in blood samples. In addition, the centrifuging time between 1-10 min (4000 rpm) was used for collecting sorbent in end of conical tube. Based on results, 5 min of centrifuge time is enough time for efficient extraction of lead. Finally, the lead ions were back-extracted from APDC/IL/NGO by changing pH and determined by F-AAS. The reusability of APDC/IL/NGO was obtained with many times extraction process by DIL-SPME procedure. The results showed, the DIL-SPME can be used for less than 7 cycles for lead extraction at optimized pH in room temperature. The absorption capacities for lead depended on chemical and physical properties of APDC/IL/NGO in bath system. The absorption capacities of APDC/IL/NGO for Pb ions examined with 50 mg L^{-1} in optimized conditions. The adsorption capacity of APDC/IL/NGO and NGO for Pb ions was achieved 154.7 mg g^{-1} and 28.9 mg g^{-1}, respectively.

3.2.5.Interference cations and anions

For extraction lead in blood samples, the effect of interference of ions was studied by DIL-SPME procedure. So, the concentrations of cations and anions in human blood such as Cu, Zn, Mn, Mg, Ca, Fe and etc. (1-2 ppm) added to 10 mL of standard solution or human blood samples in presence of 300 µg L^{-1} of lead at pH=6. The recovery of lead extraction in presence of the concomitant cations/anions couldn't decreased at pH=6. Therefore, the Pb ions can be extracted based on APDC/IL/NGO in blood samples in presence of some coexisting ions (Table 3).

3.2.6.Real sample analysis

The concentration of lead in human blood and standard samples was determined by DIL-SPME procedure. The lead was efficiently extracted based on APDC/IL/NGO adsorbent from human blood samples and obtained results were validated by electrothermal atomic absorption spectrometry (ET-AAS) and ICP-MS techniques (Table 4). In this study, the validation based on spiking real

Table 3. The effect of interference cations and anions for lead extraction by the DIL-SPME procedure

Interfering Ions in blood (A)	Mean ratio (C_A /$C_{Pb(II)}$)	Recovery (%)
	Pb(II)	Pb(II)
Co^{2+}, Fe^{2+}	550	99.3
Zn^{2+}, Cu^{2+}	850	98.1
Mn^{2+}, Mo^{2+}	600	96.5
I^- , Br^-, F^-, Cl^-	1100	97.4
Na^+, K^+	1000	99.3
Ca^{2+}, Mg^{2+}	1200	98.4
CO_3^{2-}, PO_4^{3-},NO_3^-	650	97.4
Ni^{2+}	300	98.1
Al^{3+}, V^{3+}, Cr^{3+}	900	97.7
Hg^{2+}, Ag^+	120	98.2

samples with a standard solution were achieved in human blood and serum samples by APDC/IL/NGO adsorbent (Table 5). The results demonstrated the efficient recovery for lead ions in difficulty matrixes in blood samples. The spiked samples showed a accurate results for separation/extraction/determination /preconcentration of human blood samples by APDC/IL/NGO adsorbent. As intra-day and inter-day analysis, the 40 human blood workers of battery manufacturing factories determined by same procedure ((25-55, Men, Iran) and compared to office people as control markers (Table 6).

Table 4. The validation of proposed method for lead extraction in human matrixes by ICP-MS and ET-AAS (µgL^{-1})

Samples	ICP-MS✳	DIL-SPME /F-AAS ✳	ET-AAS✳
Serum	253.8 ± 7.2	244.9 ± 10.2	248.3 ± 12.7
Blood	302.7 ± 7.8	290.6 ± 11.6	295.1 ± 14.2
Plasma	142.5 ± 3.8	139.4 ± 5.5	145.6 ± 6.9

✳Mean of three determinations ± cconfidence interval (P= 0.95, n=5),
As low LOD for ET-AAS and ICP-MS the samples diluted with DW before analysis

Table 5. Spiking real samples with a standard solution in human blood, serum and plasma samples by APDC/IL/NGO adsorbent(µgL^{-1})

Sample	Added	✳ Found	Recovery (%)
Serum	-----	123.2± 5.3	----
	50	170.9 ± 7.6	95.4
	100	225.4± 9.8	102.2
Blood	-----	111.3± 4.9	-----
	50	159.4 ± 6.1	96.2
	100	209.8± 9.2	98.5
Plasma	-----	84.5 ± 4.2	-----
	50	133.6 ± 5.8	98.2
	100	183.7 ± 8.8	99.2

✳ Mean of three determinations ± cconfidence interval (P= 0.95, n=5)

Table 6. Comparing of mean lead concentration in human blood of battery workers with control peoples by DIL-SPME procedure (μgL^{-1})

Sample	✳Mean of Subjects (n=40)		✳Mean of Controls (n=40)		✦Data Subject	
	Intra-day	Inter day	Intra-day	Inter day	r	P value
Plasma	194.2± 8.7	191.5 ± 8.6	47.1 ± 2.3	48.4 ± 2.5	0.090	<0.001
Serum	401.2 ± 19.3	397.7± 18.9	94.4 ± 4.6	90.8 ± 4.4	0.088	<0.001
Blood	382.5 ± 18.4	386.3 ± 18.6	88.2 ± 4.1	85.9± 3.9	0.101	<0.001

✳Mean of three determinations of samples ± confidence interval (P = 0.95, n =10)
✦Correlations are based on Pearson coefficients (r). Statistical significance will be observed if P < 0.001
Subject and control groups belong to *battery* workers and control peoples

Table 7. The validation of methodology for lead extraction with certified reference material (CRM, ICP-MS) by DIL-SPME procedure(μgL^{-1})

SRM	Added	Found by µ-SPE ✦	Recovery (%)
ICP-MS A	-------	120.4 ± 5.7	-------
	50	168.1 ± 7.3	95.4
	100	218.5 ± 9.9	98.1
ICP-MS B	-------	208.7 ± 9.8	-------
	50	260.1 ± 14.2	102.8
	100	305.4 ± 14.2	96.7

✦ Mean value ± standard deviation based on three replicate measurements
ICP-MS: blood analysis for lead, A=122.5 ngL^{-1}, B=210.3 (μgL^{-1})

In addition, the blood samples were validated by certified reference materials (CRM, NIST) by DIL-SPME procedure (Table 7). Based on table 4-7, the precision and accuracy of results was satisfactorily confirmed in human blood samples.

4. Conclusions

An applied adsorbent based on APDC/IL/NGO was used for separation, preconcentration and determination of lead in blood samples by the DIL-SPME procedure. The IL was helped to separate the solid phase from liquid matrixes in bottom of conical tube which was modified on NGO. By DIL-SPME procedure, the simple, perfect recovery and fast analysis was achieved for lead at pH=6.0 by APDC/IL/NGO sorbent. The modification of NGO surface with IL/APDC helped to enhance the lead extraction in blood samples. Also, some advantages of proposed method such as, fast separation, low cost, and high extraction caused to comparable to ICP-MS analyzer. The LOD and linear range(LR) has acceptable level for lead analysis in human biological samples. Therefore, the extraction and determination lead with APDC/IL modified on NGO in human blood were simply achieved based on sulfur dative bond in optimized conditions by DIL-SPME procedure before determined by F-AAS. The lead analysis in workplace air was achieved based on NIOSH method for 40 workers and range/mean concentrations in air were obtained 44.7-81.5 μgm^{-3} and 65.6 μgm^{-3}, respectively for a 200 L of air sample which was higher than standard of lead in air by NIOSH (50 μgm^{-3}).

5. Acknowledgements

The authors wish to thank from Faculty of Natural resources and Environment, Science and Research branch, Islamic Azad University, Tehran, Iran and Birjand university, Birjand, Iran.

6. References

[1] J. Briffa, E. Sinagra, R, Blundell, Heavy metal pollution in the environment and their toxicological effects on humans, Heliyon, 6 (2020) e04691.

[2] A.L. Wani, A. Ara, J.A. Usmani, Lead toxicity: A review, Int. Toxicol., 8 (2015) 55–64.

[3] Lead toxicity: what Is the biological Fate of Lead in the Body, environmental health and medicine education, Agency for toxic substances and disease registry (ATSDR), 2017. https://www.atsdr.cdc.gov/csem/csem.asp?csem=34&po=9

[4] M. Tamayo y Ortiz, M.M. Téllez-Rojo, H. Hu, M. Hernandez-Avila, R. Wright, C. Amarasiriwardena, N. Lupoli, A. Mercado-Garcia, I. Pantic, H. Lamadrid-Figueroa, Lead in candy consumed and blood lead levels of children living in Mexico City, Environ. Res., 147 (2016) 497–502

[5] J. Wieczorek, A. Baran, K. Urba ´nski, R. Mazurek, A. Klimowicz-Pawlas, Assessment of the pollution and ecological risk of lead and cadmium in soils, Environ. Geochem. Health, 40 (2018) 2325–2342.

[6] J. Ahn, M.Y. Park, M.Y. Kang, I.S. Shin, S. An, H.R. Kim, Occupational lead exposure and brain tumors: systematic review and meta-analysis, Int. J. Environ. Res. Public Health, 17 (2020) 3975.

[7] J. Sirivarasai, S. Kaojarern, S. Chanprasertyothin, P. Panpunuan, K. Petchpoung, A. Tatsaneeyapant, K. Yoovathaworn, T. Sura, S. Kaojarern, P. Sritara, Environmental lead exposure, catalase gene, and markers of antioxidant and oxidative stress relation to hypertension: An analysis based on the EGAT study, Biomed. Res. Int., 2015 (2015) 856319.

[8] F. Aarabi, M. Kusajima, T. Tohge, T. Konishi, T. Gigolashvili, M. Takamune, Y. Sasazaki, M. Watanabe, H. Nakashita, A.R. Fernie, Sulfur deficiency-induced repressor proteins optimize glucosinolate biosynthesis in plants, Sci. Adv., 2 (2016) e1601087.

[9] O. P. Ajsuvakovaa, A. A. Tinkov, Sulfhydryl groups as targets of mercury toxicity, Coord. Chem. Rev., 15 (2020) 417. http://doi.org/10.1016/j.ccr.2020.213343.

[10] Environmental Protection Agency (EPA), Basic information about lead in drinking water, 2014.

[11] United States Food and Drug Administration (FDA), Elemental impurities guidance for industry, Department of Health and Human Services, p. 41, 2017.

[12] US department of health and human services, national institute for occupational safety and health (NIOSH); Adult blood lead epidemiology and surveillance (ABLES), 2017.

[13] S. Triantafyllidou, J. Burkhardt, Variability and sampling of lead (Pb) in drinking water: Assessing potential human exposure depends on the sampling protocol, Environ. Int., 146 (2021) 106259.

[14] S. Kapitány, D. Nagy, J. Posta, A .Béni, Determination of atmospheric sulphur dioxide and sulphuric acid traces by indirect flame atomic absorption method, Microchem. J., 157 (2020) 104853.

[15] T. Amiri-Yazani, R. Zare-Dorabei, M. Rabbani, A. Mollahosseini, Highly efficient ultrasonic-assisted pre-concentration and simultaneous determination of trace amounts of Pb (II) and Cd (II) ions using modified magnetic natural clinoptilolite zeolite: Response surface methodology, Microchem. J., 146 (2019) 498-508.

[16] P. Montoro-Leal, J.C. García-Mesa, M.T. Siles Cordero, Magnetic dispersive solid phase extraction for simultaneous enrichment of cadmium and lead in environmental water samples, Microchem. J., 155 (2019) 104796.

[17] J.S.F. Pereira, D. P. Moraes, Determination of metals and metalloids in light and heavy crude oil by ICP-MS after digestion by microwave-induced combustion, Microchem. J., 96 (2010) 4-11.

[18] V. Balaram, Microwave plasma atomic emission spectrometry (MP-AES) and its applications – A critical review, Microchem. J., 159 (2020)105483.

[19] S.M. S. Khademi, A. Salemi, Development and comparison of direct immersion solid phase micro extraction Arrow-GC-MS for the determination of selected pesticides in water, Microchem. J., 164 (2021) 106006.

[20] V. CâmaraCosta, M. Limade Mello, Calibration strategies for determination of Pb content in recycled polypropylene from car batteries using laser-induced breakdown spectroscopy (LIBS), Microchem. J., 159 (2020) 105558.

[21] Y. Song, Q. Ma, H. Cheng, J. Liu, Y. Wang, Simultaneous enrichment of inorganic and organic species of lead and mercury in pg L^{-1} levels by solid phase extraction online combined with high performance liquid chromatography and inductively coupled plasma mass spectrometry, Anal. Chim. Acta, 1157 (2021) 338388.

[22] Y.-K. Li, W. Li, X. Liu, T. Yang, M.L. Chen, J.H. Wang, Functionalized magnetic composites based on the aptamer serve as novel bio-adsorbent for the separation and preconcentration of trace lead, Talanta, 203 (2019) 210-219.

[23] V. de Jesus Ferreira, J. S. Almeida, Determination of Cu, Ni, Mn, and Pb in diesel oil samples using reversed-phase vortex-assisted liquid-liquid microextraction associated with energy dispersive X-ray fluorescence spectrometry, Talanta, 222 (2021) 121514.

[24] A. H. Kame, A.Ei-Galil, E.Amr, Pre-concentration based on cloud point extraction for ultra-trace monitoring of lead (II) using flame atomic absorption spectrometry, Appl. Sci., 22 (2019) 4752. https://doi.org/10.3390/app9224752

[25] M. Ghazaghi, H. Shirkhanloo, H.Z. Mousavi, A.M. Rashidi, Ultrasound-assisted dispersive solid phase extraction of cadmium(II) and lead(II) using a hybrid nanoadsorbent composed of graphene and the zeolite clinoptilolite, Microchim. Acta, 182 (2015)1263-1272.

[26] M. Shokri, A. Beiraghi, S. Seidi, In situ emulsification microextraction using a dicationic ionic liquid followed by magnetic assisted physisorption for determination of lead prior to micro-sampling flame atomic absorption spectrometry, Anal. Chim. Acta, 889 (2015) 123-129.

[27] M. Vesali-Naseh, M. RezaVesali Naseh, P. Amer, Adsorption of Pb (II) ions from aqueous solutions using carbon nanotubes: A systematic review, J. Clean. Prod., 291 (2021) 125917.

[28] N. Rahman, M. Nasir, P.Varshney, Efficient removal of Pb(II) from water using silica gel functionalized with thiosalicylic acid: Response surface methodology for optimization, J. King Saud. Un. Sci., 33 (2021) 101232.

[29] N. Manousi, E. Rosenberg, E. A. Deliyanni, Sample preparation using graphene-oxide-derived nanomaterials for the extraction of metals, Molecules, 25 (2020) 2411. https://doi.org/10.3390/molecules25102411

[30] S. Mirza, N. Mansouri, R. Arjmandi, R. Azizinejad, Evaluation and comparison of health, safety and environmental management system in oil and petrochemical downstream industries (Case Study of Textile Factories), J. Health safe. Work, 1132-35 (2021) .

[31] W.S.J. Hummers, R.E. Offeman, Preparation of Graphitic Oxide, J. Am. Chem. Soc., 80 (1958) 1339.

[32] M.K. Abbasabadi, A. Rashidi, S. Khodabakhshi, Benzenesulfonic acid-grafted graphene as a new and green nanoadsorbent in hydrogen sulfide removal, J. Nat. Gas Sci. Eng., 28 (2016) 87-94.

[33] M. Khaleghi-Abbasabadi, D. Azarifar, Magnetic Fe3O4-supported sulfonic acid-functionalized graphene oxide (Fe3O4@GO-naphthalene-SO3H): a novel and recyclable nanocatalyst for green one-pot synthesis of 5-oxo-dihydropyrano[3,2-c]chromenes and 2-amino-3-cyano-1,4,5,6-tetrahydropyrano[3,2-c] quinolin-5-ones, Res. Chem. Intermed. 45 (2019) 2095-2118.

Anal. Methods Environ. Chem. J. 4 (2) (2021) 60-71

AMECJ

Research Article, Issue 2
Analytical Methods in Environmental Chemistry Journal
Journal home page: www.amecj.com/ir

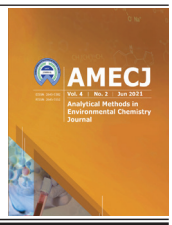

Effects of malathion exposure on glucose tolerance test in diabetic rats; emphasis on oxidative stress and blood concentration of malathion by gas chromatography mass spectrometry

Seyedeh-Azam Hosseini[a], Ali Faghihi zarandi[b] and Somayyeh Karami-Mohajeri[a,c,*]

[a] *Pharmaceutics Research Center, Institute of Neuropharmacology, Kerman University of Medical Sciences, Kerman, Iran.*
[b] *Department of Occupational Health Engineering, School of Public Health, , Kerman University of Medical Sciences, Kerman, Iran.*
[c] *Department of Toxicology and Pharmacology, School of Pharmacy, Kerman University of Medical Sciences, Kerman, Iran*

ARTICLE INFO:

Received 25 Feb 2021
Revised form 29 Apr 2021
Accepted 21 May 2021
Available online 29 Jun 2021

Keywords:
Malathion,
Blood samples,
Diabetes,
Oxidative stress,
Erythrocyte,
Magnetic graphene oxide,
Gas chromatography mass spectrometry

ABSTRACT

Malathion is one of the widely used broad-spectrum organophosphate insecticides (OPI) in Iran. Malathion affects carbohydrate metabolism, causes hyperglycemia and increases the risk of diabetes. The present study was undertaken to investigate the potential of malathion to exacerbate diabetes-induced oxidative stress and impairment in blood glucose level and glucose tolerance in a sub-acute study. Malathion concentration in blood was analyzed with gas chromatography mass spectrometry (GC-MS) after sample preparation of blood samples based on magnetic Fe_3O_4-supported graphene oxide (Fe_3O_4@ GO) nanoparticles. Type 1 diabetes was experimentally induced by intraperitoneal administration of streptozocin (65 mg kg^{-1}). Diabetic and non-diabetic rats were treated with malathion at the dose of 150 mg $kg^{-1}day^{-1}$ or 0.5-4.0 mg L^{-1} in blood for 4 weeks. Fasting blood glucose was measured every week. At the end of the study, blood samples were investigated for markers of oxidative stress. Exposure to multiple doses of malathion decreased the total antioxidant capacity of plasma and the activity of catalase and superoxide dismutase enzymes in diabetic rats. Blood glucose and glucose tolerance test (GTT) and oxidative damages did not change significantly in diabetic rats exposed to malathion. However, malathion concentration in blood caused to increase GTT in malathion-treated non-diabetic rats. Taking together, our findings provide evidence that daily exposure to malathion for 4 weeks tends to exacerbate the decrease in blood antioxidant status and protein carbonylation in diabetic rats.

1. Introduction

The agricultural application of pesticides in the world has been linked to a wide range of human health hazards through occupational, accidental, and intentional exposures [1]. It seems that among all pesticides, organophosphate insecticides (OPI) are more toxic to vertebrates with low mammalian toxicity [2, 3]. OPI inhibit acetylcholinesterase (AChE), which leads to the accumulation of acetylcholine in the cholinergic synapses and interfere with the normal function of the nervous system [4]. However, it has been shown that these pesticides have different toxicities *in vivo* and *in vitro* through AChE-independent mechanisms [5, 6].

*Corresponding Author: Somayyeh Karami-Mohajeri
Email: s_karami@kmu.ac.ir, somayyehkarami@gmail.com
https://doi.org/10.24200/amecj.v4.i02.141

OPI influences normal glucose homeostasis and carbohydrate metabolism and induces oxidative and nitrosative stress [7, 8]. Many techniques such as, UV-VIS, gas chromatography mass spectrometry, High Performance Liquid Chromatography (HPLC) and Liquid Chromatography [9, 10] were used for OPI and pesticides determination. The blood had difficulty matrixes and so must be treatment. Many sample preparation were used for treatment of blood samples for determination seven pesticides (malathion, methyl isofenphos, dichlorvos, chlorpyrifos, phenthoste, *p*,*p*′-DDD, *p*,*p*′-DDE) in blood samples based on a quick, easy, cheap, effective, rugged and safe (QuECh-ERS) sample preparation method. Occasionally, the Fe_3O_4 magnetic nanoparticles (MNPs) as the new adsorbing material was used for treatment of blood samples [11-14]. Although the foremost mechanism for hyperglycemia induced by OPI has not been recognized yet, some explanations are mentioned such as physiological stress, oxidative stress, paraoxonase enzyme inhibition, nitrosative stress, pancreatitis, cholinesterase inhibition, adrenal gland stimulation, and disturbance in liver tryptophan metabolism [15]. The human body is constantly exposed to various factors that contribute to the production of reactive oxygen species called free radicals. Imbalance between free radicals production and antioxidant systems lead to oxidative stress, which contributed to occurrence of the pathological conditions such as diabetes and development of diabetic complications [16-19]. Many toxic chemicals can generate reactive oxygen and trigger diabetes and hyperglycemia by induction of apoptosis in beta cells [20, 21]. Some evidence points to the long-term effects of OPI on glucose metabolism and increased risk of diabetes [15]. Malathion, one the of most popular OPI, has been used widely in agriculture, industry, and also for therapeutic purposes in humans (anti-louse) and animals (anti-ectoparasites) [22]. Malathion alters the pathways of carbohydrate metabolism mainly though increase in the activity of glycogen phosphorylase, phosphofructokinase, phosphoenolpyruvate carboxykinase, and hexokinase which affects glycolysis, gluconeogenesis, and glycogenolysis [15, 23]. Induction of oxidative and nitrosative stress in hepatocytes and pancreas beta cells are other contributing factors in hyperglycemia caused by Malathion [7, 23]. Activation of redox sensitive kinases and induction of oxidative stress in muscle cells after exposure to sub-toxic dose of malathion impairs insulin signaling and muscle glucose uptake and consequently causes insulin resistance state [24]. Hence, the present work has been designed to determine whether sub-acute exposure to repeated non-lethal dose of malathion can impair blood glucose control and exacerbate oxidative stress in diabetic rats. To do so, fasting blood glucose (FBG), glucose tolerance test (GTT), and biomarkers of oxidative damage were measured in non-diabetic and diabetic rats treated orally by sub-lethal dose of malathion for 4 weeks.

2. Materials and methods

2.1. Chemicals and methods

Technical-grade malathion, which contains >96% malathion, was obtained from the Shimi-Keshavarz Pesticides Production Company (Tehran, Iran). The name of malathion based on IUPAC (International Union of Pure and Applied Chemistry) is diethyl(dimethoxythiophosphorylthio) succinate; S-1,2-bis(ethoxycarbonyl) ethyl-O,O-dimethyl phosphorodithioate (CAS N.: 121-75-5, Sigma, Germany) and UV spectrum of malathion in acetonitrile (CAS N.: 75-05-08 , Merck, ACN) was shown in Schema 1. All other materials were purchased from the Merck and Sigma-Aldrich Chemical Company (St. Louis, MO). The HNO_3, HCl, polyoxyethylene octyl phenyl ether (MTX-100, CAS N: 9002-93-1, Sigma, Germany), acetone and toluene (CAS N: 108-88-3, Merck) were purchased from Merck, Germany. Anhydrous magnesium sulfate (CAS N: 10034-99-8), sodium chloride was purchased from Sigma (Germany). Acetonitrile (ACN) and methanol were purchased from Sigma Company (Germany). GC–MS (Agilent 7890A/5975C, USA) with HP-5MS column (30 m × 0.25 mm i.d.,) with flow of 1 mL per minute of

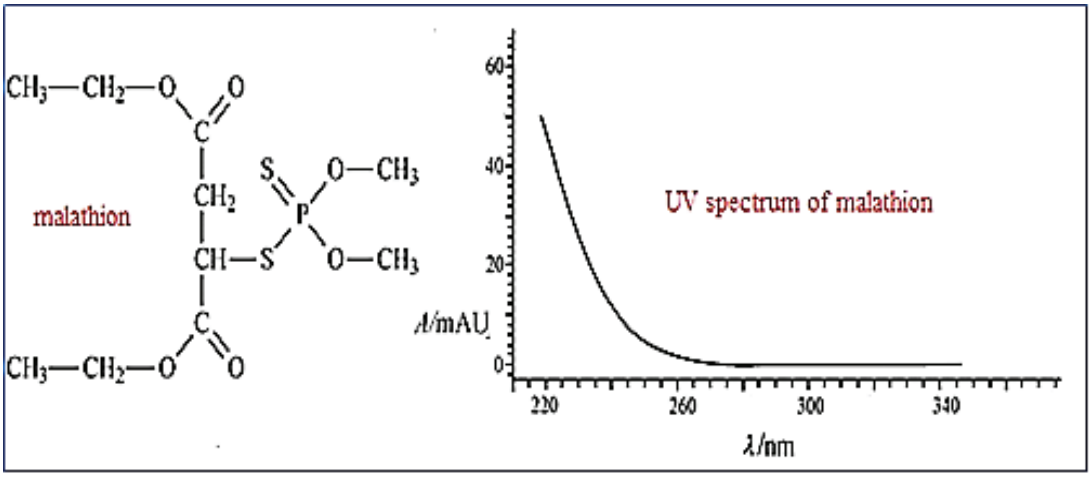

Shema 1. The structure and UV spectrum of malathion

He was used for qualitatively and quantitatively detecting pesticides in blood. Because blood is a complex matrix, and pesticides in blood are usually at low concentrations, the separation of malathion and elimination of interference in blood have needed a special sample treatment. Working standard solutions were prepared in DW. All these solutions were stored at 4 ºC without any light. The range of this study of malathion in blood is 0.3–4.4 µg mL^{-1} by GC-MS after dilution 1 mL of blood with DW.

2.2. Synthesis of magnetic Fe_3O_4-supported graphene oxide

The magnetic Fe_3O_4-supported graphene oxide (MNGO, Fe_3O_4@NGO) were prepared by co-precipitation of $FeCl_2{\cdot}4H_2O$ and $FeCl_3{\cdot}6H_2O$, in the presence of NGO [19]. firstly, a liquid solution of $FeCl_2{\cdot}4H_2O$ / $FeCl_3{\cdot}6H_2O$ was prepared (molar ratio= 1:2). The weight ratio of $FeCl_3$ / NGO in the product was m$FeCl_3$: mGO = 20:1. To prepare the magnetic graphene oxide (Fe_3O_4@NGO), 10 mg of graphene oxide mixed with 10 mL of DW and ultrasonicated for 30 min [19]. Then, 12.5 mL solution of $FeCl_2{\cdot}4H_2O$ (125 mg) and $FeCl_3{\cdot}6H_2O$ (200 mg) in DW was added to the mixture. Finally, the pH of 11 was achieved by 30% ammonia solution and the temperature was adjusted to 70 ˚C (Fig.1).

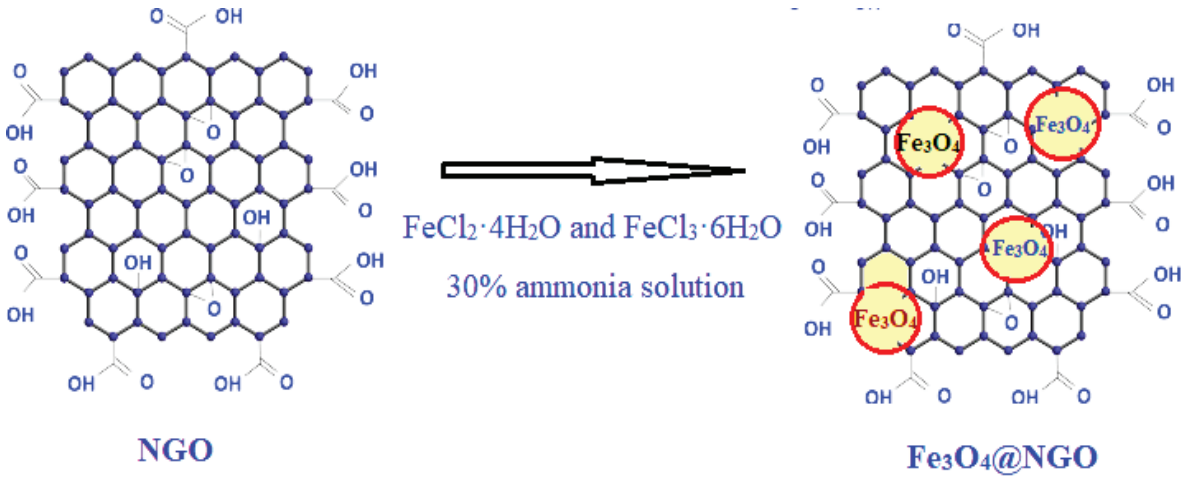

Fig.1. Synthesis of magnetic Fe_3O_4-supported graphene oxide [19]

2.3. Sample Extraction Procedure for malathion in blood

The sample preparation of blood samples in rat were prepared based on quick, easy, cheap, effective, rugged and safe (QuECh- ERS) method based on Fe_3O_4 magnetic nanoparticles (MNPs) functionalized with NGO. The free of DDC, DDT and malathion pesticide in blood samples were used as blank solution. 1 mL of rat blood sample was added into 10 mL of vial. Standard volumes of DDC, DDT and malathion pesticide were added to the vial, and then shaken for 1 min. The samples were extracted with 2 mL acetonitrile for 30 s. Anhydrous NaCl (0.1g) / $MgSO_4$ (0.3 g) were added to the mixture centrifuging at 4000 rpm for 5 min and then, the supernatant moved to 10 mL of vial include Fe_3O_4@NGO (0.04 g). The vial shake for 1 min, and the supernatant separated with an external magnet. Finally, the sample was dissolved in 50µL of acetonitrile and 1µL of solution was determined by GC–MS. The detection limits (LOD)and linear range(LR) of the QuECh- ERS method based on Fe_3O_4 @NGO obtained 0.1 µg mL^{-1} and 0.3–4.4 µg mL^{-1} with recoveries more than 95% [9-12].

2.4. Animals

Male Wistar rats weighing 211.5 ± 10.6 grams were fed with standard diet and kept under 12:12 hour light:dark cycle, at the temperature of 20 °C and relative humidity of 25 to 30%. This study received ethical approval (Code: IR.79.KMU.REC.1395-79) from the local ethical committee of the Kerman University of Medical Sciences.

2.5. Pilot experiment

A pilot test is designed to determine an oral dose of malathion which inhibits 30% of plasma ChE activity without significant physiological consequences and mortality within 4 weeks [25]. The treated groups (Ten rats in each group) received the oral doses of 75, 100, 150, and 300 mg/kg/day of malathion dissolved in corn oil for 4 weeks, while the controls received only corn oil. Blood samples were taken at the end of each week for measurement of plasma ChE activity according to the Ellman's colorimetric method with slight modification [26]. Briefly, 300 µl of 5,5′-Dithiobis(2-nitrobenzoic acid) (0.25 mM in 0.1M phosphate buffer, pH 7.4) was added to 10 µl of plasma and after 5 minutes 10 µl of acetylthiocholine iodide (3 mM) was added and the absorbance was measured at 412 nm for 5 minutes. The activity of ChE was calculated according to the molar extinction coefficient of 5-thio-2-nitrobenzoate ($13.6 \times 10^3\ M^{-1}\ cm^{-1}$) and expressed as nMol $min^{-1}mL^{-1}$. As depicted in Table 1, malathion at the dose of 150 mg $kg^{-1}day^{-1}$ during 4 weeks inhibited 30% of the plasma ChE activity (663.40±72.09) compared with the control group (1029.67±84.52) with no mortality or acute toxic effects in rats.

Table 1. Plasma cholinesterase activity as percent of inhibition (%) after 4 weeks of daily administration of oral multiple doses of malathion.

Week	Malathion (mg kg^{-1} day^{-1})				
	0	**75**	**100**	**150**	**200**
1st	99.4 ± 4.3	93.2 ± 1.8	86.6 ± 2.1***	76.4 ± 5.7***	63.8 ± 3.3***
2nd	101.4 ± 9.1	93.3 ± 1.4*	86.4 ± 2.2***	77.3 ± 5.5***	63.0 ± 2.6***
3rd	99.5 ± 5.8	91.4 ± 1.8*	85.2 ± 3.2***	71.0 ± 4.2***	59.1 ± 6.6***
4th	100.6 ± 7.5	84.5 ± 1.6***	80.8 ± 1.9***	66.7 ± 2.9***	54.9 ± 4.8***

Data was expressed as mean ± SD; n = 10; * $P < 0.05$ and *** $P < 0.001$, significantly different from the control values (One-way ANOVA followed by multiple comparison test).

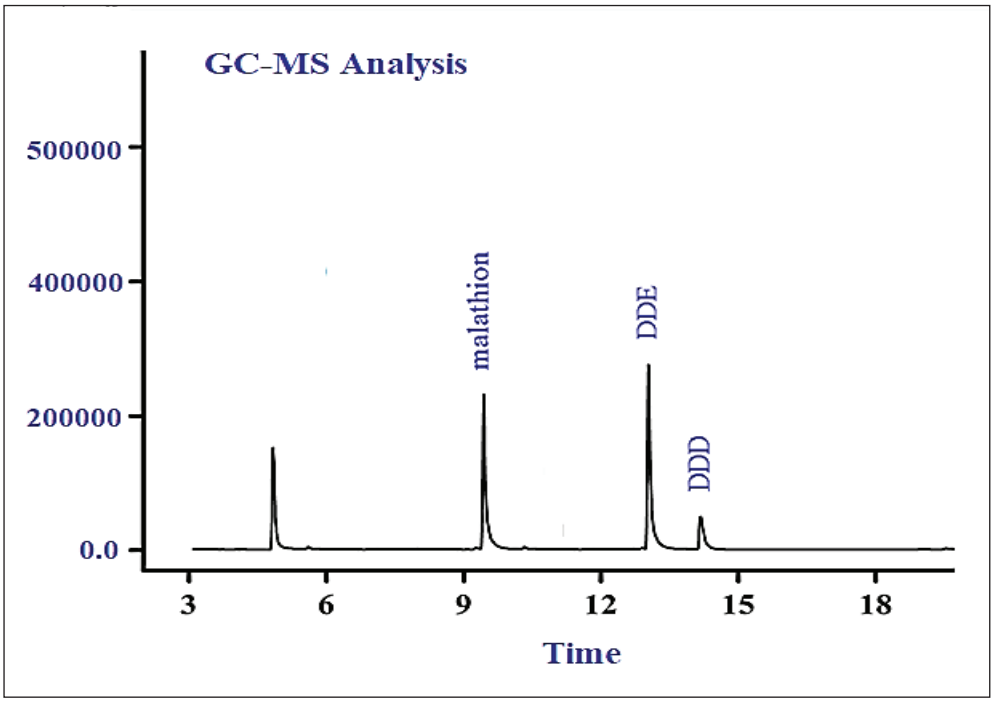

Fig.2. The Chromatographic of DDC, DDT and malathion pesticides by GC-MS

2.6. Measurement of malathion

GC–MS (Agilent 7890A/5975C, USA) with HP-5MS column (30 m × 0.25 mm i.d.,) with flow of 1 mL per minute of He was used for DDC, DDT and malathion pesticide in blood rats. The splitless injector was used. By GC–MS, the main parameters such as, the inlet and interface temperature set at 250 and 280 °C, respectively. The source of MS tuned 220 °C and ionization energy was less than 65-eV. The oven temperature was first at 100 °C (1.5 min), and increased up to 200 - 280 °C (20 - 6 °C/min). The Chromatographic of DDC, DDT and malathion pesticides was shown in Figure 2 [9-13].

2.7. Induction of diabetes in rats

Type 1 diabetes was induced by intraperitoneal injection of a single dose streptozotocin (STZ) solubilized in 0.1 M trisodium citrate buffer (pH, 4.5) at the dose of 65 mg kg^{-1}, according to the method described by Furman [27]. STZ-treated rats received 10% of sucrose instead of water for 48 h. Induction of diabetes was verified by measurement of FBG four times (1, 3 and 28 days after the beginning of treatment) to ensure that the hyperglycemia (FBG≥250 mg dL^{-1}) was established. Polyuria and polydipsia were also monitored by observation of the amount of consumed water and the frequency of bedding exchange.

2.8. Experimental design, animal treatment, and sample collection

Forty rats were randomly allocated to four groups of ten as follows:

Control: Healthy rats that only received corn oil orally.

DM: Diabetic rats received corn oil orally.

MT: Healthy rats received malathion (150 mg kg^{-1} day^{-1}, oral) for 4 weeks.

DM+MT: Diabetic rats received malathion (150 mg kg^{-1} day^{-1}, oral) for 4 weeks.

At the end of the experiment, all rats were anesthetized by ketamine (60 mg/kg) and xylazin (6 mg kg^{-1}) and after collection of blood sample through cardiac puncture sacrificed by cervical dislocation. Blood samples immediately centrifuged at 3000 g for 15 minutes for separation of plasma. To prepare hemolysate, 250 µl of distilled water was added to 50 µl of packed RBCs and mixed thoroughly. Plasma samples and hemolysate were kept at -80 °C for further experiments.

2.9. Measurement of FBG and GTT

Blood glucose was measured in the blood sample obtained by a small cut on the tip of rat's tail immediately after overnight fasting using the commercial glucose diagnostic kit of Pars Azmoon Company (Tehran, Iran). For measurement of GTT, blood glucose was recorded every 30 min after oral administration of glucose (2% w/v). Area under the curve (AUC 0-120 min) of glucose concentration from 0 to 120 minutes after administration of glucose was calculated by the trapezoidal method [28].

2.10. Measurement of oxidative stress biomarkers by spectrophotometry

2.10.1.Measurement of total antioxidant capacity of plasma

Antioxidant capacity was measured by ferric reducing antioxidant power (FRAP) method. During the reaction in acidic pH, the colorless ferric-tripyridyl triazine (Fe^{3+}-TPTZ) is reduced to blue ferrous-tripyridyl triazine (Fe^{2+}-TPTZ) [29]. To perform this experiment, 10 µl of plasma was added to 300 µl FRAP reagent (1:1:10 mixture of FeCl3, 10mM TPTZ, and 0.3M acetate buffer at pH 3.6). After incubation at 37 °C for 10 minutes, the absorbance was read at 593 nm. Finally, FRAP was expressed as mmol Fe^{2+}/mg protein according to the standard curve of $FeSO_4$.

2.10.2.Measurement of glutathione (GSH) content

According to the Elman method, thiol groups react by 5,5′-dithio-bis(2-nitrobenzoic acid) (DTNB) and produce yellow complex [30]. Briefly, 250 µL of TCA 10% were added to 500 µL of hemolysate and centrifuged at 3500 g for 35 minutes. Then, 200 µL of Tris buffer and 500 µL DTNB (10 mM in 0.1 M phosphate buffer, pH 8) were added to the supernatant and incubated in the dark at room temperature for 15 minutes. The absorbance was read at 412 nm and total thiol was expressed as nmol/mg protein according to the standard curve of GSH.

2.10.3.Measurement of superoxide dismutase (SOD) activity

SOD activity was measured based on autoxidation rate of pyrogallol at 420 nm by the Worthington method with minor modification [31]. Briefly, the absorbance of pyrogallol (2 mM pyrogallol in Tris-HCl buffer, pH 8.2) was determined kinetically alone and after the addition of 50 µl of hemolysate. The amount of SOD needed for 50% inhibition of the pyrogallol autoxidation was considered as one unit of SOD activity and expressed as U/mg protein.

2.10.4.Measurement of catalase (CAT) activity

According to Cohen method [32], 1 ml of 30 mM H_2O_2 and 50 µl of the hemolysate was added to 2 ml of phosphate buffer (50 mM, pH 7.0) and then the absorbance was measured kinetically at 240 nm. One unit of catalase activity is equal to 1 µM H_2O_2 decomposed per minute. The concentration of H_2O_2 was calculated using the following equation: H_2O_2 (µM) = (Absorbance at 240 nm × 1000)/43.6 M^{-1} cm^{-1}). Catalase activity was expressed as U/mg protein.

2.10.5.Measurement of lipid peroxidation

Malondialdehyde (MDA) as the end-product of lipid peroxidation was measured based on the absorbance of MDA-thiobarbituric acid (TBA) complex in acidic and high-temperature condition [33]. Briefly, 100 µl of hemolysate was deproteinized by TCA 10% and centrifuged at 3500 g for 35 minutes. One ml of sulfuric acid 0.05% and 800 µl of TBA (0.2%) were then added to the precipitant and boiled at 95 °C for 30 minutes. Then, MDA-TBA complex was extracted by 800 µl n-butanol and the absorbance was read at 532 nm. The level of MDA was expressed as nmol MDA/mg protein according to the MDA standard curve.

2.10.6.Measurement of protein carbonylation

Protein carbonylation was measured according to Levin et al. method [34]. Throughout the method, 100 µl of hemolysate was added to 500 µl of TCA 20%, kept at room temperature for 10 minutes, and

Table 2. Fasting blood glucose (FBG), Glucose tolerance test (GGT) and weight of rats on day 1, 3, and 28 in non-diabetic rats received corn oil (Control) and malathion (MT) and in diabetic rats received corn oil (DM) and malathion (DM + MT).

Time		Day 1	Day 3	Day 28
FBG (mg/dl)	Control	62.0 ± 9.7	74.3 ± 25.5	74.0 ± 14.7
	DM	108.4 ± 18.6	424.8 ± 28.9 ***	395.4 ± 18.1***
	MT	108.6 ± 19.3	89.1 ± 15.0	90.4 ± 21.0
	DM + MT	133.25 ± 9.1	383.2 ± 19.1***	413.7 ± 12.1***
GTT (AUC 0-120 min)	Control	9325 ± 409	NC	11990 ± 658.2
	DM	11975 ± 521	NC	47574 ± 3758***
	MT	10010.5 ± 688	NC	17886 ± 1438 *
	DM + MT	10834 ± 674	NC	50577 ± 1256***
Weight (gr)	Control	211.5 ± 10.6	213.3 ± 9.2	263.7 ± 12.33
	DM	189.4 ± 8.5	182.4 ± 12.3	158.4 ± 8.2**
	MT	198.4 ± 8.3	198.8 ± 7.7	214.6 ± 7.1
	DM + MT	212.6 ± 2.6	214.9 ± 3.1	162.7 ± 7.9***

Data was expressed as mean ± SD; n = 10; * $p < 0.05$, ** $p < 0.01$, and *** $p < 0.001$, significantly different from the control values (One-way ANOVA followed by multiple comparison test). NC: not calculated.

centrifuged. The supernatant was discarded and 1ml 4-dinitrophenylhydrazine (DNPH, 10 mM) was added to the pellet and incubated at 37 ºC for 50 minutes. Then, 1ml of TCA 20% was added and centrifuged. The remaining pellet was washed with 1mL of ethanol and ethyl acetate solution (1:1 ratio). Then, 1mL of guanidine hydrochloride 6 M was added and incubated at 37 °C for 30 minutes. After centrifugation, the supernatant was transferred to a 96-well plate and the absorbance was measured at 380 nm. The carbonyl content was calculated using the molar extinction coefficient of 22,000 M^{-1} cm^{-1} and expressed as nmol/mg protein

2.11. Measurement of protein concentration

Protein concentration in the samples was measured according to the Bradford's method [35]. Briefly, 200 µl of Bradford reagent (100 mg coomassie brilliant blue G-250 was dissolved in 50 ml 95% ethanol and then 100 ml 85% phosphoric acid and 850 ml of distilled water was added) were mixed with 50 µl of samples and bovina serum albumin (BSA) as standard in 96-well plate. After five minutes' incubation at 37 °C, the absorbance was measured at 595 nm and the protein concentration was expressed as mg mL^{-1} of samples according to the standard curve of BSA.

2.12. Statistical analysis

Data were analyzed by using commercially available SPSS software. Data was analyzed by one-way ANOVA followed by Tukey's multiple comparison test. Results were presented as mean ± SD (Standard Deviation) and p values less than 0.05 were regarded as statistically significant.

3. Results and discussion

3.1. Malathion blood concentration

The blood malathion firstly determined by GC-MS analysis after oral intake in rats. The blood analysis of malathion indicates that oral administration of malathion at the dose of 50-150 mg kg^{-1} day^{-1}caused a blood concentration of malathion in the range of 0.5–4.0 µg mL^{-1}.

3.2. Induction of diabetes in rats

As shown in Table 2, administration of STZ at the single dose of 65 mg kg^{-1} caused significant hyperglycemia (FBG = 424.8 ± 28.9 mg dL^{-1}, $p < 0.001$) and loss of body weight was compared with control group (FBG = 74.3 ± 25.5 mg dL^{-1}). Polyuria and polydipsia were other findings were observed in the diabetic rats within 4 weeks.

3.3. Effects on blood glucose

As shown in Table 2, malathion at the dose of 150 mg kg^{-1} did not result in a significant increase in FBG in diabetic rats compared with non-treated diabetic rats (p = 0.77) and in non-diabetic rats compared with control group (p = 0.72). On the other hand, malathion caused significant (p = 0.04) increase in AUC 0-120 of glucose concentration curve in non-diabetic rats. most previous studies showed that hyperglycemia in both short-term and long-term exposure to OPI happened due to disruption in glycolysis, glycogenolysis, and gluconeogenesis pathways [7] and impairment in insulin signaling and insulin-stimulated glucose uptake in muscle cells [24]. Also, a meta-analysis conducted by Ramirez-Vargas et al. (2018), revealed that blood glucose concentrations were 3.3-fold higher in malathion-exposed rats than in the control group [23]. In contrast, it should be noted that some studies show gradual increase in blood glucose and even hypoglycemia after malathion exposure [36-38]. It has been also reported that blood glucose in malathion-treated rats increased (2.2-fold) after 2 h but gradually decreased within 4 h [39]. It can be concluded that duration of exposure, dose, experimental protocols, time of blood sampling, and the mode of administration are variables which affects the toxicity of malathion. As the toxicity of malathion on carbohydrates, fats, and protein metabolism pathways is approved previously, significant effects on FBG and GTT might be obtained with increase in the number of examined animal and duration of exposure to malathion.

3.4. Effects on antioxidants level

The total antioxidant capacity of plasma in diabetic and non-diabetic rats exposed to malathion decreased significantly ($p < 0.001$) comparing to control group. Moreover, a considerable difference ($p = 0.009$) was detected in malathion-treated diabetic rats compared to diabetic rats received corn oil (Fig. 3a). GSH level in RBCs decreased significantly ($p < 0.001$) in all groups compared to control group. However, there was no considerable difference ($p = 0.13$) between diabetic and non-diabetic rats received malathion (Fig. 3b). The activity of SOD in RBCs decreased significantly in diabetic groups ($p < 0.05$), and in diabetic and non-diabetic group received malathion ($p < 0.001$) compared to control group. Malathion decreased significantly ($p = 0.0008$) the activity of SOD in diabetic rats compared to diabetic group received corn oil (Fig. 3c). The activity of CAT in erythrocyte decreased significantly ($p < 0.001$) in all groups in comparison with control group. A significant ($p = 0.007$) decrease was also observed in diabetic rats received malathion compared to diabetic groups (Fig. 3d). The results of this study indicated that both diabetes and sub-acute exposure to the sub-lethal dose of malathion reduced the activity of CAT and SOD enzymes and total antioxidant capacity of plasma and GSH level. Interestingly, malathion in diabetic rats intensified the reduction of total antioxidant capacity and the activity of antioxidant enzymes. These results are in agreement with previous studies, which have indicated that diabetic condition and exposure to OPI reduce the total antioxidant capacity of plasma [7, 40, 41]. Reduction in total thiol content which induces oxidative and nitrosative damages were also reported in OPI exposure [42-45].

3.5. Effects on lipid peroxidation and protein carbonylation

As shown in Table 3, lipid peroxidation and protein carbonylation in diabetic rats as well as in diabetic and non-diabetic rats exposed to malathion significantly ($p < 0.001$) increased compared to control group. However, despite increase in the lipid peroxidation, no significant differences were observed between lipid peroxidation level in diabetic rats and diabetic rats exposed to malathion. Protein carbonylation was significantly ($p = 0.042$) increased in diabetic rats exposed to malathion compared to diabetic rats received corn oil. Generation of free radicals disables antioxidant systems and consequently exerts further destructive effects on cellular macromolecules [7, 15, 40]. Increase in protein carbonylation and lipid peroxidation revealed in the current study was in agreement with the findings of other studies [7, 46]. OPI increases lipid peroxidation and protein carbonylation in acute and sub-acute exposure

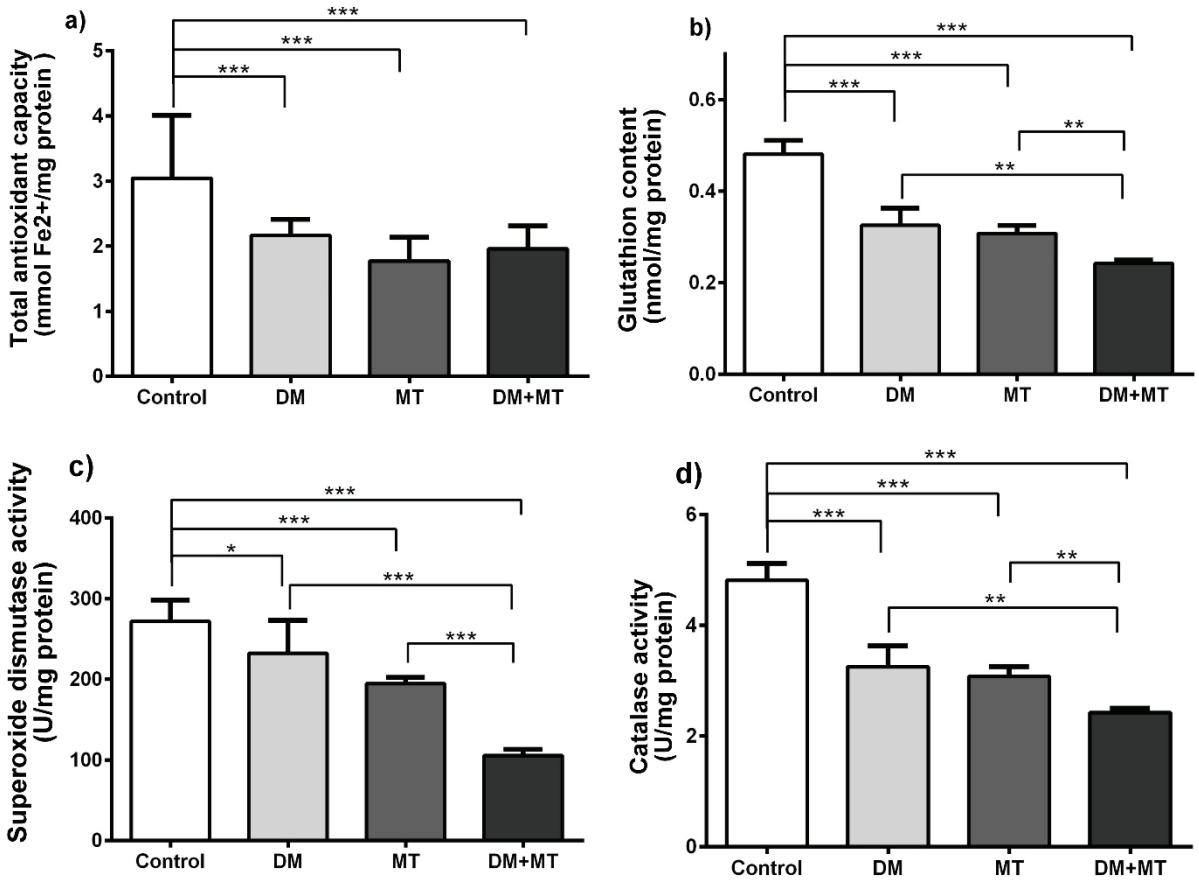

Fig. 3. Effects of malathion on antioxidants in the studied groups. **a**) Total antioxidant capacity of plasma, **b**) RBCs glutathione content, **c**) RBCs superoxide dismutase activity, **d**) RBCs catalase activity in healthy rats received corn oil (Control) and malathion (MT) and in diabetic rats received corn oil (DM) and malathion (DM + MT) after 4 weeks. Data was expressed as mean ± SD; n = 10; * $p < 0.05$, ** $p < 0.01$, and *** $p < 0.001$, significantly different between groups (One-way ANOVA followed by Tukey's multiple comparison test).

Table 3. Protein carbonylation and lipid peroxidation in non-diabetic rats received corn oil (Control) and malathion (MT) and in diabetic rats received corn oil (DM) and malathion (DM + MT) after 4 weeks.

Parameters	Control	DM	MT	DM + MT
Lipid peroxidation (nmol/mg protein)	0.64 ± 0.13	0. 86 ± 0.09***	0.92 ± 0.10***	0.99 ± 0.15***
Carbonyl protein formation (nmol/mg protein)	0.92 ± 0.15	1.12 ± 0.13**	1.20 ± 0.2**	1 45 ± 0.23***

Data was expressed as mean ± SD; n = 10; ** $p < 0.01$ and *** $p < 0.001$, significantly different from the control values (One-way ANOVA followed by multiple comparison test).

[47-49]. Elevation in lipid peroxidation in diabetic rats exposed to monocrotophos, an OPI, was also reported by Vismaya and Rajini [44]. Increase in the MDA level indicates the susceptibility of cell membrane lipids against oxidative stress induced by malathion in diabetic rats.

4. Conclusions

Taking together, the results of this study imply that malathion aggravated decline in the enzymatic antioxidant defense system. Impairment in antioxidants capacity in long-term exposure to OPI causes further oxidative damages as a proposed

mechanism for OPI-induced hyperglycemia. According to high prevalence of diabetes, it is recommended to conduct further *in vivo, in vitro,* and clinical studies to investigate effects of OPI on insulin release and blood glucose tolerance in diabetic subjects exposed to OPI. It is also recommended to evaluate effects of malathion on tissues contributing to or affected by hyperglycemia. Further consideration is also required to restrain the utilization of OPI, which are widely used in developing countries.

5. Acknowledgement

This manuscript was supported by Research Deputy of Kerman University of Medical Sciences.

6. References

[1] R.F. Clark, Insecticides: organic phosphorus compounds and carbamates. Goldfrank's Toxicological Emergencies. New York: McGraw-Hill Professional, 2002.

[2] M.D. Shah, M. Iqbal, Diazinon-induced oxidative stress and renal dysfunction in rats, Food Chem. Toxicol., 48 (2010) 3345-3353.

[3] M. Balali-Mood, H. Saber, Recent advances in the treatment of organophosphorous poisonings, Iran. J. Med. Sci., 37 (2012) 74-91.

[4] D.M. Roberts, C.K. Aaron, Management of acute organophosphorus pesticide poisoning, British Med. J., 334 (2007) 629-634.

[5] M. Abdollahi, S. Karami-Mohajeri, A comprehensive review on experimental and clinical findings in intermediate syndrome caused by organophosphate poisoning, Toxicol. Appl. Pharmacol., 258 (2012) 309-314.

[6] S. Karami-Mohajeri, S. Nikfar, M. Abdollahi, A systematic review on the nerve-muscle electrophysiology in human organophosphorus pesticide exposure, Hum. Exp. Toxicol., 33 (2014) 92-102.

[7] S. Karami-Mohajeri, M. Abdollahi, Toxic influence of organophosphate, carbamate, and organochlorine pesticides on cellular metabolism of lipids, proteins, and carbohydrates: a systematic review, Hum. Exp. Toxicol., 30 (2011) 1119-1140.

[8] M. Abdollahi, Pesticides and oxidative stress: a review, Med, Sci, Monit., 10 (2004) RA141-7.

[9] N. Brandhonneur, A micro-QuEChERS method coupled to GC-MS for the quantification of pesticides in specific maternal and fetal tissues, J. Pharm. Biomed. Anal., 104 (2015) 90-96.

[10] G. Famiglini, et al., The rapid measurement of benzodiazepines in a milk-based alcoholic beverage using QuEChERS extraction and GC-MS analysis, J. Anal. Toxicol., 39 (2015) 306-312.

[11] E. Gallardo, Determination of quinalphos in blood and urine by direct solid-phase microextraction combined with gas chromatography-mass spectrometry, J. Chromatogr. B, Anal. Technol. Biomed. Life Sci., 832 (2006) 162-168.

[12] M. Liang, Fe3O4 magnetic nanoparticle peroxidase mimetic-based colorimetric assay for the rapid detection of organophosphorus pesticide and nerve agent, Anal. Chem., 85 (2013) 308-312.

[13] X. Deng, Rapid and effective sample clean-up based on magnetic multiwalled carbon nanotubes for the determination of pesticide residues in tea by gas chromatography-mass spectrometry, Food Chem., 145 (2014) 853-858.

[14] M.K. Abbasabadi, H. Shirkhanloo, Speciation of cadmium in human blood samples based on Fe(3)O(4)-supported naphthalene-1-thiol-functionalized graphene oxide nanocomposite by ultrasound-assisted dispersive magnetic micro solid phase extraction, J. Pharm. Biomed. Anal., 189 (2020) 113455.

[15] R. Rahimi, M. Abdollahi, A review on the mechanisms involved in hyperglycemia induced by organophosphorus pesticides, Pestic. Biochem. Physiol., 88 (2007) 115-121.

[16] U. Asmat, K. Abad, K. Ismail, Diabetes mellitus and oxidative stress-A concise review, Saudi Pharm. J., 24 (2016) 547-553.

[17] U. Karunakaran, K.G. Park, A systematic

review of oxidative stress and safety of antioxidants in diabetes: focus on islets and their defense, Diabetes Metab. J., 37 (2013) 106-112.

[18] F. Giacco, M. Brownlee, Oxidative stress and diabetic complications, Circ. Res., 107 (2010) 1058-1070.

[19] S. Shahvali, A. Shahesmaeili, S. Karami-Mohajeri, The correlation between blood oxidative stress and sialic acid content in diabetic patients with nephropathy, hypertension, and hyperlipidemia, Diabetol. Int., 2019 (2019) 1-8.

[20] R. Franco, Environmental toxicity, oxidative stress and apoptosis: menage a trois, Mutat. Res., 674 (2009) 3-22.

[21] K. Van Dyke, Oxidative/nitrosative stresses trigger type I diabetes: preventable in streptozotocin rats and detectable in human disease, Ann. N Y Acad. Sci., 1203 (2010) 138-145.

[22] N.S. Babu, Effects of subchronic malathion exposure on the pharmacokinetic disposition of pefloxacin, Environ. Toxicol. Pharmacol., 22 (2006) 167-171.

[23] M.A. Ramirez-Vargas, Effects of exposure to malathion on blood glucose concentration: a meta-analysis, Environ. Sci. Pollut. Res. Int., 25 (2018) 3233-3242.

[24] S. Shrestha, Effect of sub-toxic exposure to Malathion on glucose uptake and insulin signaling in L6 myoblast derived myotubes, Drug Chem. Toxicol., 43 (2018) 1-8.

[25] J.D. Wilson, Toxicological profile for malathion. Agency for Toxic Substances and Disease Registry, 2003.

[26] G.L. Ellman, A new and rapid colorimetric determination of acetylcholinesterase activity, Biochem. Pharmacol., 7 (1961) 88-95.

[27] B.L. Furman, Streptozotocin-induced diabetic models in mice and rats, Curr. Protoc. Pharmacol., 70 (2015) 5.47.1-5.47.20.

[28] J.N. Matthews, Analysis of serial measurements in medical research, British Med. J., 300 (1990) 230-235.

[29] I.F. Benzie, J.J. Strain, The ferric reducing ability of plasma (FRAP) as a measure of "antioxidant power": the FRAP assay, Anal. Biochem., 239 (1996) 70-76.

[30] M.-L. Hu, Measurement of protein thiol groups and glutathione in plasma, Methods enzymol., 233 (1993) 380-385.

[31] C.C. Winterbourn, The estimation of red cell superoxide dismutase activity, J. Lab. Clin. Med., 85 (1975) 337-341.

[32] G. Cohen, D. Dembiec, J. Marcus, Measurement of catalase activity in tissue extracts, Anal. Biochem., 34 (1970) 30-38.

[33] D. Lapenna, Reaction conditions affecting the relationship between thiobarbituric acid reactivity and lipid peroxides in human plasma, Free Radic. Biol. Med., 31 (2001) 331-335.

[34] R.L. Levine, Carbonyl assays for determination of oxidatively modified proteins, Methods Enzymol., 233 (1994) 346-357.

[35] J.B. Hammond, N.J. Kruger, The bradford method for protein quantitation, Methods Mol. Biol., 3 (1988) 25-32.

[36] P.K. Gupta, Malathion induced biochemical changes in rat, Acta Pharmacol. Toxicol., 35 (1974) 191-194.

[37] B.O. Laley, M.A. Gibson, Association of hypoglycemia and pancreatic islet tissue with micromelia in malathion-treated chick embryos, Can. J. Zool., 55 (1977) 261-264.

[38] A.L. Arsenault, M.A. Gibson, M.E. Mader, Hypoglycemia in malathion-treated chick embryos, Can. J. Zool., 53 (1975) 1055-1057.

[39] M.A. Rodrigues, Short-term effect of malathion on rats' blood glucose and on glucose utilization by mammalian cells in vitro, Ecotoxicol. Environ. Saf., 12 (1986) 110-113.

[40] M. Trombetta, Review article: type 2 diabetes and chronic liver disease in the Verona diabetes study, Aliment. Pharmacol. Ther. (22 Suppl.) 2 (2005) 24-27.

[41] D. Jira, Toxicity hazard of organophosphate insecticide malathion identified by in vitro

methods, Neuro. Endocrinol. Lett., (33 Suppl.) 3 (2012) 53-59.
[42] I. El-Bini Dhouib, A comparative study on toxicity induced by carbosulfan and malathion in Wistar rat liver and spleen, Pestic. Biochem. Physiol., 124 (2015) 21-28.
[43] K. Begum, P.S. Rajini, Augmentation of hepatic and renal oxidative stress and disrupted glucose homeostasis by monocrotophos in streptozotocin-induced diabetic rats, Chem. Biol. Interact., 193 (2011) 240-245.
[44] Vismaya, P.S. Rajini, Exacerbation of intestinal brush border enzyme activities and oxidative stress in streptozotocin-induced diabetic rats by monocrotophos, Chem. Biol. Interact., 211 (2014) 11-19.
[45] S. Selmi, S. El-Fazaa, N. Gharbi, Oxidative stress and cholinesterase inhibition in plasma, erythrocyte and brain of rats' pups following lactational exposure to malathion, Environ. Toxicol. Pharmacol., 34 (2012) 753-760.
[46] M.B.S. de, Oxidative stress as an underlying contributor in the development of chronic complications in diabetes mellitus, Int. J. Mol. Sci., 14 (2013) 3265-3284.
[47] R.D. Handy, Chronic diazinon exposure: pathologies of spleen, thymus, blood cells, and lymph nodes are modulated by dietary protein or lipid in the mouse, Toxicol.. 172 (2002) 13-34.
[48] F.P. Possamai, Oxidative stress after acute and sub-chronic malathion intoxication in Wistar rats, Environ. Toxicol. Pharmacol., 23 (2007) 198-204.
[49] M. Akhgari, Biochemical evidence for free radical-induced lipid peroxidation as a mechanism for subchronic toxicity of malathion in blood and liver of rats, Hum. Exp. Toxicol., 22 (2003) 205-211.

Anal. Methods Environ. Chem. J. 4 (2) (2021) 72-85

AMECJ

Research Article, Issue 2
Analytical Methods in Environmental Chemistry Journal
Journal home page: www.amecj.com/ir

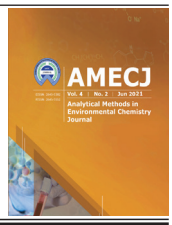

Ionic liquid functionlized on multiwall carbon nanotubes for nickel and lead determination in human serum and urine samples by micro solid-phase extraction

Arezou Lari[a], Nafiseh Esmaeili[b,*] and Homanaz Ghafari[c]

[a]*Systems Biomedicine Department, Pasteur Institute of Iran, Tehran, Iran.*
[b] *Department of chemistry, Faculty of Science, Semnan University, Semnan, Iran*
[C]*Department of pharmacology,school of medicine,Tehran university of medical sciences, P.O.Box784-13145,Tehran,Iran*

ARTICLE INFO:

Received 11 Mar 2021
Revised form 15 May 2021
Accepted 4 Jun 2021
Available online 30 Jun 2021

Keywords:
Nickel and lead,
Human samples,
Ionic liquid,
Multiwall carbon nanotubes,
Micro solid-phase extraction

ABSTRACT

In this study, a novel synthesis adsorbent, 1-(3-aminopropyl)-3-methylimidazolium hexafluorophosphate functionlized on multiwall carbon nanotubes ([Apmim][PF_6]-MWCNTs, IL@MWCNTS) was used for nickel/lead (Ni/Pb) extraction and determination by dispersive ionic liquid micro solid-phase extraction (DIL-µ-SPE) coupled to electrothermal atomic absorption spectrometry (ET-AAS). After dilution of 20 mg of IL@MWCNTS in 200 µL of acetone, the mixture was injected to 10 mL of human serum/urine samples at pH of 8.0. After sonication for 5 min, the Ni(II) / Pb(II) were extracted by ionic liquid phase and then centrifuged for 2.5 min. The upper liquid phase set aside and Ni(II) / Pb(II) loaded in adsorbent were back-extracted by acidic solution at pH=2-3. Finally, the concentration of total nickel and lead was determined by ET-AAS. By optimizing, the limit of detection, linear range, and enrichment factor for nickel and lead were obtained (0.05 µg L^{-1}; 0.1 µg L^{-1}), (0.2-5.8 µg L^{-1}; 0.4-30 µg L^{-1}) and 24.7; 5.1, respectively (RSD less than 5%). Also, the capacity absorption of IL@MWCNTS for nickel and lead ions were achieved 149.3 mg g^{-1} and 162.5 mg g^{-1}, respectively. The DIL-µ-SPE procedure was validated for nickel and lead extraction by spiking of real samples and ICP-MS analyzer.

1. Introduction

Lead and nickel (Pb, Ni) have toxic effects and use in different industries. Heavy metals as non-essential elements have widely distributed in the environment (air, soils, waters) and humans. Human exposure of heavy metals cause to various diseases such as cancer. Pb and Ni is a naturally occurring element found in small amounts in the earth's crust [1]. While it has some beneficial uses, it can be toxic to humans and animals, and cause to health effects. The most exposure of lead and nickel related to human activities including, the fossil fuels, gasoline, the industrial facilities, the nickel cadmium battery, and paint factories. Lead and nickel compounds have been used in a wide variety of products found in different industries, including paint, ceramics, pipes and plumbing materials, gasoline, batteries, and cosmetics [2, 3]. High levels of human exposure to Ni and Pb metals cause to damage the most of human organ systems such as, the central nervous system (CNS), kidneys, liver, bones and gastrointestinal system. Lead can also effect on hemoglobin synthesis and cause to anemia effects or accumulate in the bones. Depending on the level of exposure,

*Corresponding Author: Nafiseh Esmaeili
Email: esmaeilin@gmail.com, esmaeilin@semnana.ac.ir
https://doi.org/10.24200/amecj.v4.i02.144

the lead and nickel can adversely effect on the nervous system, immune system, reproductive and the cardiovascular system [4-7]. Infants and young children are especially sensitive to lead exposures, which may contribute to behavioral problems, learning deficits and lowered IQ [8]. Lead can also be emitted into the environment from industrial sources and contaminated sites, such as former lead smelters. While natural levels of lead in soil range between 50 and 400 parts per million, mining, smelting and refining activities have resulted in substantial increases the lead levels in the environment, especially near mining and smelting sites. Lead can be added to soils and sediments through deposition from sources of lead by air pollution. Lead can be added to proteins and amino acids which was caused neurological problems [9,10]. Due to the environmental protection agency (EPA), the maximum contaminant level (MCL) for Pb in waters is zero and has no effect in humans [2]. Also, the National toxicology program (NTP) announced that the lead concentration in blood and serum must be less than 50 µg L^{-1} in children. The variable lead values in human blood/serum was about 250 -300 µg L^{-1} which was reported by food and drug administration (FDA) [11]. As references, the standard blood lead levels are below 25 mg dL^{-1} or 250 microgram per liter. The permissible exposure level in the ambient (air, water, soil, etc.) environment has been reported [12-14]. Nickel (Ni) caused to acute disease in humans [15]. Ni(II) can be enter to waters from waste water of different industries such as battery and electroplating factories [16]. Nickel complex to various proteins and enzyme in the human body. Nickel toxicity caused to many problems in human systems or organs such as renal, liver, brain, cardiovascular system, immune system and heart. The symptoms diseases included lung dysfunction and cancer was seen for nickel exposure [17]. Oral values for rats range from 67-9000 mg Ni per kg (ATSDR). Toxic effects of oral exposure to nickel usually involve the kidneys (ATSDR). Normal range for Ni in healthy peoples is 0.2 µgL^{-1} in serum and less than 3.0 µgL^{-1} in human urine. [18,19]. Nickel (II) in urine and serum samples determined with UV-VIS spectrophotometry and flame atomic absorption spectrometry techniques [20]. Recently, the various techniques such as, the inductively coupled plasma(ICP), the inductively coupled plasma mass spectrometry(ICP-MS) [21], the flame atomic absorption spectrometry F-AAS [22], the X-ray fluorescence spectrometry [23] and the electrothermal atomic absorption spectrometry (ET-AAS) were used to determine Ni and Pb ions in different matrixes [24]. Due to ultra-trace concentration of Pb and Ni in human samples (urine and serum) and difficulty matrices in human biological samples, the sample treatment was used. For Examples, the solid phase extraction(SPE) [25], the magnetic dispersive micro-solid phase extraction (MD-µ-SPE) [26,27], the dispersive micro solid phase microextraction (D-SPME) [28], the needle hub in-syringe solid phase extraction (NHS-SPE) [29], and liquid-liquid microextraction (LLME) [30, 31] were used. Among them, the dispersive micro solid-phase extraction D-µ-SPE was mostly used for determination of heavy metals such as Ni and Pb in water and humans. Task ionic liquids were used for extraction of heavy metals from liquid phase by N, S groups. The D-µ-SPE procedure have advantages such as easy to use, simple, high recovery and efficient extraction. In this process, the adsorbent properties are main factor for heavy metal extraction by D-µ-SPE procedure. The high surface area of nanoparticles caused to increase the extraction recovery and absorption capacity. Recently, the various nanostructures were used for extraction Pb and Ni in waters, human urine and serum samples [32, 33]. In this study a novel ionic liquid ([Apmim][PF_6]) functionalized on MWCNTs (IL-MWCNTs) was used for extraction of Ni and Pb ions in human urine and serum samples by the DIL-µ-SPE procedure. The Ni and Pb concentration was determined by the ET-AAS after sample preparation. The main parameters on lead and nickel extraction were studied and evaluated.

Table 1. The ET-AAS conditions for lead and nickel determination.

Features	Value Pb	Value Ni
Linear range, µg L^{-1}	3-90	5-85
Working range, µg L^{-1}	3-150	5-145
Wavelength, nm	283.3,217.0	232.0
Lamp current, mA	5.0	4.0
Slit, nm	0.5	0.2
Mode	Peak Area	Peak Area
Auto Sampler (µL)	1-100	1-100
LOD	0.75	1.25
LLOQ	3.0	5.0
R^2	0.9998	0.9997

2. Materials and Methods

2.1. Apparatus

The AAS (GBC, 932, AUS) based on furnace accessory (Pal 3000) and deuterium (D_2) /hollow-cathode lamp (Ni, Pb) was used. The sample was transferred to 2 mL of PVC tube in Pal3000 as auto-sampler accessory. The conditions of ET-AAS were shown in Table 1. The lead determination was achieved by injecting 20 µL of sample to graphite tube with auto-sampler in three steps of drying, ashing, and atomization. The ICP-MS (PerkinElmer, USA) was used for ultra-trace Ni and Pb analysis in different matrixes. The conditions of ICP-MS were tuned for Ni and Pb determination in samples (1200 W, 12 L min^{-1} per 1 s). The auxiliary gas flow was adjusted 1.2 L min^{-1}. The quantitative analysis of lead and nickel were obtained in PPT concentration by ICP-MS analyzer (<10 ppt). The range of pH values of the serum and urine samples were measured by pH meter (Metrohm) and adjusted by favorite buffer solution. The shaker accessory (USA, Domingo Lab) by stirring speed between 10~210 PRM and working platform of 315×218 mm (12.5"×8.5") with voltage 220V was used. The Eppendorf centrifuge offers 24–place capacity in an aerosol-tight rotor and speeds up to 21,300 × g was used (Laboratory centrifuge model 5418 R, Eppendorf, Germany). was used by the DIL-µ-SPE procedure. The polypropylene syringe and conical tube were purchased from Sigma (Germany). Fourier transform infrared (FT-IR) spectra were obtained by a Perkin Elmer Spectrum (65 FT-IR). X-ray diffraction (XRD) was reported by a X'Pert PRO X-ray diffractometer. Scanning electron microscopy (SEM) images were achieved using a Tescan Mira-3.

2.2. Reagents

In this study, the analytical grade of reagents was prepared from Merck / Sigma Aldrich (Germany). The standard solution of lead (Pb^{2+}) was purchased from Merck CO. (Germany) with a concentration of 1000 mg L^{-1} in 1 % HNO_3. The standard stock solutions (1000 mg L^{-1}) of Ni (II), were purchased from Merck (Darmstadt, Germany). Another concentration of lead and nickel was daily prepared by dilution of the standard lead solution with DW. Ultrapure water was purchased from Millipore Company (Bedford, USA) for dilution of solutions or standards. The pH was adjusted by sodium phosphate buffer solution for pH 5.7-8.2. The reagents such as acetonitrile (CAS N.: 75-05-08, Merck), polyoxyethylene octyl phenyl ether (TX-100, CAS N: 9002-93-1, Sigma, Germany), and toluene (CAS N: 108-88-3, Merck), HNO_3, xylene, HCl, ethanol, and acetone, were prepared from Merck,

Germany. MWCNTs adsorbent prepared from RIPI company in Iran. aminoopropyltrimethoxysilane (APTMS) was prepared from Sigma, Germany.

2.3. Synthesis of [Apmim][PF_6]-MWCNTs

The carboxylic acid of MWCNTs was prepared by the acid treatment procedure according to previous reports [34]. Then, the carboxylic acid (COOH) on MWCNTs was treated with $NaBH_4$ / CH_3OH, and COOH were reduced to CH_2OH groups. Typically, in a 100 mL flask / condenser / magnetic stirrer (MSB), the sodium borohydride (0.5 g) added to 5 g of MWCNTs-COOH and in presence of methanol refluxed / cooled/ filtered / washed with methanol. Then 2.0 g of MWCNTs –OH were added to 3-aminoopropyltrimethoxysilane (APTMS) in xylene (50 ml) and heated. Then, the product was filtered, washed with ethanol. Finally, Immobilization of the carbonyl group on the MWCNTs was accomplished by stirring the aminopropyl-functionalized CNTs in an ethanolic solution of terephthalaldehyde (0.5 g) for 3 h at 70 °C. An ethanolic solution carbonyl-functionalized MWCNTs were moved to ultrasonic bath for 15 minutes. After the sonication, a solution of [Apmim][PF_6]in EtOH (10 mL) was added dropwise to mentioned suspension during 10 min at 80 °C. The reaction mixture was refluxed for 4 h at 80 °C by N_2[34].

2.4. General procedure

By the DIL-µ-SPE procedure, 10 mL of human urine and serum sample was used for extraction Pb and Ni by IL-MWCNTs. Firstly, 10 mL of human samples and standard solution containing 0.2 µg L^{-1}; 0.4 µg L^{-1} (lower limit) and 5.5 µg L^{-1}; 30 µg L^{-1} (upper limit) for Ni and Pb was used, respectively at pH of 8.0. Then, 20 mg of IL-MWCNTs mixed with 0.2 mL of acetone and injected to 10 mL samples /standard solution in PVC centrifuge conical tube. The mixture was shaken for 6 min and Pb/Ni ions were extracted by amine group of [Apmim][PF_6] at optimized pH. Then, the adsorbent was collected from liquid phase by centrifuging of samples. Then, the Ni loaded on adsorbent was back extracted with 0.2 mL of nitric acid (0.3 M) and diluted with 0.2 mL of DW. Also, the lead loaded on adsorbent was back extracted with 0.2 mL of nitric acid (0.3 M) and diluted with DW up 2 mL. Finally, the solution was determined by ET-AAS (Fig.1, Table 2). The recovery of extraction with IL-MWCNTs adsorbent was obtained for Pb/Ni concentration by the equation 1. The C_A is the primary concentrations and C_S is the secondary concentration of Pb(II)/Ni(II), which was determined by ET-AAS (n=10, Eq. 1).

$$\text{Recovery\%} = (C_A\text{-}C_S)/C_A \times 100 \qquad \text{(Eq.1)}$$

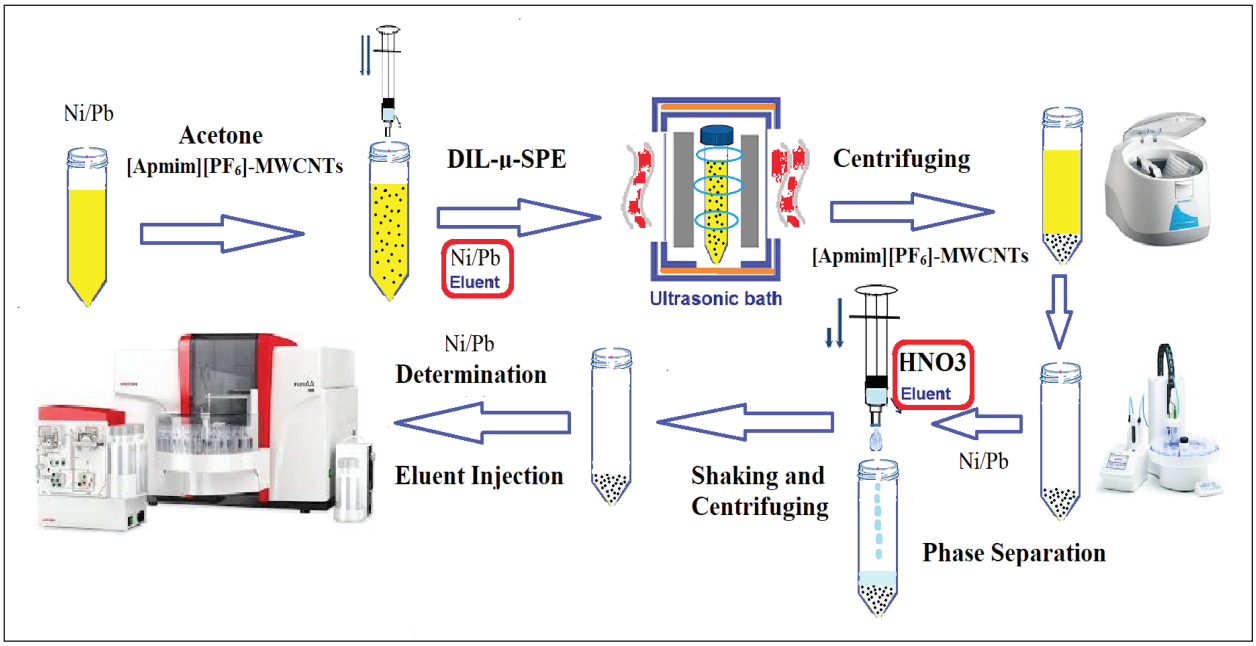

Fig. 1. The DIL-µ-SPE procedure based on IL-MWCNTs for Pb and Ni extraction

Table 2. The analytical features for determination lead and nickel by DIL-µ-SPE procedure coupled to ET-AAS

Features	Value Pb	Value Ni
Working pH	7.5-8.5	8.0
Amount of Il-MWCNTs(mg)	18	20
Sample volume of serum (mL)	10 .0	10.0
Sample volume of urine, water (mL)	15.0	12.0
Volume of sample injection (µL)	20	20
Linear range for serum (µg L^{-1})	0.4-30	0.2-5.8
Mean RSD %, n=10	4.2	3.9
LOD for urine or serum (µg L^{-1})	0.1	0.05
Enrichment factor for urine or serum	5.1	24.7
Volume and concentration of HNO_3	0.2 mL, 0.3 M	0.2 mL, 0.2 M
Shaking/Centrifuging time	6.0 min, 4.0 min	6.0 min, 4.0 min
Correlation coefficient	R^2 = 0.9997	R^2 = 0.9995

3. Results and discussion

The lead and nickel were extracted and determined based on the IL-MWCNTs nanostructures which characterized by scanning electron microscopy (SEM), X-ray diffraction spectroscopy (XRD), and Fourier transform infrared spectroscopy (FT-IR).

3.1. X-ray diffraction spectroscopy (XRD)

The powder XRD patterns of pristine MWCNTs (a) and [Apmim][PF_6] immobilized on MWCNTs (b) are shown in Figure 2. The XRD of the MWCNTs and IL-MWCNTs were compared. The two characteristic graphitic peaks, at a 2θ value (28° and 45°) corresponding to the peaks of the (002) and (100) planes of hexagonal graphite MWCNT, respectively, are present in the XRD pattern of both measured samples. As shown in Figure 2, after functionalized of [Apmim][PF_6] on MWCNTs, no new peaks were seen, and the characteristic peaks of MWCNTs didn't change.

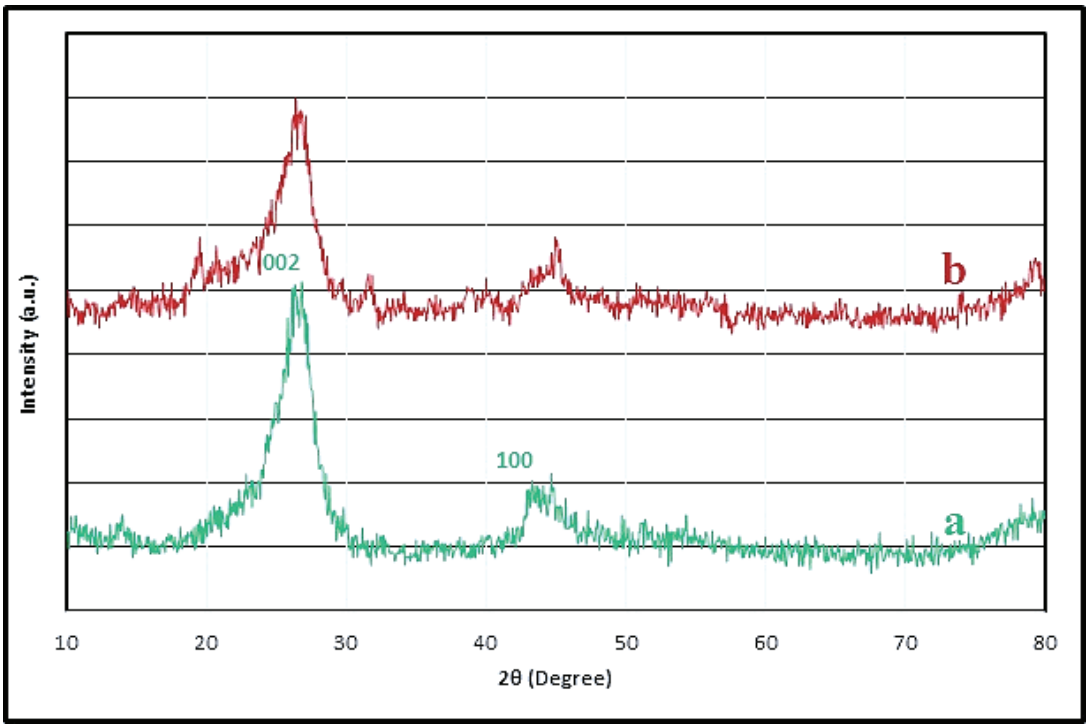

Fig. 2. The XRD of a) MWCNTs and b) IL-MWCNTs

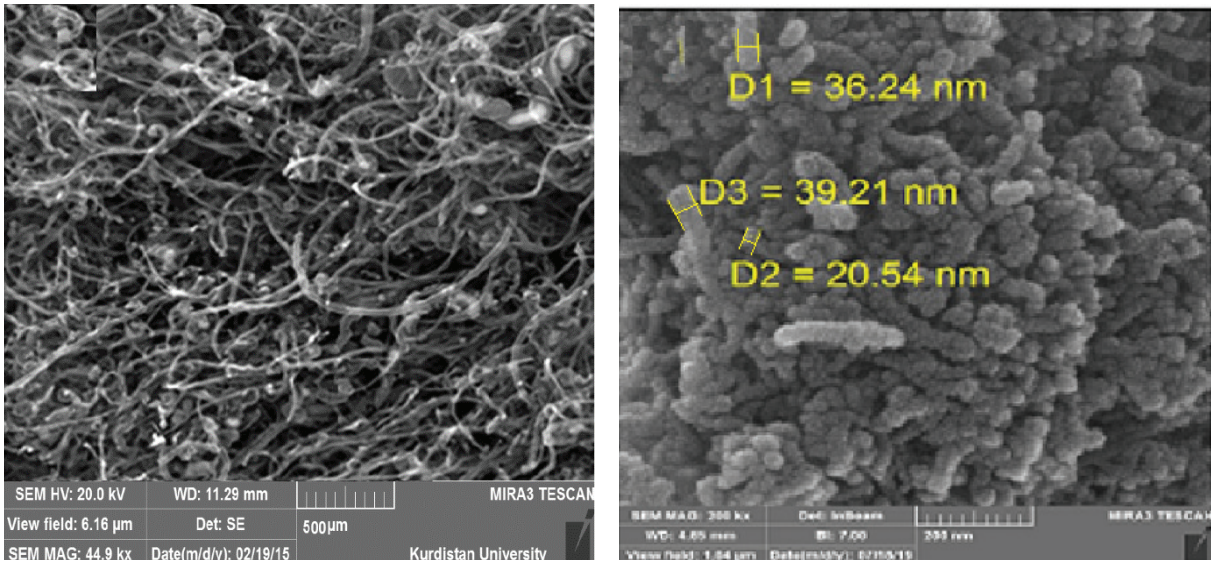

Fig. 3 . FE-SEM images of [Apmim][PF_6] immobilized on MWCNTs

3.2. Field emission scanning electron microscopy (FE-SEM)

FE-SEM images of [Apmim][PF_6] immobilized on MWCNTs are shown in Figure 3. It showed that the nanotubes have previous form and save their nature as MWCNTs. Due to FE-SEM images with different scale bars, a clear change in the morphology of [Apmim][PF_6] immobilized on MWCNTs were seen that showed the ionic liquid has been immobilized on the MWCNTs. The FE-SEM showed that, the IL-MWCNTs have nano size between 20-60 nm.

3.3. Fourier transform infrared spectroscopy (FT-IR)

The FT-IR spectra of [Apmim][PF_6]-MWCNTs are shown in Figure 4. This FTIR spectrum showed that the oxidation and covalently bond of the pristine MWCNTs. The peak of 1717 cm^{-1} is showed to the carbonyl bond (CO) due to oxidation functionalities. Also, the peak at 3437-3439 cm^{-1} was assigned to the stretching of O-H groups on the inner surface of oxidized MWCNTs. The supporting of the aminopropylsilane group on OH by treatment with APTMS was confirmed by the appearance of a sharp peak at around 1094 cm^{-1} which is attributed to the O-Si-O bond constructed between MWCNTs and ionic liquid moieties. The IR peak at 2922 and 2854 cm^{-1} were related to asymmetric and symmetric vibration absorptions, respectively, for the aliphatic CH_2 groups (C–H) of chlorosilane coupling agent and butyl chain of [Apmim][PF_6].

3.4. Optimization of DIL-µ-SPE procedure

The DIL-µ-SPE procedure was used based on IL-MWCNTs as a new adsorbent for determination lead and nickel in human urine and serum samples. High efficient recoveries, low RSD / LOD and variable linear ranges were obtained by optimizing of parameters such as, pH, amount of IL-MWCNTs, HNO_3 volume and concentration, the urine/serum volume, and the capacity of adsorption for extraction of Pb and Ni ions in human biological samples.

3.4.1. The pH optimization

The pH of urine and serum sample has a main role for adsorption of lead and nickel ions on IL-MWCNTs by DIL-µ-SPE procedure. The effect of pH range on the extraction of Pb and Ni with adsorbent was studied for Ni and Pb concentration between 0.2-5.5 µg L^{-1} and 0.4-30 µg L^{-1}, respectively (Fig. 5). Based on results, the recovery for Ni (II) and Pb(II) ions were increased at pH range of 8.0 more than 96%. Also, the extraction recoveries decreased at pH more than 8.5 and less than 7. So, the pH of 8 was selected

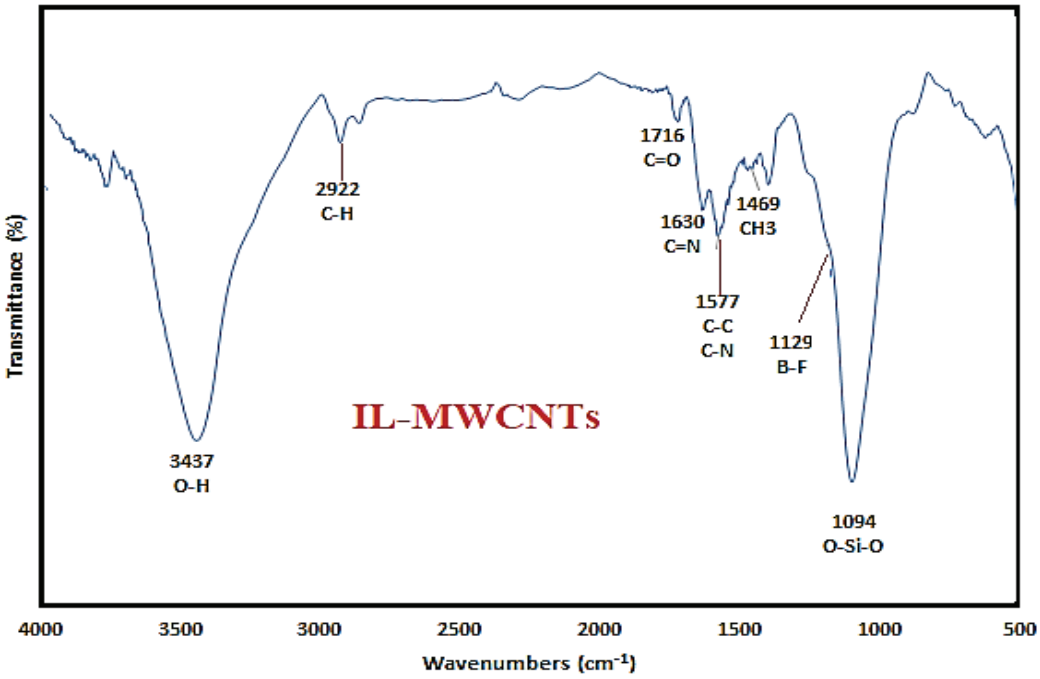

Fig.4. The FT-IR spectra of IL-MWCNTs

as optimal pH by the DIL-µ-SPE procedure. The adsorption mechanism on the IL-MWCNTs was achieved based on deprotonated amine groups (Pb^{2+}/Ni^{2+}→M…..-NH_2─IL) with the positively charged of metals in optimized pH. At lower pH, the surface of IL-MWCNTs have positively charged due to the H^+ protonation. Therefore, the extraction efficiencies were reduced by the similar charge law between Pb^{2+}/Ni^{2+and} positively charged of $^+NH_2$ of IL. Moreover, at pH of 8.0, the NH_2 group of IL had negative charge (-) and caused to increase adsorption adsorbent. The results showed, high recovery for extraction Pb /Ni were achieved at pH=8. In addition, the extraction efficiency was obtained about 30% in low pH as physically adsorption.

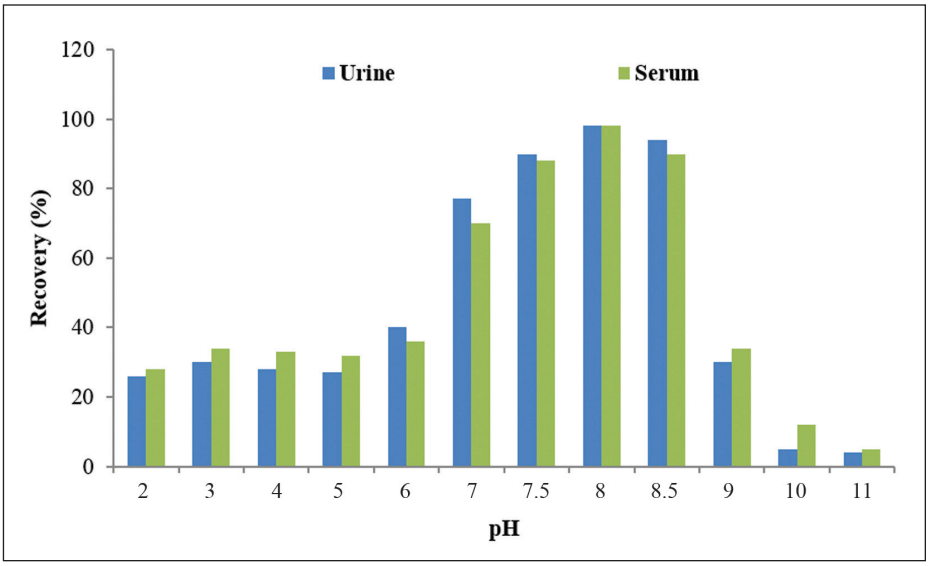

Fig. 5. The effect of pH on Pb/Ni extraction by the DIL-µ-SPE procedure

3.4.2. Optimization of amount of IL-MWCNTs

By the DIL-µ-SPE procedure, the amount of IL-MWCNTs was optimized for extraction of Ni(II) and Pb(II) in urine and serum samples. In this study, the amount of 5-40 mg of IL-MWCNTs was studied. The results showed that the 18 mg of IL-MWCNTs had high extraction for Ni(II) and Pb(II) in urine and serum samples in optimized conditions. Therefore, 20 mg of IL-MWCNTs was selected as optimal amount of IL-MWCNTs (Fig. 6). The more amount of IL-MWCNTs had no effect on the extraction recovery of Pb/Ni at pH=8.

3.4.3. Effect of eluent

The volume and concentration of eluents for lead and nickel extraction in urine and serum samples was studied. By the DIL-µ-SPE procedure, the various mineral acids were selected as elution phase for back extraction Pb(II) and Ni(II) from IL-MWCNTs phase at low pH. At low pH, the covalent bond between metal and amine group break down and Ni/Pb ions release in liquid phase. The different volumes from 100 to 500 µL and concentration between 0.1-0.5 mol L^{-1} were used as eluent phase (HCl, HNO_3, H_2SO_4 and H_3PO_4) by the DIL-µ-SPE method. The results showed that the 0.2 mol L^{-1} of HNO_3 (0.2 mL) had quantitatively back extracted Pb/Ni ions from IL-MWCNTs (Figs. 7). So, the HNO_3 was used for further works.

3.4.4.Sample volume optimization

The sample volume affected on the recoveries of Pb(II) and Ni(II) ions at pH=8. In this research, the various sample volumes of urine and serum from 1 to 20 mL were studied for Pb(II) and Ni(II) extraction in presence of the concentration between 0.2-5.5 µg L^{-1} and 0.4-30 µg L^{-1} for nickel and lead, respectively by the DIL-µ-SPE procedure. The results showed, the high extraction recoveries less than 12 mL and 15 mL for lead and nickel in urine samples were obtained, respectively. Also, the good recoveries less than 10 mL for lead and nickel in serum samples was achieved. Moreover, the extraction efficiency Pb(II) and Ni(II) ions was reduced by increasing more than 10 mL samples. Therefore, 10 mL was used as the optimal sample volume by proposed procedure (Fig. 8).

3.4.5.Time of extraction

The interaction of IL-MWCNTs with Pb(II) and Ni(II) ions is main factor for extraction process by DIL-µ-SPE procedure. So, the time dispersion of the IL-MWCNTs for metal extraction in the urine and serum samples were calculated. The high interaction caused to increase the extraction of metals in liquid phase. The effect of the ultrasonic time was evaluated based on IL-MWCNTs adsorbent at PH=8. The results showed, the maximum recovery was obtained about 6.0 min.

3.5. Reusability and Adsorption capacity

The reusability of IL-MWCNTs for extraction of with Pb(II) and Ni(II) ions was examined for several analyses by the DIL-µ-SPE method. The good recovery based on 19 times of extraction and back extraction cycles was obtained for Pb(II) and Ni(II) by IL-MWCNTs. Also, the absorption capacities IL- MWCNTs and MWCNTs for Pb(II) and Ni(II) extraction in urine and serum samples were achieved based on amine group of IL and surface area of MWCNTs. For this propose, 20 mg of IL-MWCNTs and MWCNTs were added to 10 mL of standard solution with concentration of 10 mg L^{-1} of Pb(II) and Ni(II) in batch system at optimized pH. By results, the adsorption capacity of MWCNTs and IL- MWCNTs for Ni(II) and Pb(II) was found 21.4/26.7 mg g^{-1} and 149.3 / 162.5 mg g^{-1}, respectively.

3.6. The effect of concomitant ions

The effect of interference ions on Pb(II) and Ni(II) extraction was studied in human urine and serum samples by DIL-µ-SPE procedure (Table 3). In optimized conditions, the various interfering ions in human biological samples was added to 10 mL of Pb(II) and Ni(II) of standard solution with concentration of 30 µg L^{-1} and 5.5 µg L^{-1}, respectively. The results showed, the main concomitant ions had no effect on the metal extraction at pH=8. The IL-MWCNTs had good

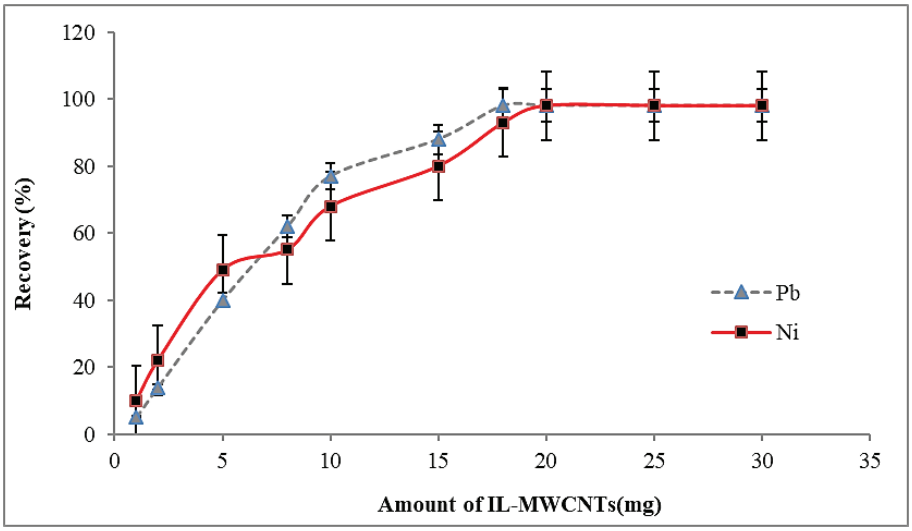

Fig. 6. The effect of amount of Il-MWCNTs on Pb/Ni extraction by the DIL-µ-SPE procedure

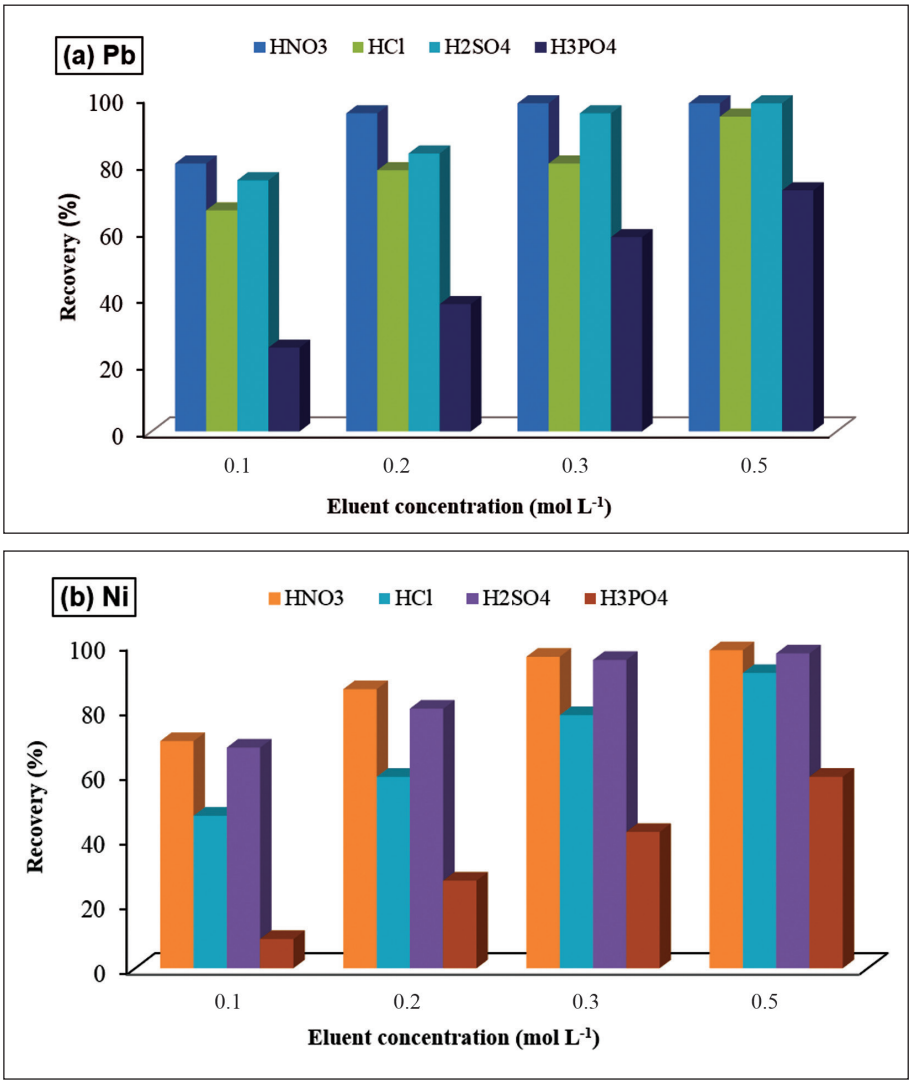

Fig. 7. The effect of eluent for back-extraction of a) lead and b) nickel from IL-MWCNTs by the DIL-µ-SPE procedure

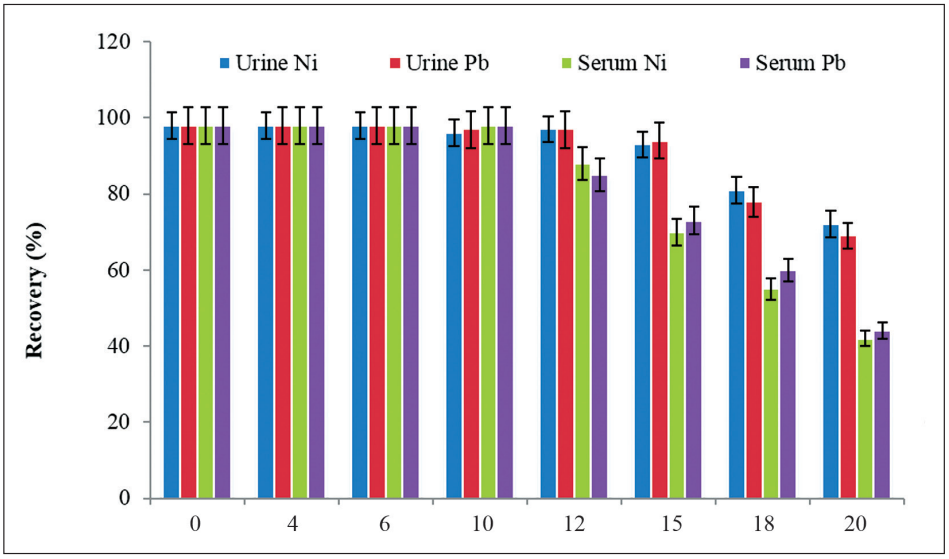

Fig. 8. The effect of sample volume on lead and nickel extraction in urine and blood samples by the DIL-µ-SPE procedure

Table 3. The effect of interference ions on Pb(II) and Ni(II) extraction in human urine and serum samples by the DIL-µ-SPE procedure

Interfering Ions(CA)	Mean ratio ($CA/C_{Pb(II)}$; or $CA/C_{Ni(II)}$)		Recovery (%)	
	Pb(II)	Ni(II)	Pb(II)	Ni(II)
Cr^{3+}, As^{3+}	900	800	98.8	97.4
Zn^{2+}, Cu^{2+}	750	600	97.2	98.5
Cd^{2+}	700	300	97.0	95.8
I^- , Br^-, F^- , Cl^-	1200	1100	99.2	98.6
Al^{3+}, V^{3+}	650	700	98.0	96.9
Na^+, K^+, Cl^-,Ca^{2+}, Mg^{2+}	900	800	97.5	97.1
Co^{2+}, Mn^{2+}	600	800	99.1	97.7
Hg^{2+}	50	80	96.6	97.3
Ag^+	200	150	98.0	98.7
SCN^- , $S_2O_3^{2-}$, CH_3COO^-, NO_3^-	800	900	97.6	99.4

extraction for Pb(II) and Ni(II) in present of the interference ions. The ethical committee of Semnan University confirmed the project for determining metals in the different matrices (ECSU, Project No. 8051127-01) with student proposal number(SN-9228558001).

3.7. Real sample analysis

The Pb(II) and Ni(II) ions was determined in urine and serum samples based on IL-MWCNTs by the DIL-µ-SPE procedure coupled to ET-AAS. By optimizing parameters, the means of 10 times determinations, for Pb(II) and Ni(II) ions were calculated. The human urine and serum samples were spiked with Pb(II) and Ni(II) standard solutions for 0.4-30 µg L^{-1} and 0.2-5.8 µg L^{-1} at pH=8, respectively (Table 4 and 5). The results showed us, the spiking real samples

has favorite accuracy and pricision for lead and nickel analysis in difficulty matrixes. The mean extraction efficiency of spiked urine and serum samples for Pb(II) and Ni(II) ions were obtained from 95.2% to 104.3% (RSD% < 5%) for ten samples. The spike samples demonstrated that the proposed method have satisfactory results for extraction and determination Pb(II) and Ni(II) ions in human biological samples. In addition, the Pb(II) and Ni(II) ions concentration in urine and serum samples was mesured with ICP-MS and compared to DIL-µ-SPE/ET-AAS procedure

Table 4. Validation of lead determination(Pb) based on spiking of human serum, blood, plasma and urine samples by DIL-µ-SPE procedure

Human Sample*	Spike (µg L^{-1})	*Found (µg L^{-1})	Recovery (%)
Blood	---	14.7 ± 0.6	---
	15	29.8 ± 1.3	100.6
Serum	---	15.2 ± 0.7	---
	15	30.1 ± 1.4	99.3
Urine	---	8.4 ± 0.3	
	10	18.2 ± 0.9	98.0
	---	5.5 ± 0.2	---
Plasma	5.0	10.3 ± 0.5	96.2

*Mean of three determinations of samples ± confidence interval (P = 0.95, n =10)
All samples volumes diluted with DW (1:10), Dilution factor =10

Table 5. Validation of nickel determination (Ni) based on spiking of human serum, blood, plasma and urine samples by DIL-µ-SPE procedure

Human Sample*	Spike (µg L^{-1})	*Found (µg L^{-1})	Recovery (%)
Blood	---	2.22 ± 0.12	---
	2.5	4.63 ± 0.18	96.4
Serum	---	2.65 ± 0.11	---
	2.5	5.27 ± 0.28	104.8
Urine	---	1.35 ± 0.06	99.3
	1.5	2.84 ± 0.12	
Plasma	---	0.52 ± 0.02	---
	0.5	1.01 ± 0.05	98.0

*Mean of three determinations of samples ± confidence interval (P = 0.95, n =10)

Table 6. Comparing of DIL-µ-SPE /ET-FAAS with ICP-MS method for mean concentration of Pb and Ni in human samples (**µg** L^{-1})

Sample	ICP-MS	ICP-MS	*IL-MWCNTs /ET-AAS	*IL-MWCNTs /ET-AAS
	Pb	Ni	Pb	Ni
Blood	29.56± 0.96	2.53 ± 0.04	28.82± 1.42	2.41 ± 0.11
Urine	18.13 ± 0.35	1.87± 0.03	17.49 ± 0.77	1.95 ± 0.09
Serum	27.48 ± 0.81	4.68 ± 0.08	27.06 ± 1.32	4.43 ± 0.23

*Mean of three determinations of samples ± confidence interval (P = 0.95, N =10),
The lead samples diluted with DW (1:10)

(Table 6). The precision and accuracy of results showed the validation of methodology for the Pb(II)/ Ni(II) determination by IL-MWCNTs adsorbent.

4. Conclusions

A simple and efficient method based on ILMWCNTs adsorbent was used for separation and determination of nickel and lead in urine and serum samples by ET-AAS. By the DIL-µ-SPE procedure, high recovery and efficient extraction was obtained at optimized conditions. The linear range and working range for Ni(II) and Pb(II) was achieved 0.2-3.42 µg L^{-1}/0.4-17.6 µg L^{-1} and 0.2-5.8 µg L^{-1}/0.4-30 µg L^{-1} for 10 mL of urine and serum samples, respectively. The mean correlation coefficient and enrichment factor for Ni(II) and Pb(II) were obtained 0.9997/0.9995 and 24.7/5.1, respectively. The NH2 group in IL-MWCNTs was coordinated with Ni(II) and Pb(II) cations and separated from liquid phase by centrifuging process. The high adsorption capacities, recovery, enrichment and favorite reusability caused to consider the DIL-µ-SPE procedure as a new methodology for nickel and lead extraction in human samples with low LOD and RSD (>5%) in optimized conditions. The validation methodology based on spiking samples and ICP-MS analysis showed, the DIL-µ-SPE method can be used as applied techniques for Ni(II) and Pb(II) determination in human samples.

5. Acknowledgements

The authors wish to thank Semnan University, Iran. The ethical committee of Semnan University confirmed the project for determining metals in the different matrices (ECSU, Project No. 8051127-01) with student proposal number (SN:9228558001).

6. References

[1] World Health Organization (WHO), Preventing disease through healthy environments: exposure to lead: a major public health concern, 2019.

[2] Environmental Protection Agency (USEPA) Basic Information About Lead in Drinking Water, 2014.

[3] Agency for Toxic Substances and Disease Registry, Division of Toxicology and Human Health Sciences, 1600 Clifton Road NE, Mailstop S102-1, Atlanta, GA 30333, revision 2019.

[4] Agency for Toxic Substances and Disease Registry (ATSDR), Toxicological profile for Lead,Atlanta, GA: U.S. Department of Health and Human Services, Public Health Service, 2019.

[5] Agency for Toxic Substances and Disease Registry (ATSDR), Toxicological profile for Nickel. Atlanta, GA: U.S. Department of Health and Human Services, Public Health Service, 2005.

[6] A.A. Ab Latif Wani, J.A. Usmani, Lead toxicity: a review, Interdiscip. toxicol., 8 (2015) 55-64.

[7] G. Flora, D. Gupta, A. Tiwari, Toxicity of lead: a review with recent updates, Interdiscip. toxicol., 5 (2012) 47-58.

[8] T. Dignam, R. B. Kaufmann, L. LeStourgeon, M. Jean Brown, Control of lead sources in the United States, public health progress and current challenges to eliminating lead exposure, J. Public Health Manag. Pract., (2019) S13–S22. PMC6522252, https://doi.org/10.1097/PHH.0000000000000889.

[9] M. Kirberger, J.J. Yang, Structural differences between Pb^{2+} and Ca^{2+}binding sites in proteins: implications with respect to toxicity, J. Inorg. Biochem., 102 (2008) 1901–1909.

[10] J.S. Magyar, T.-C. Weng, C.M. Stern, D.F. Dye, B.W. Rous, J.C. Payne, B.M. Bridgewater, A. Mijovilovich, G. Parkin, J.M. Zaleski, Reexamination of lead (II) coordination preferences in sulfur-rich sites: implications for a critical mechanism of lead poisoning, J. Am. Chem. Soc., 127 (2005) 9495-9505.

[11] United States Food and Drug Administration (USFDA), Elemental impurities guidance for industry, Department of Health and Human Services, p. 41, 2017.

[12] B.C. Schwarcz, L. Chilton, B. Shirley, S. Seifert, Childhood lead exposure associated with the use of kajal, an eye cosmetic from Afghanistan Albuquerque, New Mexico,

Morb. Mortal Wkly. Rep., 62 (2013) 917-919.
[13] K.L. Caldwell, P.Y. Cheng, J.M. Jarrett, Measurement challenges at low blood lead levels, Pediatrics., 140 (2017) e20170272. https://doi.org/10.1542/peds.2017-0272
[14] D.C. Bellinger, Neurological and behavioral consequences of childhood lead exposure. PLOS Med., 5 (2008) e115. https://doi.org/10.1371/journal.pmed.0050115.pdf.
[15] A. Abbas, A.M. Al-Amer, T. Laoui, M.J. Al-Marri, M.S. Nasser, M. Khraisheh, Heavy metal removal from aqueous solution by advanced carbon nanotubes: critical review of adsorption applications, Sep. Purifi. Technol., 157 (2016) 141-61.
[16] S. Feng, X. Wang, G. Wei, P. Peng, Y. Yang, Z. Cao, Leachates of municipal solid waste incineration bottom ash from Macao: Heavy metal concentrations and genotoxicity, Chemosphere., 67 (2007) 1133-1137.
[17] S.K. Seilkop, A.R. Oller, Respiratory cancer risks associated with low-level nickel exposure: An integrated assessment based on animal, epidemiological, and mechanistic data, Regul. Toxicol. Pharm., 37 (2003) 173–190.
[18] Agency for Toxic Substances and Disease Registry, Division of Toxicology and Human Health Sciences, 1600 Clifton Road NE, Mailstop S102-1, Atlanta, GA 30333, revision 2019.
[19] Agency for Toxic Substances and Disease Registry (ATSDR), Toxicological profile for Nickel. Atlanta, GA: U.S. Department of Health and Human Services, Public Health Service, 2005.
[20] A. Fadhil Khudhair, M. Khudhair Hassan, H. F. Alesary , A. S. Abbas, Simple pre-concentration method for the determination of nickel(II) in urine samples using UV-VIS spectrophotometry and flame atomic absorption spectrometry techniques, Indones. J. Chem., 19 (2019) 638 – 649.
[21] S. Orecchio, D. Amorello, Determination of trace elements in gluten-free food for celiac people by ICP-MS, Microchem. J., 116 (2014) 163-172.
[22] M. Arjomandi, H. Shirkhanloo, A review: Analytical methods for heavy metals determination in environment and human samples, Anal. Methods Environ. Chem. J., 2 (2019) 97-126.
[23] J. Shan Qun, W. Xiang Yu, S. Jin Lyu, Analysis of nickel distribution by synchrotron radiation X-ray fluorescence in nickel-induced early- and late-phase allergic contact dermatitis in Hartley guinea pigs, Chinese Med. J., 132 (2019)1959-1964.
[24] A. Baysal, S. Akman, A rapid solid sampling method for determination of nickel and copper along human hair by ETAAS, Microchem. J., 98 (2011) 291-296
[25] M. Eftekhari, M. Gheibi, M. Akrami, F. Iranzad, Solid-phase extraction of ultra-trace levels of lead using tannic acid-coated graphene oxide as an efficient adsorbent followed by electrothermal atomic absorption spectrometry; response surface methodology–central composite design, New J. Chem., 42 (2018) 1159-1168.
[26] M. Rajabi M. Abolhosseini, Magnetic dispersive micro-solid phase extraction merged with micro-sampling flame atomic absorption spectrometry using (Zn-Al LDH)-(PTh/DBSNa)-Fe_3O_4 nanosorbent for effective trace determination of nickel(II) and cadmium(II) in food samples, Microchem. J., 159 (2020) 105450.
[27] S. Azimi, Z. Es'haghi, A magnetized nanoparticle based solid-phase extraction procedure followed by inductively coupled plasma atomic emission spectrometry to determine arsenic, lead and cadmium in water, milk, Indian rice and red tea, Bull. Environ. Contam. Toxicol., 98 (2017) 830-836.
[28] W. Ding, X. Wang, T. Liu., Preconcentration/extraction of trace bisphenols in milks using a novel effervescent reaction-assisted

dispersive solid-phase extraction based on magnetic nickel-based N-doped graphene tubes, Microchem. J., 150 (2019) 104109.

[29] M. Shirani, F. Salari, S. Habibollahi, A. Akbari, Needle hub in-syringe solid phase extraction based a novel functionalized biopolyamide for simultaneous green separation/ preconcentration and determination of cobalt, nickel, and chromium (III) in food and environmental samples with micro sampling flame atomic absorption spectrometry, Microchem. J., 152 (2020) 104340.

[30] S. M. Sorouraddin, M. A. Farajzadeh H. Nasiri, Picoline based-homogeneous liquid–liquid microextraction of cobalt(II) and nickel(II) at trace levels from a high volume of an aqueous sample, Anal. Methods, 11 (2019) 1379-1386.

[31] L. Khoshmaram, Air-assisted liquid–liquid microextraction combined with flame atomic absorption spectrometry for determination of trace Pb in biological and aqueous samples, Int. J. Environ. Anal. Chem., 101 (2021) 838-848.

[32] H. Shirkhanloo, S. Davari Ahranjani, A lead analysis based on amine functionalized bimodal mesoporous silica nanoparticles in human biological samples by ultrasound assisted-ionic liquid trap-micro solid phase extraction, J. Pharm. Biomed. Aanl., 157 (2018) 1-9.

[33] H. Shirkhanloo, Z. Karamzadeh, A novel biostructure sorbent based on CysSB/MetSB@ MWCNTs for separation of nickel and cobalt in biological samples by ultrasound assisted-dispersive ionic liquid-suspension solid phase micro extraction, J. Pharm. Biomed. Anal., 172 (2019) 285-294.

[34] N. Esmaeili, J. Rakhtshah, E. Kolvari, H. Shirkhanloo, Ultrasound assisted-dispersive-modification solid-phase extraction using task-specific ionic liquid immobilized on multiwall carbon nanotubes for speciation and determinationmercury in water samples, Microchem. J., 154 (2020) 104632.

AMECJ

Research Article, Issue 2
Analytical Methods in Environmental Chemistry Journal
Journal home page: www.amecj.com/ir

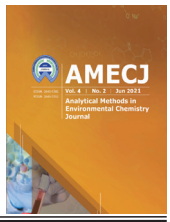

Determination of fenthion in environmental water samples by dispersive liquid–liquid microextraction coupled with spectrofluorimetric and chemometrics methods

Tahereh Eskandari[a], Ali Niazi[b,*], Mohammad Hossein Fatemi[c] and Mohammad Javad Chaichi[c]
[a]*Department of Chemistry, Arak Branch, Islamic Azad University, Arak, Iran*
[b] *Department of Chemistry, Central Tehran Branch, Islamic Azad University, Tehran. Iran*
[c] *Department of Analytical Chemistry, Faculty of Chemistry, Mazandaran University, Babolsar, Iran*

ARTICLE INFO:
Received 15 Feb 2021
Revised form 24 Apr 2021
Accepted 20 May 2021
Available online 30 Jun 2021

Keywords:
Fenthion,
Pesticides,
Organophosphoruse pesticides,
Dispersive liquid–liquid icroextraction,
Box–Behnken design,
Spectrofluorimetry

ABSTRACT
In the present study, a simple, rapid and efficient dispersive liquid–liquid microextraction (DLLME) coupled with spectrofluorimetry (SFM) and chemometrics methods have been proposed for the preconcentration and determination of fenthion in water samples. Box–Behnken design was applied for multivariate optimization of the extraction conditions (sample pH, the volume of dispersive solvent and volume of extraction solvent). Analysis of variance was performed to study the statistical significance of the variables, their interactions and the model. Under the optimum conditions, the calibration graph was linear in the range of 5.0–110 ng mL^{-1} with the detection limit of 1.23 ng mL^{-1} ($3S_b/m$). Parallel factor analysis (PARAFAC) and partial least square (PLS) modelling were applied for the multivariate calibration of the spectrofluorimetric data. The orthogonal signal correction (OSC) was applied for preprocessing of data matrices and the prediction results of model, and the analysis results were statistically compared. The accuracy of the methods, evaluated by the root mean square error of prediction (RMSEP) for fenthion by OSC-PARAFAC and OSC-PLS models were 0.37 and 0.78, respectively. The proposed procedure could be successfully applied for the determination of fenthion in water samples.

1. Introduction

The organophosphorous pesticides (OPPs) have been widely used in agriculture for crop production and fruit tree treatment, but many of them are identified as highly toxic compounds [1–3]. They are released into the environment from manufacturing, transportation and agriculture applications. OPPs have been found in ground waters, surface waters, lagoons and drinking water. Fenthion (O,O-Dimethyl O-[3-methyl-4-(methylsulfanyl)phenyl] phosphorothioate) is a contact and stomach organophosphorous pesticide widely used in the control of many sucking, biting pests, especially fruit flies, stem borers and mosquitoes on crops such as alfalfa, rice, sugar, vegetables and forests. Fenthion is toxic for the human and animal health [4–6]. The toxicological effect of fenthion, is almost entirely due to the inhibition of acetylcholinesterase in the nervous system, resulting in respiratory, myocardial and neuromuscular transmission impairment [5, 7]. Due to the low concentration of the analytes and the complex matrix of the samples, a preliminary sample preconcentration and a separation

*Corresponding Author: Ali Niazi
Email: ali.niazi@gmail.com, ali.niazi@iauctb.ac.ir
https://doi.org/10.24200/amecj.v4.i02.138

technique are required. Thus, different extraction processes have been used for separation and pre-concentration of trace pesticide residues, such as solid phase extraction method (SPE) [8–11], solid phase microextraction (SPME) [12], [13], single drop microextraction (SDME) [14] and dispersive liquid–liquid microextraction (DLLME) [15–17]. In the last decades, liquid–phase microextraction (LPME), based on the miniaturization of traditional LLE technique by greatly reducing the use of organic solvent has been reported as an alternative for sample preparations. One of the most popular LPME techniques is dispersive liquid-liquid microextraction (DLLME) which is widely used as a preconcentration method [18-21]. DLLME was developed by Assadi and co-workers [16]. By consisting of the formation of a cloudy solution promoted by the fast addition in the aqueous sample of a mixture of extractor and dispersive solvents. The tiny droplets formed and dispersed among the aqueous sample solution are further joined and sedimented in the bottom of a conical test tube by centrifugation. This method provides many advantages including rapidity, simplicity of operation, high recovery and enrichment factor. After sample preparation, the determination of OPPs in different sample matrices was carried out by using gas chromatography mass spectrometry (GC-MS) [9, 22], gas chromatography (GC) [23–25] and high-performance liquid chromatography (HPLC) [26,27]. Fluorescence spectrometry is a sensitive, selective and relatively low cost method for the quantitative analysis of pesticides and other pollutants [28–30]. Different experimental variables can affect the extraction yield in the DLLME procedure; therefore, a multivariate approach has been widely used for their optimization. Statistical methods are useful to determine the effects of variables on the extraction procedure. The response surface methodology (RSM) based on statistical design of experiments (DOEs) has been extensively used for modelling and optimization in various analytical procedures [31–36]. Response surface methodology (RSM) is powerful multivariate technique that used for building empirical model via collection of mathematical and statistical method. The main advantage of RSM is that it reduces the number of experiment because several factors can be varied simultaneously for optimization and as a result saves time, energy, and chemicals [16,37,38]. Box–Behnken design is the most common and efficient design used in RSM. Box–Behnken design is a second order multivariate technique based on three level partial factorial designs. Box–Behnken is a spherical, rotatable or nearly rotatable that consists of a central point and with the midpoints of the edges of the variable space [15–17], [33, 34]. Two dimensional excitation emission (EEM) fluorescence data can be obtained by measuring the emission spectra at various excitation wavelengths. In recent years, application of multi-way data analysis techniques has increased significantly in the analytical chemistry. There are several multivariate calibration procedures that can be used for the treatment of EEM fluorescence data, in order to quantify the compounds, present in a mixture [39]. In fluorescence analysis, parallel factor analysis (PARAFAC) [28], [40–44] and partial least-squares regression (PLS) [34, 43], [45–47] has been mostly applied for the analyses of three-way data obtained as series of emission spectra measured for different excitations. PLS is a factor analysis method that has been used in multicomponent quantitative analysis from several spectral data, such as IR, UV-visible or fluorescence [47]. Partial Least Squares (PLS) regression is a method to predict the response variable based on predictor variables and to describe their common structure. The main advantage of PLS calibration procedures is that they can model a system even in the presence of interfering signals, provided that they are included in the calibration step. PARAFAC is a multi-way decomposition method that has investigated to be useful for the analysis of second-order calibration. The main advantages of the PARAFAC model are the uniqueness, simplicity of its solutions and quantification of an analyte, even in the presence of unknown interferences (the second-order advantage) [40, 44].The orthogonal signal correction (OSC) is a useful pre-processing step that improves the chemometrics model

by filtering systematic variation in the spectra not associated with the concentration [40].

The aim of this paper is to develop a fast, sensitive and inexpensive spectrofluorimetric method coupled with PARAFAC modelling for the determination and preconcentration of fenthion in environmental water samples using DLLME procedure. Also, the effects of various experimental variables, including sample pH, the volume of extraction solvent and volume of dispersive solvent were investigated and optimized using Box–Behnken design.

2. Experimental

2.1. Chemicals and reagents

All chemicals and solvents, such as methanol, ethanol, acetonitrile, chloroform, carbon tetrachloride, chlorobenzene, and dichloromethane were purchased from Sigma–Aldrich and Merck. fenthion standards were obtained from Dr. Ehrenstorfer (Augsburg, Germany). All of the reagents used in this work were of analytical grade. Chloroform, carbon tetrachloride, chlorobenzene and dichloromethane purchased from Sigma, Germany. A buffer solution was prepared using universal buffer solution. Universal buffer solutions were prepared by mixing phosphoric, acetic, and boric acid. A stock solution of Fenthion ($C_{10}H_5O_3PS_2$, 1000 mg L^{-1}) was prepared by dissolving appropriate amounts of analyte in methanol, stored under dark conditions in refrigerator (Schema 1) and synthesized by condensation of 4-methylmercapto-m-cresol and dimethyl phosphorochloridothionate. Working standard solutions were obtained daily by appropriately diluting this stock solution with ultrapure water.

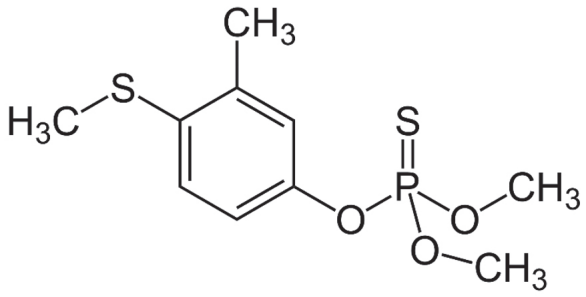

Schema1: Picture of Fenthion as an organothiophosphate insecticide

2.2. Apparatus and software

The pH was determined with a model 780 Metrohm pH-meter with combined glass–calomel electrode. A centrifuge (Sigma) was used to accelerate the phase separation process. A PerkinElmer, LS 45 Spectrofluorimeter enhanced by 150 W Xe lamp was coupled with a computer and equipped with a 300 µL quartz microcell which was used for recording the spectra using Windows 7 operating system. All the measurements were done at the exciting wavelength of 200-300 nm for every 10 nm, and at the emission wavelength in the 300-500 nm range for every 1 nm. Box–Behnken design and statistical analysis were performed with Minitab Version 16. The programs for PLS, PARAFAC, and OSC calculation were written in MATLAB 2018 and run on a personal computer (CPU 3.0 GHz and RAM 4 GB) equipped with the Windows 7 operating system. The applied OSC version is based on the Wold et al. algorithm.

2.3. Experimental procedure

10 mL of sample solution containing 5.0–110.0 ng mL^{-1} of Fenthion, and 1.0 mL of buffer solution (pH was adjusted to 10.0) was poured into a test tube with a conical bottom. Then an appropriate mixture of disperser solvent (methanol, 600 µL) and extraction solvent (chlorobenzene, 220 µL) was rapidly injected into the sample tube. In this step, a cloudy solution was immediately formed in the test tube and then, it was centrifuged for 1 min at 3000 rpm to separate the phases. Finally, the upper aqueous solution was removed by syringe, and the sediment phase was used for subsequent measurement by spectrofluorimetric which was shown in Fig.1.

3. Result and discussion

3.1. Selection of extraction and dispersive solvent

The selection of an appropriate extraction solvent is very important for a DLLME procedure. It must have some properties, such as higher density than water, good extraction efficiency of the analytes, and low solubility in water. Chloroform, carbon

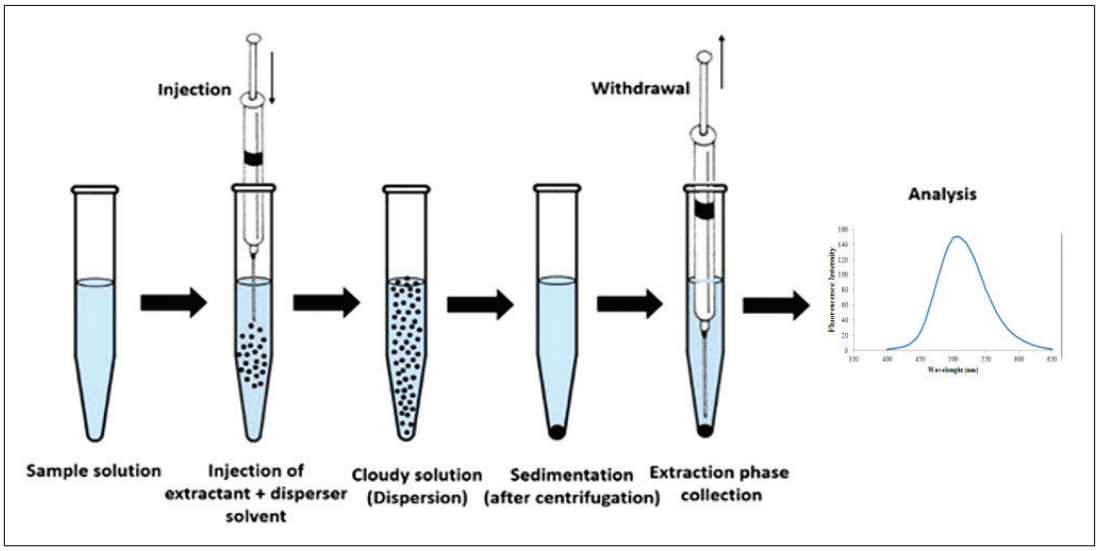

Fig.1. Dispersive liquid–liquid microextraction (DLLME) procedure.

tetrachloride, chlorobenzene and dichloromethane were studied as extraction solvents. The results showed that among the solvents tested, chlorobenzene has the highest recovery in comparison with the other tested solvents. Therefore, chlorobenzene was chosen for further experiments. The dispersive solvent should be miscible with the organic extraction solvent and the aqueous phase. Suitable dispersive solvent can increase the surface area for transferring the analyte from sample to extraction solvent. Thereby, ethanol, methanol, acetonitrile and acetone are selected for this purpose. The results indicated that the best recovery was obtained by using methanol. Thus in this study methanol was selected as suitable disperser solvent.

3.2. Effect of pH and salt addition

The extraction efficiency for analyte can be affected by adjusting the pH of the aqueous solution. The effect of pH variation on extraction efficiency was investigated in the range of 1-12 and the optimal pH was found to be 10 (Fig. 2). The influence of salt addition is also an important factor for extraction. Salt addition can improve extraction yield in DLLME, especially for those analytes with a lower solubility, as a result of a salting out effect. Therefore, NaCl in the concentration range of 1–15% (w/v) was studied as a salting agent and no significant effect on the extraction efficiency was observed. Considering the obtained results, no addition of salt was chosen in the further analysis.

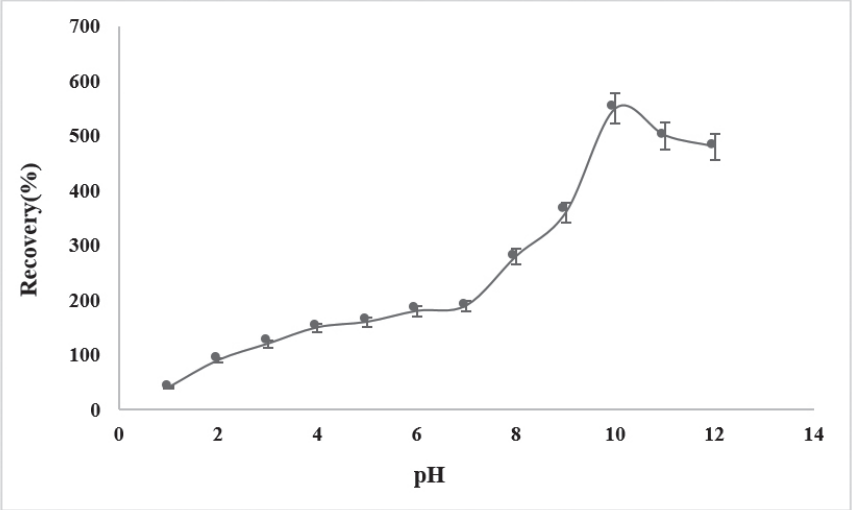

Fig. 2. The effect of pH variation on extraction efficiency

3.3. Effect of extraction and centrifugation time

In DLLME, extraction time is defined as the interval time between injection of the extraction mixture into the aqueous sample and starting to centrifuge. The effect of the extraction time was studied in the range of 1–10 min. The experimental results showed that time has no impact on extraction efficiency. This means that the transfer of the analyte from aqueous phase to the extraction solvent was fast, which was the advantage of DLLME procedure. Therefore, 1 min was defined as extraction time. Centrifugation is a critical step in the DLLME technique, in order to achieve the phase separation of extraction phase from the aqueous phase. So, the effect of centrifugation time was also examined in the ranges of 1–5 min. It was observed that by increasing the centrifugation time, the response remained constant. Therefore, the time and rate of centrifugation had no significant effect on the extraction efficiency. According to this result, 1 min was selected as the optimum centrifuge time, in the following study.

3.4. Box–Behnken analysis

Box–Behnken experimental design was used to optimize and evaluate the main effects and interaction effects of the process variables on the recovery. The sample pH (X_1), the volume of extraction solvent (X_2) and volume of dispersive solvent (X_3) were selected as the three independent variables as showed in Table 1.

The number of experiments (N) required for the development of Box– Behnken design was defined as $N = 2k(k-1)+C_0$, (where k was the number of factors and C_0 is the number of central points). Thus, a total of 15 runs were carried out for optimizing these three variables at three levels (low, medium and high). The Box–Behnken design matrix and the recovery are presented in Table 2. According to Box–Behnken matrix, a total of 15 tests containing 3 replicates at the center point were performed in random order.An empirical relationship between the response and the variables can be presented by the flowing equation (Eq.1):

$$Y = \beta_0 + \sum \beta_i X_i + \sum \beta_i X_i^2 + \sum \beta_j X_i X_j + \varepsilon$$

(Eq. 1)

Where Y is the predicted response and X_i represented the effect of the independent variables. Thus, X_i^2 and X_iX_j represented the quadratic, and interaction terms respectively[7]. β_i, β_{ii} and $\beta_{ij\ (i\neq j)}$ were the coefficient of linear, quadratic and interaction, respectively. β_0 and ε represented the constant and the random error, respectively.

Experimental data were fitted to a second-order polynomial mathematical equation. Analysis of variance (ANOVA) was applied to the analysis of experimental data at 95% confidence interval so that the significance of each term was evaluated by their corresponding *p*-values which are presented in Table 3.

According to Table 3, it was concluded that all the linear (X_1, X_2, X_3 and X_4) and quadratic terms (X_1^2, X_2^2, X_3^2 and X_4^2), were significant at 5% probability level. As shown in Table 3, the interaction between sample pH and volume of extraction solvent (X_1X_2) and the volume of extraction solvent and dispersive solvent (X_2X_3) were significant. The polynomial model is represented in Equation 2:

$$"Y" = -2068{\cdot}95 + 311{\cdot}71X_1 + 1{\cdot}2X_2 + 1{\cdot}56X_3 - 14{\cdot}98X_1^2 - 0{\cdot}01X_2^2 - 0{\cdot}03X_3^2 + 0{\cdot}04X_1X_2 + 0{\cdot}01X_2X_3$$

(Eq.2)

The 3D response surface graphs of the effect between each factor were shown in Figure 3. The plot in Figure 3 displayed that the recovery increased with the increase of initial solution pH ranging from 9 to 10. However, pH values higher than 10 reduced the recovery. Also, the response first increased with extraction solvent volume approximately 220 µL, and thereafter decreased. The optimum values of the tested variables were obtained as follows: X_1= 10.0, X_2= 220.0 µL and X_3= 600.0 µL.

Table 1. Variables and their levels in Box-Behnken design.

Factors	Symbol	Level		
		Low (-1)	Medium (0)	High (+1)
pH	X_1	9	10	11
V_{ext} (µL)	X_2	100.0	200.0	300.0
V_{disp} (µL)	X_3	500.0	600.0	700.0

Table 2. Box-Behnken design matrix with obtained result.

Run No.	Actual level of factors			Recovery (%)
	X_1	X_2	X_3	
1	10.0	100.0	500.0	59.2
2	10.0	300.0	700.0	78.4
3	10.0	200.0	600.0	97.1
4	9.0	300.0	600.0	77.6
5	11.0	300.0	600.0	69.5
6	11.0	200.0	700.0	73.2
7	10.0	100.0	700.0	71.2
8	9.0	100.0	600.0	60.4
9	10.0	200.0	600.0	95.7
10	11.0	200.0	500.0	68.5
11	11.0	100.0	600.0	70.1
12	10.0	300.0	500.0	81.3
13	10.0	200.0	600.0	96.5
14	9.0	200.0	500.0	65.2
15	9.0	200.0	700.0	71.5

Table 3. Analysis of variance evaluation of linear, quadratic, and interaction terms for each response variable.

Variables	DF[a]	SS[b]	MS[c]	F-values	p-value
Model	9	2092.19	232.465	50.44	0.000
X_1	1	820.22	820.222	177.97	0.000
X_2	1	379.47	379.466	82.33	0.000
X_3	1	374.70	374.700	81.30	0.000
X_1^2	1	828.46	828.463	179.76	0.000
X_2^2	1	536.50	536.503	116.41	0.000
X_3^2	1	518.85	518.848	112.58	0.000
X_1X_2	1	79.21	79.210	17.19	0.009
X_1X_3	1	0.64	0.640	0.14	0.725
X_2X_3	1	55.50	55.502	12.04	0.018
Residual	5	23.04	4.609	-----	-----
Lack-of-Fit	3	22.06	7.352	14.90	0.064
Pure Error	2	0.99	0.493	-----	-----
Total	14				

R^2 = 98.91; Adjusted R^2 = 96.95.
[a] DF: degree of freedom.
[b] SS: sum of squares.
[c] MS: mean square.

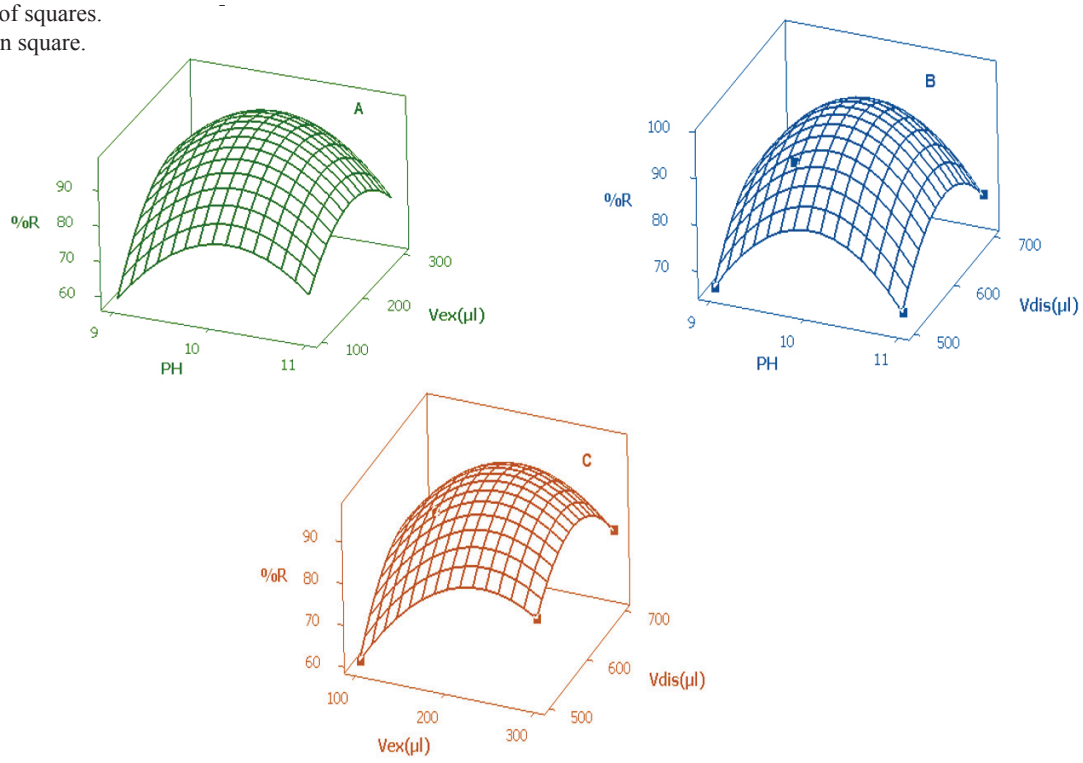

Fig.3. Three dimensional response surface plots representing the effect of process variable on recovery (A): (A) pH–volume of extraction solvent (V_{ext}); (B) pH–volume of dispersive solvent (V_{dis}); (C) volume of extraction solvent–volume of dispersive solvent.

3.5. Statistical analysis

The suitability of the model was analyzed by ANOVA and the results shown in Table 3. The analysis of variance of regression model demonstrated that the model was highly significant at probability level (p-value is below 0.05). Also, the quality of the fitted model was studied by the coefficients of determination and adjusted the determination coefficient. The coefficient of determination R^2 and adjusted R^2 values were 0.9891 and 0.9695, respectively. In other words, the model could explain 98.91% of the variability in the response. The validation of the goodness of fit was evaluated by the lack of fit test. The lack of fit *p*-value of 0.064 implies the lack of fit is not significant and it means that the quadratic polynomial model fit the data well.

3.6. Analytical figures of merit

The linear range, repeatability, reproducibility and limit of detections (LODs) for fenthion were investigated under the optimized conditions to evaluate the proposed procedure performance. The Linearity was obtained over the range of 5.0–110.0 ng mL^{-1} with a calibration curve (I=0.024+0.3745C) and with a correlation coefficient (r^2) of 0.9870. The limit of detection which is defined as $3S_b/m$ (where S_b is the standard deviation of the blank signals for ten replicate, and m is the slope of the calibration curve after extraction) was calculated to be 1.23 ng mL^{-1}. Precision, accuracy and stability were evaluated by repeatability (intra-day) and reproducibility (inter-day) analyses. The precision of the method was determined by analysing 5 samples on the same day (intra-day) or 5 samples on consecutive days (inter-day), and represented as RSD%. The intra-day precision was 2.74 % and the inter–day precision was 3.82 %. Finally, the enrichment factor (EF) (calculated from the ratio of the slopes of the calibration curves obtained with and without pre-concentration) of 80.12 for Fenthion were determined.

3.7. Partial least squares analysis

PLS model was prepared and recorded for an excitation wavelength in the 200-300 nm range for each 10 nm, while emission wavelength was in the range of 300-500 nm for every nm. 15 samples were used for calibration set and five samples not used for building the PLS calibration model were selected as a validation test. Using the PLS and OSC-PLS methods, the concentration of fenthion in the validation set were calculated. The predicted concentrations of analyte with these methods are shown in Table 4. In the PLS model, the number of factors was determined by the cross-validation (leave-one-out) method components and the predicted residual error sum of squares (PRESS) was calculated. As shown in Table 4, the optimum number of factors of PLS for fenthion (N.F. = 5) was larger than the theoretically expected value of 1.

OSC is a preprocessing technique that improves the calibration model by removing the information from the spectrofluorimetric data that unrelated to target variables based on constrained principal component analysis. Therefore, the spectral data were preprocessed by OSC method. The results (Table 4) showed that OSC preprocessing has reduced the number of factors (N.F. = 3).

3.8. Parallel factor analysis

The data was then arranged in a 10 × 11 × 251 three-dimensional array consisting of 11 solutions with different fenthion concentrations in the rows (5.0-110.0 ng mL^{-1}), 200 emission wavelengths in the columns, and 10 excitation wavelengths in the slices. For the evaluation of the predictive ability of a multivariate calibration model, the root mean square error of prediction (RMSEP) and relative standard error of prediction (RSEP) were also applied. The obtained results were summarized in Table 4. The RMSEP and RSEP values with OSC-PARAFAC were 0.37, 0.45% for fenthion, respectively. These results confirmed that the OSC-PARAFAC method provided high prediction ability with low RMSEP values with respect to PLS method. Statistical parameters of the linear relationship between the proportion loadings calculated by PARAFAC and OSC-PARAFAC are shown in Table 5.

Table 4. Added and obtained results of the prediction set of fenthion using different methods (ng mL^{-1}).

Added fenthion (ng mL^{-1})	Founded fenthion (ng mL^{-1})			
	PLS	**OSC-PLS**	**PARAFAC**	**OSC-PARAFAC**
15.0	15.7	15.4	14.7	15.1
35.0	36.2	35.8	34.6	35.5
55.0	56.3	56.1	55.8	55.3
75.0	74.2	74.5	75.8	75.5
95.0	92.2	93.6	94.5	95.4
Number of factor	5	3	2	1
PRESS	2.81	1.23	-	-
RMSEP	0.92	0.78	0.64	0.37
RSEP	1.46	1.21	0.74	0.45

Table 5. Statistical parameters of the linear relationship between the proportion loadings calculated by PARAFAC and OSC-PARAFAC.

Parameters	PARAFAC[a]	OSC-PARAFAC[b]
Number of data point	11	11
Intercept	0.0841	0.0103
Standard deviation of intercept	0.4531	0.1381
Slope	0.1241	0.3681
Standard deviation of slope	0.2140	0.0985
Correlation coefficient	0.9412	0.9826

[a] PARAFAC: parallel factor analysis;
[b] OSC-PARAFAC: orthogonal signal correction parallel factor analysis.

3.9. Application of the method in synthesis and real matrix samples

In order to investigate the applicability of the optimized methods for real samples, it was used to the preconcentration and determination of the fenthion in spiked water sample and real samples including three water samples (tap, river and waste water). The concentrations of fenthion were determined by the OSC-PLS, and OSC-PARAFAC and the results are summarized in Table 6. Moreover, the OSC-PARAFAC model was better than OSC-PLS model in terms of the determination of fenthion in complex matrices, without considerable error. The results demonstrated that satisfactory recovery for fenthion could be obtained using the proposed procedures. Hence, the OSC-PARAFAC model was able to predict the concentrations of fenthion in the real matrix samples.

Table 6. Application of the proposed method for the determination of fenthion in real samples.

Sample	Added	Found (ng mL^{-1})			
		OSC-PLS	Recovery (%)	OSC-PARAFAC	Recovery (%)
Tap water	-	N.D.[a]	-	N.D.	-
	50.0	52.3	104.6	50.6	101.2
River water	-	N.D.	-	N.D.	-
	50.0	48.7	97.4	49.3	98.6
Waste water	-	N.D.	-	N.D.	-
	50.0	51.7	103.4	48.6	97.2

[a] N.D.: Not Detected.

4. Conclusions

A simple and efficient DLLME coupled with spectrofluorimetry was developed for the extraction and determination of fenthion in water samples. The proposed method has numerous advantages such as, simplicity and rapidity of extraction and analysis that reduced the organic solvent consumption within a short time. In this study, the RSM based on the BBD was successfully used for optimization of variable the DLLME method that led to a saving of experimental time and materials. PLS and PARAFAC multivariate calibration models, with and without OSC pre-processing, were used for Modelling second-order fluorescence signals and quantification of fenthion. The predicted values obtained by application of OSC-PARAFAC model showed the high predictive ability compared with OSC-PLS method, which explained that the tolerance limit of three-way calibration methods for the matrix effect was better than that of the two-way methods. Therefore, the proposed procedure can be successfully applied for analysis and monitoring of fenthion in water samples.

5. Acknowledgment

The authors are grateful to the Department of Chemistry, Arak Branch, Islamic Azad University, Central Tehran Branch, Islamic Azad University and Faculty of Chemistry, Mazandaran University, Iran

6. reference 37 (2013)

[1] O. Espinoza-Navarro, C. Ponce-LaRosa, E. Bustos-Obregón, Organophosphorous pesticides: their effects on biosentinel species and humans, control and application in Chile, Int. J. Morphol., 35 (2017) 1069–1074.

[2] K. Vala Ragnarsdottir, Environmental fate and toxicology of organophosphate pesticides, J. Geol. Soc., 157 (2000) 859–876.

[3] P. Sánchez Lizardi, M. K. O'Rourke, R. J. Morris, The effects of organophosphate pesticide exposure on hispanic children's cognitive and behavioral functioning, J. Pediatr. Psychol., 33 (2007) 91–101.

[4] A. S. H. Derbalah, H. Wakatsuki, T. Yamazaki, H. Sakugawa, Photodegradation kinetics of fenitrothion in various aqueous media and its effect on steroid hormones biosynthesis, Geochem. J., 38 (2004) 201–213.

[5] R. A. Cheke, Effects of the organophosphate fenthion for control of the redbilled quelea Quelea quelea on cholinesterase and haemoglobin concentrations in the blood of target and non-target birds, Ecotoxicol., 21(2012) 1761–1770.

[6] T. Galeano Díaz, A. Guiberteau Cabanillas, M. D. López Soto, J. M. Ortiz, Determination of fenthion and fenthion-sulfoxide, in olive oil and in river water, by square-wave adsorptive-stripping voltammetry, Talanta, 76 (2008) 809–814.

[7] Y. Zhou, An experimental design approach using response surface techniques to obtain optimal liquid chromatography and mass spectrometry conditions to determine the al-

kaloids in Meconopsi species, J. Chromatogr. A, 1216 (2009) 7013–7023.
[8] S. Boulanouar, S. Mezzache, A. Combès, V. Pichon, Molecularly imprinted polymers for the determination of organophosphorus pesticides in complex samples, Talanta, 176 (2018) 465–478.
[9] T.-K. Ly, T.-D. Ho, P. Behra, Determination of 400 pesticide residues in green tea leaves by UPLC-MS/MS and GC-MS/MS combined with QuEChERS extraction and mixed-mode SPE clean-up method, Food Chemistry, 326 (2020) 126928.
[10] F. Tokay, S. Bağdat, Solid phase extraction and preconcentration of some metal ions using Schiff base immobilised silica gel followed by ICP-OES, Int. J. Environ. Anal. Chem., 00 (2019)1–12.
[11] P. Sun, Y. L. Gao, C. Xu, Y. F. Lian, Determination of six organophosphorus pesticides in water samples by three-dimensional graphene aerogel-based solid-phase extraction combined with gas chromatography/mass spectrometry, RSC Adv., 8 (2018) 10277–10283.
[12] X. C. Huang, J. K. Ma, R. X. Feng, S. L. Wei, Simultaneous determination of five organophosphorus pesticide residues in different food samples by solid-phase microextraction fibers coupled with high-performance liquid chromatography, J. Sci. Food Agric., 99 (2019) 6998–7007.
[13] S. Manafi Khoshmanesh, H. Hamishehkar, H. Razmi, Trace analysis of organophosphorus pesticide residues in fruit juices and vegetables by an electrochemically fabricated solid-phase microextraction fiber coated with a layer-by-layer graphenized graphite/graphene oxide/polyaniline nanocomposite, Anal. Methods, 12 (2020) 3268–3276.
[14] N. S. Pano-Farias, S. G. Ceballos-Magaña, R. Muñiz-Valencia, J. M. Jurado, Á. Alcázar, I. A. Aguayo-Villarreal, Direct immersion single drop micro-extraction method for multiclass pesticides analysis in mango using GC–MS, Food Chem., 237 (2017) 30–38.
[15] A. Niazi, N. Khorshidi, P. Ghaemmaghami, "Microwave-assisted of dispersive liquid-liquid microextraction and spectrophotometric determination of uranium after optimization based on Box-Behnken design and chemometrics methods, Spectrochim. Acta - Part A: Mol. Biomol. Spect., 135 (2015) 69–75.
[16] F. Assadian, A. Niazi, Application of response surface modeling and chemometrics methods for the determination of ofloxacin in human urine using dispersive liquid-liquid microextraction combined with spectrofluorimetry, J. Brazilian Chem. Soc., 28 (2017) 2291–2300.
[17] A. Niazi, S. Habibi, M. Ramezani, Spectrophotometric determination of bismuth in water samples by dispersive liquid-liquid microextraction after multivariate optimization based on box-behnken, J. Chilean Chem. Soc., 58 (2013) 1899–1901.
[18] L. Mousavi, Z.Tamiji, MR. Khoshayand,Applications and opportunities of experimental design for the dispersive liquid-liquid microextraction method - A review, Talanta, 190 (2018) 335-356
[19] C. M. Monzón, C. M. Teglia, M. R. Delfino, H. C. Goicoechea, Chemometric optimization and validation of a novel dispersive liquid-liquid microextraction-HPLC method for gliclazide, glibenclamide and glimepiride quantitation in serum samples, Microchem. J., 127 (2016) 113–119.
[20] S. Veyseh, A. Niazi, Talanta A novel aeration-assisted homogenous liquid – liquid microextration for determination of thorium and uranium in water and hair samples by inductively coupled plasma-mass spectroscopy, Talanta, 147 (2016) 117–123.
[21] J. I. Cacho, N. Campillo, P. Viñas, M. Hernández-Córdoba, In situ ionic liquid dispersive liquid-liquid microextraction coupled to gas chromatography-mass spectrometry for the determination of organophosphorus pesticides, J. Chromatogr. A, 1559 (2018) 95–101.
[22] H. Malekzadeh, M. H. Fatemi, Analysis of flavor volatiles of some Iranian rice cultivars by

optimized static headspace gas chromatography-mass spectrometry, J. Iran. Chem. Soc., 12 (2015) 2245–2251.

[23] V. Kostik, Development and validation of a method for the simultaneous determination of 20 organophosphorus pesticide residues in corn by accelerated solvent extraction and gas chromatography with nitrogen phosphorus detection, Am. J. Appl. Chem., 2 (2014) 46.

[24] A. Bidari, M. R. Ganjali, P. Norouzi, M. R. M. Hosseini, Y. Assadi, Sample preparation method for the analysis of some organophosphorus pesticides residues in tomato by ultrasound-assisted solvent extraction followed by dispersive liquid-liquid microextraction, Food Chem.,126 (2011)1840–1844.

[25] J. Sherma, Review of thin-layer chromatography in pesticide analysis: 2014–2016, J. Liquid Chromatogr. Related Technol., 40 (2017) 226–238.

[26] J. Hassan, M. Sarkouhi, Miniaturized counter current liquid-liquid extraction for organophosphorus pesticides determination, Arab. J. Chem., 9 (2016) 38–42.

[27] T. T. Hu, C. M. Lu, H. Li, Z. X. Zhang, Y. H. Zhao, J. Li, Determination of Eleven organophosphorus pesticide residues in textiles by using HPLC-HRMS, Anal. Sci., 33 (2017) 1027–1032.

[28] N. Ferretto, M. Tedetti, C. Guigue, S. Mounier, R. Redon, M. Goutx, Identification and quantification of known polycyclic aromatic hydrocarbons and pesticides in complex mixtures using fluorescence excitation-emission matrices and parallel factor analysis, Chemosphere, 107 (2014) 344–353.

[29] J. Dong, P. Li, S. Wang, J. Wei, Y. Yang, Fluorometric determination of pesticides and organophosphates using nanoceria as a phosphatase mimic and an inner filter effect on carbon nanodots, Microchim. Acta, 186 (2019) 66.

[30] H. C. Liang, N. Bilon, M. T. Hay, Analytical methods for pesticide residues, Water Environ. Res., 86 (2014) 2132–2155.

[31] W. M. Marget, M. D. Morris, Central composite experimental designs for multiple responses with different models, Technometrics, 61 (2019) 524-532.

[32] N. Khorshidi, A. Niazi, Optimization of pyrocatechol violet biosorption by Robinia pseudoacacia leaf powder using response surface methodology: Kinetic, isotherm and thermodynamic studies, J. Water Reuse Desal., 6 (2016) 333–344.

[33] Z. Zhang, H. Zheng, Optimization for decolorization of azo dye acid green 20 by ultrasound and H2O2 using response surface methodology, J. Hazard. Mater., 172 (2009) 1388–1393.

[34] F. B. Shahri, A. Niazi, Synthesis of modi fi ed maghemite nanoparticles and its application for removal of Acridine Orange from aqueous solutions by using Box-Behnken design, J. Magn. Magn. Mater., 396 (2015) 318–326.

[35] M. H. Dehghani, Production and application of a treated bentonite–chitosan composite for the efficient removal of humic acid from aqueous solution, Chem. Eng. Res. Design, 140 (2018) 102–115.

[36] S. G. Tuncel, T. Topal, Multifactorial optimization approach for determination of polycyclic aromatic hydrocarbons in sea sediments of Turkish Mediterranean Coast, *A*m. J. Anal. Chem. 2 (2011) 783–794.

[37] R. Bhaumik, N. K. Mondal, S. Chattoraj, J. K. Datta, E. T. Al, Application of Response Surface Methodology for Optimization of Fluoride Removal Mechanism by Newely Developed Biomaterial, Am. J. Anal. Chem., 4 (2013 404–419.

[38] M. Z. Mohamad Zulhelmi, A. Rasyidah, S. Faraziehan, K. Mohamad Anuar, Response surface methodology approach for optimization of biosorption process for removal of binary metals by immobilized saccharomyces cerevisiae, Appl. Mech. Mater., 661(2014) 51–57.

[39] X. Yan, H. Li, X. Wang, X. Su, A novel fluorescence probing strategy for the determination of parathion-methyl, Talanta, 131(2015) 88–94.

[40] M. L. Nahorniak, K. S. Booksh, Optimizing the implementation of the PARAFAC method for near-real time calibration of excitation–emission fluorescence analysis, J. Chemom., 17 (2004) 608–617.

[41] S. Elcoroaristizabal, A. De Juan, J. Antonio, I. Elorduy, N. Durana, L. Alonso, Chemometric determination of PAHs in aerosol samples by fluorescence spectroscopy and second-order data analysis algorithms, J. Chemom., 28 (2014) 260–271.

[42] A. Niazi, M. Sadeghi, PARAFAC and PLS applied to spectrophotometric determination of tetracycline in pharmaceutical formulation and biological fluids, Chem. Pharm. Bull., 54 (2006) 711–713.

[43] J. Ghasemi, A. Niazi, Two- and three-way chemometrics methods applied for spectrophotometric determination of lorazepam in pharmaceutical formulations and biological fluids, Anal. Chim. Acta, 533 (2005)169–177.

[44] K. Kumar, A. Kumar Mishra, Parallel factor (PARAFAC) analysis on total synchronous fluorescence spectroscopy (TSFS) data sets in excitation-emission matrix fluorescence (EEMF) layout: Certain practical aspects, Chemom. Intell. Lab. Syst., 147 (2015) 121–130.

[45] J. U. Ghasemi, A. Niazi, Simultaneous determination of cobalt and nickel, comparison of prediction ability of PCR and PLS using original, first and second derivative spectra, Microchem. J., 68 (2001) 1-11.

[46] A. Niazi, M. Goodarzi, Orthogonal signal correction–partial least squares method for simultaneous spectrophotometric determination of cypermethrin and tetramethrin. Spectrochim. Acta Part A, 62 (2008)1165-1169.

[47] S. Wold, M. Sjöström, L. Eriksson, PLS-regression: A basic tool of chemometrics, Chemom. Intell. Lab. Syst., 58 (2001) 109–130.